Introduction of Hydrophilicity onto Silicon Oxide and Titanium Oxide by Non-equilibrium Atmospheric Pressure Plasma

Chen Long

Department of Production Science and Technology, Gunma University

March 2019

Contents

Contents 1
Chapter 1 General introduction 3
1. Definition and classification of plasma 3
1.1 Definition of plasma 3
1.2 Classification of Plasma 3
2. Non-equilibrium atmospheric pressure plasma 4
2.1 Dielectric barrier discharges (DBDs) 5
2.2 Corona discharges 5
2.3 Atmospheric pressure plasma jet (APPJ) 6
3 Application of non-equilibrium plasma 7
3.1 The application of non-equilibrium plasma for reduction to metal ions 8
3.2 The application of non-equilibrium plasma for reduction to graphene material 9
3.3 The application of non-equilibrium plasma-assisted reduction to synthesis of metal nanoparticles 11
3.4 Deposition of coatings by non-equilibrium atmospheric pressure plasma 12
3.5 Surface modification treatments by non-equilibrium atmospheric pressure plasma 13
4 Objectives of this study 13
References 15
Chapter 2 Introduction of hydrophilicity onto oxidized Si wafer surfaces by non-equilibrium atmospheric pressure plasma with Ar and Ar/H_2 as working gas 31
1 Introduction 31
2 Experimental details 32
2.1 Non-equilibrium atmospheric pressure plasma device 32
2.2 Sample preparation 32
2.3 Surface characterization. 33
3 Results and discussion 33
3.1 XPS analysis of oxidized Si wafer surfaces 33
3.1.1 XPS analysis of oxidized Si wafer 33
3.1.2 XPS analysis of oxidized Si wafer after plasma treatment 34
3.2 Contact angle of water on oxidized Si wafer surfaces 35
4 Conclusions 36
References 37
Chapter 3 Introduction of hydrophilicity onto oxidized Si wafer surfaces by non-equilibrium atmospheric pressure plasma with addition of water vapor 53
1 Introduction 53
2 Experimental details 54
2.1 Structure of bubbling system 54
2.2 Sample preparation 54
2.3 Surface characterization 55
2.4 Analysis of surface hydroxy group by derivatization XPS 55
2.4.1 Derivatization reaction 57
2.4.2 XPS measurements 57

3 Results and discussion 58
3.1 Results of oxidized Si wafer surfaces 58
3.1.1 XPS analysis of oxidized Si wafer 58
3.1.2 Contact angle of water on oxidized Si wafer surfaces 58
3.1.3 Analysis of surface hydroxy group by derivatization XPS 59
3.2 Results of quartz glasses 60
3.2.1 XPS analysis of quartz glass 60
3.2.2 Contact angle of water on quartz glasses 61
3.3 Stability of hydroxy group 61
4 Comparison of hydrophilicity introduced by different plasma methods 62
5 Conclusions 63
References 64
Chapter 4 Comparison of hydrophilicity on TiO_2 film surfaces introduced by non-equilibrium atmospheric pressure plasma with or without addition of water vapor 85
1 Introduction 85
2 Experimental details 86
2.1 Sample preparation 86
2.2 Surface characterization 87
3 Results and discussion 87
3.1 XPS analysis of TiO_2 surfaces 87
3.2 Contact angle of water on TiO_2 film surfaces 89
3.3 Stability of hydroxy group 90
4 Application of non-equilibrium atmospheric pressure plasma treatment to dye-sensitized solar cell 90
4.1 Measurement of dye adsorption 91
4.2 Quantity of dye adsorption 93
5 Conclusions 93
References 94
Chapter 5 Conclusions and prospect 115
1 Conclusions 115
2 Prospect 118
List of publications 119
Acknowledgement 120

Chapter 1 General introduction

1. Definition and classification of plasma

1.1 Definition of plasma

Plasma, a word proposed by Langmuir, is often considered the fourth state of matter except solid, liquid and gas and it represents 97% of the universe [1, 2]. A commonly accepted definition is plasma is a partially or fully ionized gas. Plasma discharges can create an abundance of energetic gas phase species, such as ions, electrons, photon and neutral particles [3].

1.2 Classification of Plasma

According to the type of the energy transferred to plasma, the properties of plasma can change by electron density and electron temperature. These two parameters can classify plasmas into different categories (as shown in Fig. 1-1) [4]. In general, there are two main categories for plasma depending on plasma's characterized temperature: Equilibrium plasma (thermal plasma) and non-equilibrium plasma (cold plasma). Both of these two kinds of plasma can be generated in laboratory or industrial environment by applying direct or alternating high voltage on a gas [5].

For thermal plasma, transitions and chemical reactions are controlled by collisions, not by radiative processes. In addition, collision phenomena are micro-reversible in thermal plasma that is to say each kind of collision is balanced by its inverse (excitation/deexcitation; ionization/recombination; kinetic balance) [6]. Therefore, in thermal plasma the electron temperature is equal to the gas temperature which depends on the temperature of heavy particles.

Non-equilibrium plasma can be described by two temperatures: heavy particle temperature (T_h)

and electron temperature (T_e). The heavy particles can be kept "cold" (near ambient temperature, 300 K) while the electron can be made "hot", above 1×10^4 K. Because of the big mass difference between heavy particles and electrons, the gas temperature (T_g) (or plasma temperature) is determined by T_h, in other words $T_g \approx T_h$. Therefore non-equilibrium is also called cold plasma, because of the lower heavy particle temperature. Non-equilibrium plasmas are as particular use in industry because of their ability to promote specific types of gas-phase reactions and species that can modify bulk materials [2].

2. Non-equilibrium atmospheric pressure plasma

The effect of gas pressure on electron temperature (T_e) and gas temperature (T_g) is shown in Fig. 1-2 [7]. At relatively lower pressure (10^{-4} ~ 10^{-2} kPa) T_g is much lower than electron temperature. The heavy particles are excited or ionized by inelastic collisions with electrons. The inelastic collisions do not raise the T_g. But collisions in the plasma can intensify when the gas pressure becomes higher. They lead to both plasma chemistry (by inelastic collisions) and heavy particles heating (by elastic collisions). Then, the difference between T_e and T_g decreases, and plasma state is close to the thermal equilibrium state. How to prevent heavy particles from achieving thermal equilibrium is very important to generate non-equilibrium plasma at atmospheric pressure. The density of the feeding power affects the plasma state (thermal equilibrium or non-equilibrium) to a great extent. Namely, a high density of feeding power induces atmospheric pressure thermal equilibrium plasma; while a low power density or a pulsed power supply lead to non-equilibrium atmospheric pressure plasma.

One merit of atmospheric pressure plasma is that, unlike low-pressure or vacuum plasma, it does

not require vacuum or low-pressure devices, which are very expensive vacuum equipment with high maintenance cost.

The various types of electrical discharge that can be used to generate non-thermal plasmas at atmospheric pressure [8-9]. These discharges which occur in an appropriate gaseous atmosphere are: dielectric barrier discharge (DBD), corona discharge, as well as some types of radio-frequency (RF) discharges and microwave (MW) discharges [10].

2.1 Dielectric barrier discharges (DBDs)

Dielectric barrier discharges (DBD) have been known for more than one century [11]. The DBD's unique combination of non-equilibrium and quasi-continuous behavior has attracted great interests in a wide application and become the focus of many fundamental researches [12]. DBD are also called "silent" and "atmospheric-pressure-glow" discharges [9, 13]. DBDs are based on the use of a dielectric barrier in the discharge gap. It was used to stop electric currents and prevents the formation of electric currents. A schematic illustration of DBD discharge is shown in Fig. 1-3. It consists of two metal electrodes, in which at least one is coated with a dielectric layer. The gap is on the order of several millimeter, and the applied voltage is about 20 kV. The plasma is generated through a series of micro arcs, lasting for 10–100 ns, and randomly distributed in space and time. These streamers are believed to be ~100 μ m in diameter and are separated from each other by about 2 cm [9, 13-14].

2.2 Corona discharges

Corona discharges appear as luminous glow localized in space around a point tip in a highly non--uniform electric field. The physics of this source is well understood [15-18]. The corona discharge

is basically a Townsend discharge. It occurs prior to the electrical breakdown. Fig. 1-4 shows a schematic of a point-to-plane corona. The apparatus consists of a metal tip, with a radius of about 3mm, a planar electrode separated from the tip by a distance of 4–16 mm, and the DC power supply is pulsed [18].

2.3 Atmospheric pressure plasma jet (APPJ)

The atmospheric pressure plasma jet (APPJ) is a truly non-thermal plasma which is demonstrated by the vast difference in ion and electron temperatures from thermal plasma [19]. Shown in Fig. 1-5 is a schematic of an atmospheric-pressure plasma jet [9]. This new source consists of two concentric electrodes without any dielectric between electrodes [20-21], and through which a mixture of helium, argon, oxygen, and other gases flow. By applying 13.56 MHz RF power to the inner electrode at a voltage between 100-250 V, the gas discharge is ignited. The gas temperature of the discharge is typically between 50-300 ℃, so thermal damage to materials can be easily avoided.

The ionized gas from the plasma jet exits through a nozzle, directing to a substrate a few millimeters down-stream. This source has been used to etch polyimide, tungsten, silicon dioxide and so on [22], as well as to deposit silicon dioxide films by plasma-assisted chemical vapor deposition [23].

Both DBDs and RF discharges can be used to generate atmospheric pressure plasma. In DBDs, dielectric materials are used to cover one or both electrodes, and the high voltage in the frequency range of several kHz is applied to ignite the discharge. It would cause a drop of the voltage across the plasma with charging accumulation on the dielectric layer, which covers the electrodes, so DBDs are self-pulsed discharges that can restrict the discharge current and avoid arcing. RF discharges

have also been used to generate non-equilibrium atmospheric pressure plasma jet with devices that are similar to DBDs or with devices where the electrodes are bare metal [24-27]. With bare metal electrodes, glow-to-arc transition would occur easily. Therefore, the electrodes have to be cooled and the gas flow rate has to be adjusted to a certain level to reduce the risk of glow-to-arc transition. RF driven plasma devices require impedance matching between the power source and the plasma to optimize the dissipated power in the plasma and minimize the reflected power.

3 Application of non-equilibrium plasma

In recent years, non-equilibrium plasma has become a very popular tool in various fields, especially surface treatment, as shown in Fig. 1-5 [19]. In case of plasma-solid interactions, we can classify them into 3 categories. The first one is where material is removed from the solid surface by plasma-induced etching or ablation (as shown in Fig. 1.5 b). Secondly, material is added to the surface in the form of thin film deposit, a process known under the collective name "plasma-enhanced chemical vapor deposition (PECVD)" (as shown in Fig. 1.5 c). Finally, materials are not added or removed from the solid, but the surface is chemically and/or physically modified during its exposure to particles and radiation from the plasma [5] (as shown in Fig. 1.5 d & e).

Non-equilibrium plasma can be divided into low-pressure (LP) and atmospheric pressure (AP) according to the working pressure. Energetic electrons, which are generally thought to be the reducing agents for LP plasma, can reduce the metal ions with positive standard potentials using inert gases as the working gas [28]. In contrast, hydrogen-containing gases (e.g., H_2, CH_4, NH_3 [29-34], etc.) are often used as working gases for AP plasma, and the generated active hydrogen species (e.g., excited hydrogen atoms and molecules, etc.) are deemed as the reducing agents. These active

hydrogen species are more powerful for reduction than energetic electrons. They may not only reduce metal ions with positive standard potentials, but also some with negative values [35]. Moreover, the process is operated at atmospheric pressure, and no expensive or sophisticated vacuum systems are required.

There are so many applications of the surface process mentioned above, even in industrially important applications. There can be little doubt that the electronics industry, energy and environment have been the principal driving forces for the advancement of plasma processing. In the next section some reductive and surface modification's applications of plasma for these fields will be shown.

3.1 The application of non-equilibrium plasma for reduction to metal ions

Supported metal nanoparticles are usually served as heterogeneous catalysts owing to their unique properties [36, 37] and play an important role in energy conversion, nanoelectronics and storage [38, 39]. The controllable size and structure of catalysts are crucial to their properties. But there is also a challenge in catalysis field: pollution to our environment and high material wastes and energy consumption during the preparation of heterogeneous catalysts [40]. Among many preparation methods, plasma has attracted remarkable attention.

Non-equilibrium plasma has recently been shown to be an efficient method for reducing supported metal [41]. This reduction process can take several minutes to tens of minutes, and the metal nanoparticles which prepared by plasma are homogeneously distributed on the supports with smaller size. Because in room temperature, electron reduction via non-hydrogen discharge is excellent for

size control though fast nucleation and slow crystal growth. Plasma is a simple, easy, cheap and energy-efficient way to reduce supported metal ions. For those metal ions that cannot be reduced by non-hydrogen glow discharge [42], hydrogen non-equilibrium plasma can be applied to reduce them [43-47].

Zhoujun Wang [48] et al. used Ar glow discharge plasma to reduce $RhCl_3$ impregnated Al_2O_3 powder at room temperature. They also revealed that Ar plasma reduction induced a high dispersion of Rh nanoparticles on the support with average particle size of 1.2 nm. Xuzhen Wang [49] et al. prepared graphene sheets supported monometal (Ni, Co) or bimetal (Ni-Co) nanoparticle composites with the assistance of DBD plasma at low temperature. Graphene oxide and metal ions (Ni^{2+}, Co^{2+}) can be simultaneously reduced by H_2 plasma in atmosphere. Lanbo Di [40] et al. demonstrated a new non-equilibrium atmospheric pressure plasma method for reducing supported metal ions: TiO_2 (P25) supported $HAuCl_4$, $AgNO_3$, H_2PtCl_6, and Pd $(NO_3)_2$ can be reduced into their metallic states by carbon monoxide non-equilibrium plasma in atmosphere for 9 min. Additionally they found the Au nanoparticles generated by CO plasma and those generated by H_2 plasma exist in a metallic state and exhibit similar particle sizes.

3.2 The application of non-equilibrium plasma for reduction to graphene material

Graphene, due to its unique properties of high electron mobility which mainly originates from its two-dimensional structure [50, 51] has many potential applications in transparent conductive films [52, 53], field effect transistors (FETs) [54], lithium-ion batteries [55], supercapacitors [56], organic photovoltaic cells [57, 58], electron field emitters [59], ultrasensitive sensors [60], hydrogen storage [62,

[63], as well as in nano-biotechnologies [64, 65]. There are two main process used for reduction of graphene oxide (GO) to produce graphene or reduced GO. The first approach is the typical reduction in solution by chemical reducing agents such as hydrazine (N_2H_4) [66, 68] or sodium7 borohydride ($NaBH_4$) [68], there are also more reductive agents but they are usually highly toxic or the process requires very long time [69, 70]. Thus, for chemical reduction, the treatment is time-consuming and commonly ineffective, often requiring additional annealing steps [53, 71]. Moreover, there will be a dangerous and environmentally toxic chemical that can introduce impurities in reduced GO [72, 73]. The second approach, which is more common, is based on thermal reduction using high temperature in H_2 or Ar or ultrahigh vacuum (UHV) environments in order to remove oxygen effectively [74, 75]. But for thermal reduction, the required high temperature will damage many substrates such as polymers, plastics and textiles, severely limiting its applicability. [76].

Compared with chemical and thermal reduction approaches, plasma discharges offer a unique advantage because non-equilibrium reactions can be performed at low temperature and high purity [77]. In the case of GO, the generation of atomic hydrogen can remove oxygen functional groups effectively without damaging the substrate [71]. Faisal Alotaibi [78] et al. used a new method based on scanning atmospheric plasma to enhance an ultrafast reduction of GO and prepare highly conductive graphene films. This ultrafast GO films reduction process can be completed in 60 s at room temperature. It is possible for this process to achieve the effect of conventional chemical and thermal reduction process. M. Baraket [79] et al. reduced GO by using electron beam-generated plasmas in gas mixtures of argon and methane. Seung Whan Lee [80] et al. demonstrated reduction of GO at low temperature (70℃) and atmospheric pressure via H_2 plasma-assisted chemistry. The highly effective removal of oxygen functional groups and lower resistance GO films were obtained. They also found

that plasma method can mitigate ion-induced sputter removal or damage.

3.3 The application of non-equilibrium plasma-assisted reduction to synthesis of metal nanoparticles

Metal nanoparticles can be used to prepare nanoparticle films for electronic circuitry [81] and flexible electronics [82] which are used in applications like display [83], batteries [84 85], stretchable circuits [86 87] and flexible sensors [86-92]. There are a lot of different methods to synthesize metal nanoparticles. But many of them require multi-step processes [90]. As for the plasma treatment, like the reduction of graphene introduced in last part, there is availability of high-energy atomic hydrogen to enable the chemical reactions to proceed rapidly, and it will not damage the substrates during process. Moreover, it does not require the restricted conditions of high temperature or vacuum. [93].

Copper is the most significant circuit material for electronic devices and components [94 95], due to its low cost and high conductivity [96]. However, copper is easily oxidized in the air to form a thin copper oxide layer which is thought to be mechanically weak [97]. The oxidation of copper has always been a serious problem in the process of wiring circuit boards by soldering [98]. So various methods were used to reduce and sinter copper nano-particles. K. Takeda [99] reduced the copper sheet by atmospheric pressure Ar /H_2 plasma at 90 °C. In the former study of our lab [21], non-equilibrium atmospheric pressure plasma jet generated by three kinds of plasma torches, i. e. an APC plasma torch, a beam plasma torch, and a beam plasma torch with an air-cooling system of electrode was used to reduce and sinter copper nano-particles. The results showed that the oxidized copper nano-particles could be reduced at ambient temperature with 1 minute in atmosphere, and be sintered at ambient temperature within 7 minutes in atmosphere. For the application of plasma to other metals,

A. R. Dayal and D. R. Sadedin [93] used plasma reactor which had a transient traveling arc to study hydrogen for in-flight reduction of metal oxide particles. The results suggested that atomic hydrogen existing throughout the volume of plasma reactor was sufficient to reduce particles of FeO, Cr_2O_3, and TiO_2.

3.4 Deposition of coatings by non-equilibrium atmospheric pressure plasma

Plasma enhanced chemical vapor deposition (PECVD) is currently used in automotive, aerospace industries and microelectronics [99]. There are variety of deposition of thin films such as amorphous materials, oxides, nitrides, metal alloys, and doped materials [100-105]. PECVD allows film formation over large areas and on fragile materials such as polymers [3]. It requires supplying an additional precursor as a vapor. Silicon–organics, metal–organics or various solutions may be used as precursors. Liquid precursors are atomized or vaporized for transferring into the working volume of the APPJ system [106]. The thickness of deposited films can be controlled by changing plasma parameters such as RF power, chamber pressure, deposition time, as well as working gas composition.

The most widely investigated application of PECVD is on oxides, and the features of reduction of plasma are also studied. Deposition of TiO_2 thin films by PECVD and TiO_x ($0 < x < 2$) thin film synthesized by plasma assisted reduction were reported by Shuxia Ren et al. [107]. To generate oxygen vacancies in TiO_2 thin film, hydrogen (H_2) was introduced into the PECVD chamber to initiate plasma assisted H_2 reduction. The result showed that TiO_x ($x = 1.48$, 1.05 and 0.77) thin films synthesized by plasma assisted chemical vapor deposition and reduction. Although most

applications of APPJs have involved the deposition of oxides, the use of this method for preparation of a metal coating has also been reported [108]. RF APPJ was used for the direct deposition of Cu coatings on polyamide substrates. Adding a fractional amount of H_2 gas into the Ar gas reduced the reaction of oxidized Cu films, because oxidization of the Cu film is inevitable due to the presence of oxygen in air.

3.5 Surface modification treatments by non-equilibrium atmospheric pressure plasma

Plasma treatments are most widely used to modify material surfaces, especially the surface of polymeric materials. The goals of these treatments can vary widely [109]. The purposes include surface activation for higher adhesion, surface cleaning, and improvement of hydrophilic or hydrophobic properties and etching of polymers. It was shown that APPJs can be very effective in materials processing and suitable for materials sensitive to thermal damage. It has been reported that both Kapton and polyimide have been successfully etched by APPJ [110, 111]. APPJ can also be used for cleaning of metal surface by using oxygen highly diluted in helium or argon gas [112]. The oxygen active species are capable of removing many organic materials on the metal surface with the release of water and carbon dioxide. Other surface modifications of oxides and metals have also been demonstrated [113-115]. In most cases, the exhaust gas from APPJ system is harmless and can be discharged to the atmosphere without further processing. As an environmental-friendly technology, it is expected that APPJ will be more widely used in the future.

4 Objectives of this study

As mentioned earlier, non-equilibrium plasmas have energetic electrons (low pressure) or active

hydrogen species (atmospheric pressure) which can play a role as reducing agents. For the processes which are operated at atmospheric pressure, the active hydrogen species are more powerful than energetic electrons. Moreover, this process is more advantageous in term of cost and operation flexibility. So far, there are many reports about the reduction process operated by a variety of non-equilibrium atmospheric pressure plasma jets.

In this thesis, silicon oxide and titanium oxide surface are irradiated by non-equilibrium atmospheric pressure plasma in order to introduce hydrophilicity to their surface. The purpose of this thesis is to find out the optimum plasma irradiation conditions for the hydrophilicity introduction, and also to clarify the surface structure of the irradiated oxides. And more, it is aimed to explore the possibility of its application.

A new type of capacitive coupled RF plasma device (named of "APC") was used to generate non-equilibrium plasma at atmospheric pressure. In order to study the elemental composition on the surface of sample and plasma treatment effect, the measurements by X-ray photoelectron spectroscopy (XPS) and contact angle of water were conducted.

Chapter 2 explains the construction of "APC plasma torch" and the experimental setup used for plasma-treatment. Plasma-treatment with pure Ar and Ar/H_2 as working gas is used to introduce hydrophilicity effect on thermally oxidized Si wafer surface. Thermal oxidization process was operated at 900 °C in muffle furnace, then plasma irradiation under different treatment period was carried out and XPS and contact angle analyses were carried out.

Chapter 3 describes the construction of APC plasma torch with Ar/water vapor. Oxidized Si wafers were irradiated by Ar /H_2O plasma in different treatment periods and analyzed in terms of XPS and contact angle in order to investigate the influence of the structure of silicon oxide on the

introduction of hydrophilicity by non-equilibrium atmospheric pressure plasma, quartz glass was treated with Ar/H_2O plasma. Furthermore, the stability of the hydrophilicity of the silicon oxide surface introduced by Ar/H_2O plasma, change with time in the contact angle was observed. Surface thermally oxidized Si wafers and quartz glass were stored in air and in vacuo after Ar/H_2O plasma treatment. Moreover, hydrophilicity introduced by different plasma methods shown in chapter 2 and 3 are compared and summarized.

Based on the above results, in chapter 4, the influence of non-equilibrium atmospheric pressure plasma on titanium oxide is studied. As a sample, a titanium oxide film prepared by coating titanium oxide nanoparticles on a glass plate was used. Ar/H_2O plasma was generated with using APC. The stability of hydroxy group on the wafers treated by Ar/H_2O plasma is investigated as well. In this chapter, the application of plasma to dye-sensitized solar cell (DSSC) is also discussed.

References

[1] I. Langmuir. Oscillations in ionized gases. Proc. Natl. Acad. Sci. U.S.A., 14(8): 627-637, 1928.

[2] D. Merche, N. Vandencasteele, F. Reniers. Atmospheric plasmas for thin film deposition: A critical review. Thin Solid Films, 520: 4219–4236, 2012.

[3] K. J. Trevino. Understanding the molecular-level chemistry of H_2O plasmas. Doctor thesis, Fort Collins, Colorado State University, 2011

[4] C. Tendero, C. Tixier, P. Tristant. Atmospheric pressure plasmas: A review. Spectrochimica Acta Part B, 61 (1): 2-30, 2006.

[5] R. d'Agostino, P. Favia, C. Oehr, M. R. Wertheimer. Low-Temperature Plasma Processing of Materials: Past, Present, and Future. Plasma Process. Polym., 2 (1): 7-15, 2005.

[6] M. D. Calzada, M. Moisan, A. Gamero, A. Sola. Experimental investigation and characterization of the departure from local thermodynamic equilibrium along a surface-wave-sustained discharge at atmospheric pressure. J. Appl. Phys., 80 (46): 46-55, 1996.

[7] M. I. Boulos. Thermal Plasmas: Fundamental and Applications. Volume I, Plenum Press, New York, ISBN: 0-306-44607-3: 452, 1994.

[8] A. Fridman, A. Chirokov, A. Gutsol. Non-thermal atmospheric pressure discharges. J. Phys. D.: Appl. Phys., 38: R1-R24, 2005.

[9] A. Schütze, J. Y. Jeong, S. E. Babayan, J. Park, G. S. Selwyn and R. F. Hicks. The Atmospheric Pressure Plasma Jet: A Review and Comparison to Other Plasma Sources. IEEE Trans. Plasm. Sci. , 26: 1685-1694, 1998.

[10] S. E. Alexandrov and M. L. Hitchman. Chemical Vapor Deposition Enhanced by Atmospheric Pressure Non-thermal Non-equilibrium Plasmas. Chem. Vap. Deposition, 11: 457-468, 2005.

[11] U. Kogelschatz. Dielectric-Barrier Discharges: Their History, Discharge Physics, and Industrial Applications. Plasma Chem. Plasma Process, 23 (1): 1-46, 2003.

[12] V. Nehra, A. Kumar, H. K. Dwivedi. Atmospheric non-thermal plasma sources. Int. J. Eng., 2 (1): 53-68, 2008.

[13] B. Eliasson and U. Kogelschatz. Nonequilibrium volume plasma chem-ical processing. IEEE Trans. Plasma Sci., 19 (6): 1063–1077, 1991.

[14] J. Salge. Plasma-assisted deposition at atmospheric pressure. Surf. Coat. Technol., 80 (1–2): 1–7. , 1996

[15] M. Goldman and R. S. Sigmond. Corona and insulation. IEEE Trans. Elect. Insulation, EI-17 (2): 90–105, 1982.

[16] Y. P. Raizer, Gas Discharge Physics. New York: Springer-Verlag, 1991.

[17] J. S. Chang, P. A. Lawless, and T. Yamamoto, “Corona discharge processes,” IEEE Trans. Plasma Sci., 19, Dec: 1152–1166. 1991.

[18] M. Goldman and N. Goldman. “Corona discharges,” in Gaseous Electronics. vol. 1, M. N. Hirsh and H. J. Oskam, Eds. New York: Academic: 219–290 1978.

[19] G. S. Selwyn, H. Herrmann, J. Park, I. Henins, Materials processing using an atmospheric pressure plasma jet. Physics Division Progress Report: 189, 1999–2000,.

[20] J. Laimer, H. Störi. Recent Advances in the Research on Non-Equilibrium Atmospheric Pressure Plasma Jets. Plasma Process. Polym., 4(3): 266-274, 2007.

[21] G. L. Zhang, Reduction and sintering of copper nano-particles by non-equilibrium atmospheric pressure plasma jet, Kiryu: Gunma University, 2012.

[22] J. Y. Jeong, S. E. Babayan, V. J. Tu, J. Park, R. F. Hicks, and G. S. Selwyn. Etching materials with an atmospheric-pressure plasma jet. Plasma Source Sci. Technol., 7 (3): 282–285, 1998.

[23] S. E. Babayan, J. Y. Jeong, V. J. Tu, J. Park, G. S. Selwyn, and R. F. Hicks. Deposition of silicon dioxide films with an atmospheric pressure plasma jet. Plasma Source Sci. Technol., 7 (3): 286–288, 1998.

[24] X. M. Fei, Characterization, Comparison and Application of Two Types of Atmospheric Pressure Cold Argon Plasma Jets, Kiryu: Gunma University, 2011.

[25] J. Laimer, H. Störi, Glow Discharges Observed in Capacitive Radio-Frequency Atmospheric-Pressure Plasma Jets. Plasma Process. Polym., 3 (8): 573-586, 2006.

[26] J. J. Shi, M. G. Kong. Mode Characteristics of radio-frequency atmospheric glow discharges. IEEE. Trans. Plasma Sci., 33 (22): 624-630, 2005.

[27] J. Park, I. Henins, H. W. Herrmann, G. S. Selwayn. Discharge phenomena of an atmospheric pressure radio-frequency capacitive plasma source. J. Appl. Phys., 89 (1): 20-28, 2001.

[28] C. J. Liu, M. Y. Li, J. Q. Wang, X. T. Zhou, Q. T. Guo, J. M. Yan. Plasma methods for preparing green catalysts: current status and perspective. Chin J Catal., 37 (3): 340–348, 2016.

[29] L. B. Di, X. L. Zhang, Z. J. Xu, K. Wang. Atmospheric-pressure cold plasma for preparation of high performance Pt/TiO_2 photocatalyst and its mechanism. Plasma Chem Plasma Process, 34: 301–311, 2014.

[30] B. Qi, L. B. Di, W. J. Xu, X. L. Zhang. Dry plasma reduction to prepare a high performance Pd/C catalyst at atmospheric pressure for CO oxidation. J Mater Chem A, 2: 11885–11890, 2014.

[31] L. B. Di, Z. Li, D-W Park, B. Lee, X. L. Zhang. Atmospheric-pressure cold plasma for synthesizing Pd/FeO_x catalysts with enhanced low-temperature CO oxidation activity. Jpn J Appl Phys., 56: 060301, 2017

[32] W. Y. Xu, X. Z. Wang, Q. Zhou, B. Meng, J. T. Zhao, J. S. Qiu, Y. Gogotsi. Low-temperature plasma-assisted preparation of graphene supported palladium nanoparticles with high hydrodesulfurization activity. J Mater Chem., 22:14363–14368, 2012.

[33] W. Hua, L. J. Jin, He XF, J. H. Liu, H. Q. Hu. Preparation of Ni/MgO catalyst for CO_2 reforming of methane by dielectric-barrier discharge plasma. Catal Commu., 11(11): 968–972, 2011.

[34] H. J. Gallon, X. Tu , M. V. Twigg, J. C. Whitehead. Plasma-assisted methane reduction of a NiO catalyst—low temperature activation of methane and formation of carbon nanofibers. Appl Catal B, 106(3–4): 616–620, 2011.

[35] S. Z. Hu, F. Y. Li, Z. P. Fan, J. Z. Gui. Improved photocatalytic hydrogen production property over $Ni/NiO/N–TiO_{2-x}$ heterojunction nanocomposite prepared by NH_3 plasma treatment. J Power

Sources, 250: 30–39, 2014.

[36] A. Y. Khodakov, W. Chu, P. Fongarland. Advances in the development of novel cobalt Fischer–Tropsch catalysts for synthesis of long-chain hydrocarbons and clean fuels. Chem Rev. 107 (5):1692–1744, 2007.

[37] H. Yang, Z. H. Wang, Y. Y. Zheng, L. Q. He, C. Zhan, X, H. Lu, Z. Q. Tian, P. P. Fang, Y. X. Tong. Tunable wavelength enhanced photoelectrochemical cells from surface plasmon resonance. J. Am Chem. Soc. 138 (50): 16204–16207, 2016

[38] A. S. Aririco`, P. Bruce, B. Scrosati, J. M. Tarascon, W. V. Schalkwijk. Nanostructured materials for advanced energy conversion and storage devices. Nat Mater, 4: 366–377, 2006.

[39] G. Prieto, J. Zečević, H. Friedrich, K.P. De Jong, P.E. De Jongh. Towards stable catalysts by controlling collective properties of supported metal nanoparticles. Nat Mater, 12: 34–39, 2013.

[40] C. J. Liu, M. Y. Li, et al., Plasma methods for preparing green catalysts: Current status and perspective. Chinese Journal of Catalysis, 37: 340 – 348, 2016.

[41] L. B. Di, X. L. Zhang, et al., Feasibility of Atmospheric-Pressure CO Cold Plasma for Reduction of Supported Metal Ions. Plasma Chem. Plasma Process, 37:1535–1549, 2017.

[42] C. J. Liu, Y. Zhao, et al., Perspectives on Electron-Assisted Reduction for Preparation of Highly Dispersed Noble Metal Catalysts. ACS Sustainable Chem. Eng., 2 (1): 3–13, 2014.

[43] W. Chu, J. Xu, J. Hong, T. Lin, A. Khodakov. Design of efficient Fischer Tropsch cobalt catalysts via plasma enhancement: Reducibility and performance. Catalysis Today, 256: 41-48, 2015.

[44] H. Penga, Y. Maa, W. M. Liu, et al., Methane dry reforming on Ni/$La_2Zr_2O_7$ treated by plasma in different atmospheres. Journal of Energy Chemistry, 24 (4), 2015: 416-424.

[45] P. Estifaee, M. Haghighi, et al., The beneficial use of non-thermal plasma in synthesis of

Ni/Al_2O_3–MgO nanocatalyst used in hydrogen production from reforming of CH_4/CO_2 greenhouse gases. Journal of Power Sources, 257: 364-373, 2014.

[46] J. Karuppiah, Y. S. Mok. Plasma-reduced $Ni/\gamma–Al_2O_3$ and $CeO_2–Ni/\gamma–Al_2O_3$ catalysts for improving dry reforming of propane. International Journal of Hydrogen Energy, 39 (29): 16329-16338, 2015.

[47] W. J. Xu, et al., Enhanced activity for CO oxidation over Pd/Al_2O_3 catalysts prepared by atmospheric-pressure cold plasma. Catalysis Today. 256: 148-152, 2015.

[48] Z. J. Wang, Yu. Zhao, L. Cui, H. Y. Du, and C. J. Liu. CO_2 reforming of methane over argon plasma reduced Rh/Al_2O_3 catalyst: a case study of alternative catalyst reduction via non-hydrogen plasmas. Green Chem., 9: 554-559, 2007.

[49] X. Z. Wang, W. Y. Xua, et al., Synthesis of metallic Ni-Co/graphene catalysts with enhanced hydrodesulfurization activity via a low-temperature plasma approach. Catalysis Today, 256: 203-208, 2015.

[50] C. N. Rao, A. K Sood. K. S. Subrahmanyam, et al., A. Graphene: The New Two-Dimensional Nanomaterial. Angew. Chem., Int. Ed., 48: 7752−7777, 2009.

[51] S. P., P.; T. H. Nok, X. L, F.; Klaus, M. Patterned Graphene Electrodes from Solution-Processed Graphite Oxide Films for Organic Field-Effect Transistors. Adv. Mater., 21, 3488−3491, 2009.

[52] X, Wang, L. J. Zhi, K, Mullen. Transparent, Conductive Graphene Electrodes for Dye-Sensitized Solar Cells. Nano Lett., 8: 323−327, 2008.

[53] G. Eda, G. Fanchini, M. Chhowalla. Large-area ultrathin films of reduced graphene oxide as a transparent and flexible electronic material. Nat. Nanotechnol., 3: 270−274, 2008.

[54] T. Mori, Y. Kikuzawa, H. Takeuchi. N-Type Field-Effect Transistor Based on a Fluorinated-

Graphene. Org. Electron., 9:328−332, 2008.

[55] E. Yoo, J. Kim, E. Hosono, H. Zhou, T. Kudo, I. Honma. Large Reversible Li Storage of Graphene Nanosheet Families for Use in Rechargeable Lithium Ion Batteries. Nano Lett., 8: 2277−2282, 2008.

[56] S. R. C. Vivekchand,; C. S. Rout, K. S. Subrahmanyam, A. Govindaraj, C. N. R. Rao. Graphene-Based Electrochemical Supercapacitors. J. Chem. Sci., 120: 9−13, 2008.

[57] Q. Liu, Z. F. Liu, X. Y. Zhang, N. Zhang, L. Y. Yang, S. G. Yin, Y. S. Chen. Solution-Processed Bulk Heterojunction Organic Solar Cells Based on an Oligothiophene Derivative. Appl. Phys. Lett. 92: 223303, 2008.

[58] X. Wang, L. J. Zhi, N. Tsao, Z. Tomovic,; J. L. Li. Transparent Carbon Films As Electrodes in Organic Solar Cells. Angew. Chem., Int. Ed. 47: 2990−2992, 2008.

[59] Z. S. Wu, S. Pei, W. Ren, D. Tang, L. Gao; B. Liu, F. Li, C. Liu, H. M. Cheng. Field Emission of Single-Layer Graphene Films Prepared by Electrophoretic Deposition. Adv. Mater, 21: 1756−1760, 2009.

[60] F. Schedin, A. K. Geim, S. V. Morozov, E. W. Hill, P. Blake, M. I. Katsnelson, K. S. Novoselov. Detection of Individual Gas Molecules Adsorbed on Graphene. Nat. Mater, 6: 652−655, 2007.

[61] D. C. Elias, R. R. Nair, et al., Control of graphene's properties by reversible hydrogenation: evidence for graphene. Science, 323: 610–613, 2009.

[62] R. Strobel, J. Garche, P. T. Moseley, L. Jorissen, G. Wolf. Hydrogen storage by carbon materials. J Power Sour. 159: 781–801, 2006.

[63] J. O, Sofo, A. S. Chaudhari, G. D. Barber. Graphane: a two-dimensional hydrocarbon. Phys Rev. B 75 (15-15): 1–4, 2007.

[64] N. Chopra, L. G. Bachas, M. R. Knecht. Fabrication and biofunctionalization of carbon-encapsulated Au nanoparticles. Chem Mater, 21 (7): 1176–1178, 2009.

[65] C. Shan, H, Yang, J. Song, D. Han, A. Ivaska, L. Niu. Direct electrochemistry of glucose oxidase and biosensing for glucose based on graphene. Anal Chem. 81 (6): 2378–2382, 2009.

[66] I. Jung, D. Dikin, ect. Effect of Water Vapor on Electrical Properties of Individual Reduced Graphene Oxide Sheets. J. Phys. Chem., C 112: 20264−20268, 2008.

[67] S. Gilje, S. Han,; M. Wang. K. L. Wang, R. B. Kaner. Chemical Route to Graphene for Device Applications. Nano Lett., 7 (11): 3394−3398, 2007.

[68] H. J. Shin, K. K. Kim, A. Benayad, et al., Efficient reduction of graphite oxide by sodium borohydride and its effect on electrical conductance. Adv. Funct. Mater, 19 (12): 1987−1992, 2009.

[69] S. Pei, H. M. Cheng. The reduction of graphene oxide. Carbon, 50 (9): 3210-3228, 2012.

[70] Y. Wang, Z. Shi, J. Yin. Facile synthesis of soluble graphene via a green reduction of graphene oxide in tea solution and its biocomposites, ACS Appl. Mater. Interfaces, 3 (4): 1127-1133, 2011.

[71] C Gómez-Navarro, R. T. Weitz, et al., Electronic Transport Properties of Individual Chemically Reduced Graphene Oxide Sheets. Nano Lett., 7 (11): 3499−3503, 2007.

[72] S. Stankovich, D. A. Dikin, et al., Synthesis of Graphene-Based Nanosheets via Chemical Reduction of Exfoliated Graphite Oxide. Carbon, 45 (11): 1558−1565, 2007.

[73] S. Stankovich, D. A. Dikin, et al., Graphene-Based Composite Materials. Nature, 442: 282−286, 2006.

[74] C. Mattevi, G. Eda, S. Agnoli, et al., Evolution of Electrical, Chemical, and Structural Properties of Transparent and Conducting Chemically Derived Graphene. Thin Films. Adv. Funct. Mater, 19: 2577−2583, 2009.

[75] D. Yang, A. Velamakanni, et al., Chemical Analysis of Graphene Oxide Films after Heat and Chemical Treatments by X-Ray Photoelectron and Micro-Raman Spectroscopy. Carbon, 47 (1): 145−152, 2009.

[76] S. W. Lee, et al., Plasma-assisted reduction of graphene oxide at low temperature and atmospheric pressure for flexible conductor applications. J. Phys. Chem. Lett., 3 (6): 772-777, 2012.

[77] M. A. Liebermann; A. J. Lichtenberg. Principles of Plasma Discharges and Materials Processing. John Wiley & Sons: Hoboken, NJ, 2005.

[78] F. Alotaibi, T. T. Tung, et al., Scanning atmospheric plasma for ultrafast reduction of graphene oxide and fabrication of highly conductive graphene films and patterns. Carbon, 127: 113-121, 2018.

[79] M. Baraket, S. G. Walton, Z. Wei, et al., Reduction of graphene oxide by electron beam generated plasmas produced in methane/argon mixtures. Carbon, 48 (12): 3382-3390, 2010.

[80] S. W. Lee, C. Mattevi, M. Chhowalla, and R. M. Sankaran. Plasma-Assisted Reduction of Graphene Oxide at Low Temperature and Atmospheric Pressure for Flexible Conductor Applications. J. Phys. Chem. Lett., 3 (6): 772−777, 2012.

[81] T. Ebine，et al.， Nano Silver Dispersion and Nano Silver Ink for Printing Fine Patterns (in Japanese), DIC Technical Review, 14: 40-41, 2008.

[82] J. Yeo, S. Hong, D. Lee, et al., Next Generation Non-Vacuum, maskless, Low Temperature Nanoparticle Ink Laser Digital Direct Metal Patterning for a Large Area Flexible Electronics. Direct Digital Metal Patterning, 8 (7): 1-9, 2012.

[83] Nathan, A. et al., Amorphous silicon thin film transistor circuit integration for organic LED displays on glass and plastic. IEEE J. Solid-St. Circ., 39 (9): 1477–1486, 2004.

[84] M. Koo, K. I. Park, et al., Bendable inorganic thin-film battery for fully flexible electronic

systems. Nano Lett., 12 (9): 4810-4816, 2012.

[85] A. M. Gaikwad, G. L. Whiting, D. A. Steingart and A. C. Arias. Highly flexible, printed alkaline batteries based on mesh-embedded electrodes. Adv. Mater., 23 (29): 3251-3259, 2011.

[86] M. Park, J. Im, M. Shin, et al., Highly stretchable electric circuits from a composite material of silver nanoparticles and elastomeric fibres. Nat. Nanotechnol, 7: 803-809, 2012.

[87] F. Xu, X. Wang, Y. Zhu and Y. Zhu. Wavy ribbons of carbon nanotubes for stretchable conductors. Adv. Funct. Mater., 22 (6): 1279-1283, 2012.

[88] J. H. Lee, D. Yang, S. Kim, I. Park. Stretchable strain sensor based on metal nanoparticle thin film for human motion detection & flexible pressure sensing devices. Korea Advanced Institute of Science and Technology, Republic of Korea Fabrication of Stretchable Strain Sensors based on Silver. 1 (June): 2624–2627, 2013.

[89] V. F. Curto, C. Fay, et al., Real-time sweat pH monitoring based on a wearable chemical barcode micro-fluidic platform incorporating ionic liquids. Sensor. Actuat. B-Chem., 171-172: 1327-1334, 2012.

[90] H. Kudo, T. Sawada, et al., A flexible and wearable glucose sensor based on functional polymers with Soft-MEMS techniques. Biosensors and Bioelectronics, 22 (4): 558-562, 2006.

[91] S. Takamatsu, T. Kobayashi, N. Shibayama, K. Miyake and T. Itoh. Fabric pressure sensor array fabricated with die-coating and weaving techniques. Sensor. Actuat. A-Phys., 184: 57-63, 2012.

[92] Y. Miyoshi, K. Miyajima, ect. Flexible humidity sensor in a sandwich configuration with a hydrophilic porous membrane. Sensor. Actuat. B-Chem., 142 (1): 28-32, 2009.

[93] A. R. Dayal and D. R. Sadedin. Application of Pulsed Traveling Hydrogen Arcs for Metal Oxide Reduction. Plasma Chemistry and Plasma Processing, 23 (4): 627-649, 2003.

[94] S. Ono, S. Teii, Y. Suzuki, T. Suganuma. Effect of gas composition on metal surface cleaning using atmospheric pressure microwave plasma. Thin Solid Films, 518 (3): 981-986, 2009.

[95] M. Ghoranneviss, F. Yaghobian, M. Farbod, M. Eshghabadi. Effects of different substrate materials on synthesis of Cu nanoparticles. Appl. Phys. 9 (1): S124-S127, 2009.

[96] P. K. Khanna, S. Gaikwad, P. V. Adhyapak, N. Singh, R. Marimuthu, Mater. Latt., 61: 4711, 2007.

[97] Y. Sawasa, H. Tamaru, M. Kogoma, M. Kawase, K. Hashimoto. The reduction of copper oxide thin films with hydrogen plasma generated by an atmospheric-pressure glow discharge. J. Phys. D: Appl. Phys., 29 (10): 2539, 1996.

[98] A. Manara, V. Sirtori, L. Mammarella. Optical ellipsometry and electron spectroscopy studies of copper oxidation related to copper on printed circuit boardsSurf. Interface Anal., 18 (1), 32-38: 1992.

[99] K. Takeda, H. Inui, H. Kondo, K. Ishikawa, M. Sekine, M. Hori. Behavior of hydrogen radical on reduction of copper oxide in atmospheric pressure remote plasma using H_2/Ar mixture gases. 30th ICPIG, Belfast, Northern Ireland, UK, August 28th – September 2nd: D14, 2011.

[100] M. Moravej, R. F. Hicks. Atmospheric Plasma Deposition of Coatings Using a Capacitive Discharge Source. Chem. Vap. Deposition, 11: 469-476, 2005.

[101] G. Cicala, G. Bruno, P. Capezzuto. Plasma deposition chemistry of amorphous silicon–carbon alloys from fluorinated gas. Journal of vacuum science & technology A-vacuum surfaces and films, 16: 2762-767, 1998.

[102] G. Bruno, P. Capezzuto, G. Cicala. RF glow discharge of SiF_4-H_2 mixtures: Diagnostics and modeling of the a-Si plasma deposition process. Journal of Applied physics, 69 (10): 7256-7266,

1991.

[103] K. H. A. Bogart, S. K. Ramirez, L. A. Gonzales, G. R. Bogart, and E. R. Fisher. Deposition of SiO_2 films from novel alkoxysilane /O_2 plasmas. Journal of vacuum science & technology A-vacuum surfaces and films, 16: 3175-3184, 1998.

[104] K. M. Byun and W. J. Lee. Deposition characteristics of low dielectric constant Si of films prepared by ECR PECVD. Metals and Materials-Korea, 6 (2): 155-160, 2000.

[105] P. Favia, G. Caporiccio, R. d'Agostino. Plasma deposition of thin films from a fluorine-containing cyclosiloxane. Journal of polymer science part a-polymer chemistry. 32 (1): 121-130, 1994.

[106] T. GÜNGÖR and H. HÜSEYİN. Effects of substrate temperature on properties of a-SiN_x:H films. J. Phys., 26: 269-275, 2002.

[107] O. V. Penkov, M. Khadem, W. S. Lim, D. E. Kim. A review of recent applications of atmospheric pressure plasma jets for materials processing. J. Coat. Technol. Res., 12 (2): 225–235, 2015.

[108] S. X. Ren, L. Z. Tang, Q. Sun, Z. H. Li, H. F. Yang, J. J. Zhao. The structure, oxygen vacancies and magnetic properties of TiO_x ($0 < x < 2$) synthesized by plasma assisted chemical vapor deposition and reduction. Materials Letters, 228: 212–215, 2018.

[109] P. Zhao, W. Zheng, J. Watanabe, Y. D. Meng, N. Masaaki. Highly Conductive Cu Thin Film Deposition on Polyimide by RF-Driven Atmospheric Pressure Plasma Jets under Nitrogen Atmosphere. Plasma Process. Polym., 12: 431–438, 2015.

[110] J. Y. Jeong, S. E. Babayan, et al., Etching materials with an atmospheric-pressure plasma jet. Plasma Sources Sci. Technol. 7 (3): 282-285, 1998.

[111] J. Y. Jeong, S. E. Babayan, et al., Etching polyimide with a nonequilibrium atmospheric-pressure plasma jet. Vacuum. Sci. Technol A. 17 (5): 2581-2585, 1999.

[112] M. Laroussi, T. Akan. Arc-free atmospheric pressure cold plasma jets: A Review. Plasma Process, Polym. 4 (9): 777-788, 2007.

[113] V. J. Tu, J. Y. Jeong, A. Schutze, et al., Tantalum etching with a nonthermal atmospheric-pressure plasma, Vacuum Sci. Technol. A, 18 (6): 2799-2805, 2000.

[114] X. Yang, M. Moravej, et al., Etching of uranium oxide with a non-thermal, atmospheric pressure plasma. J. Nucl. Mater, 324 (2-3): 134-139, 2004.

[115] Y. Kim, J. Park, L. A. Rosocha, H. L. Teslow. Measurements of dioxygen fluoride (O_2F) in an atmospheric pressure plasma jet. Appl. Phys. Lett., 87 (1): 011502, 2005.

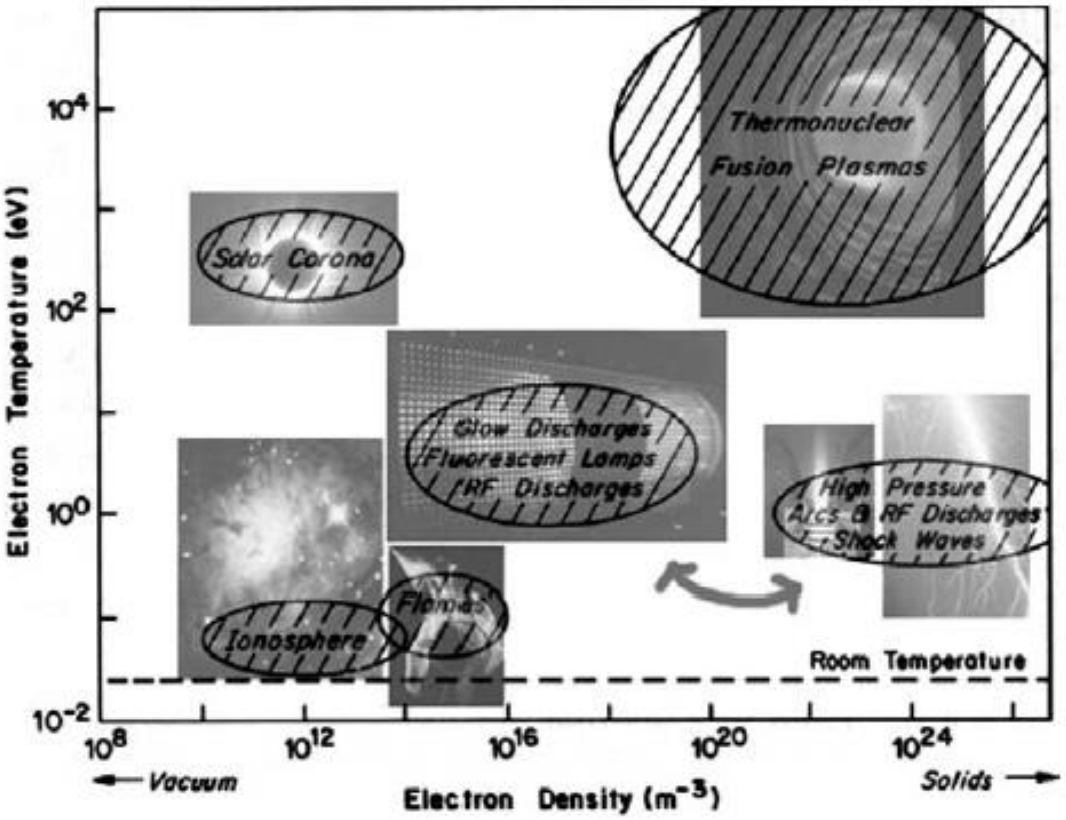

Fig. 1-1 Schematic of plasma classification [4]

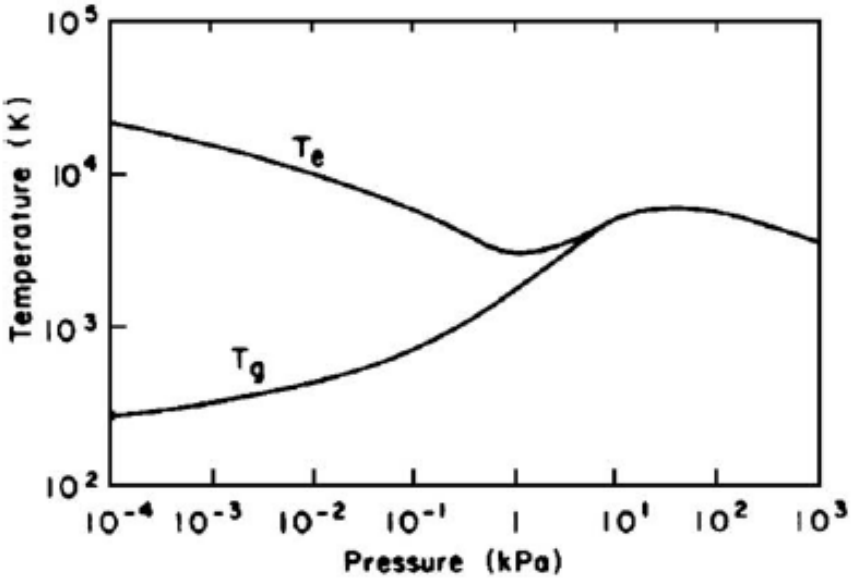

Fig. 1-2 Variation of electron and heavy particle temperature with pressure [7].

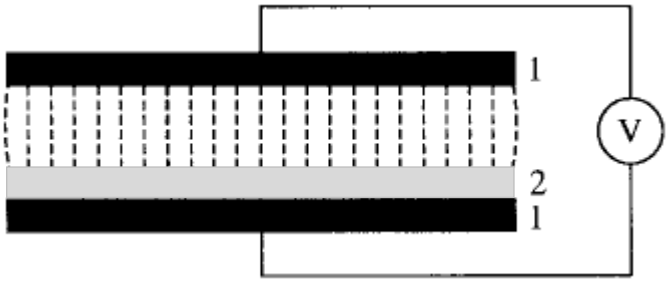

Fig. 1-3 Schematic of a silent discharge: 1) metallic electrodes and 2) dielectric barrier coating [11].

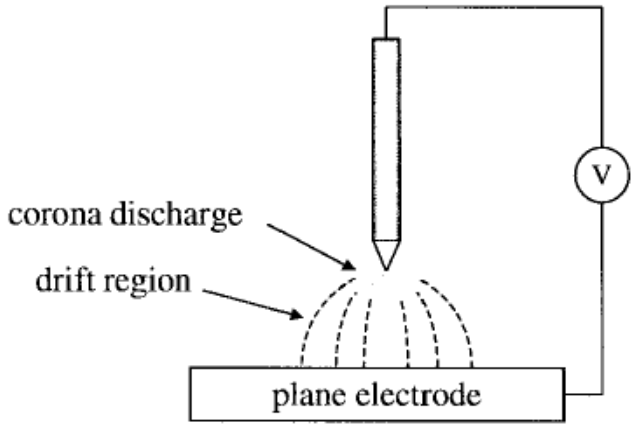

Fig. 1-4 Schematic of a corona discharge [9].

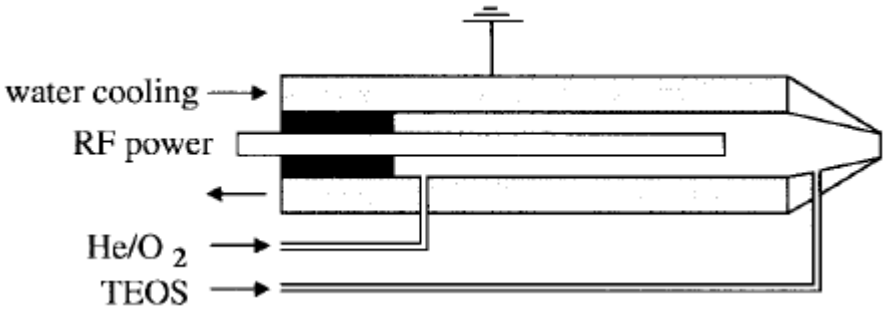

Fig. 1-5 Schematic of the atmospheric-pressure plasma jet for the deposition of silica films [9].

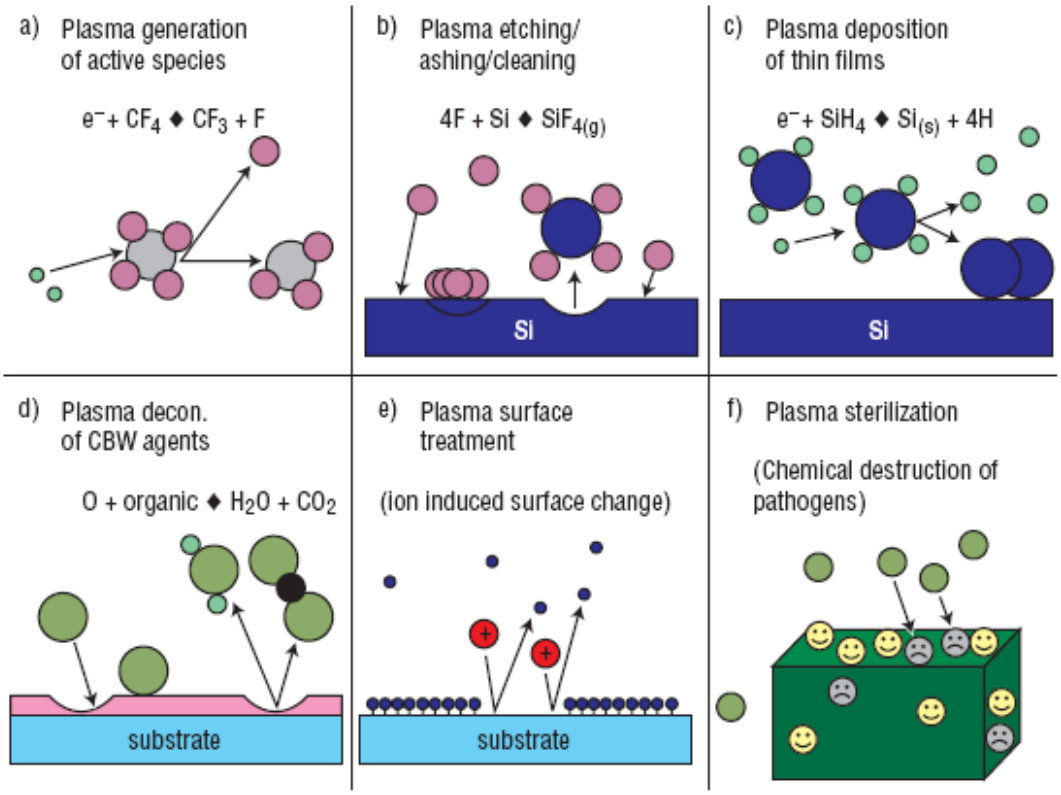

Fig. 1-6 Diagram of the fundamental processes used in plasma processing of materials [13].

Chapter 2 Introduction of hydrophilicity onto oxidized Si wafer surfaces by non-equilibrium atmospheric pressure plasma with Ar and Ar/H_2 as working gas

1 Introduction

Silica (SiO_2) is one of the most common materials on the earth [1, 2]. The applications of SiO_2 in varieties of fields and technologies are still growing. The surface properties of SiO_2 are crucial to many fields including catalysis, optical-fiber communication and microelectronics [3]. Surface processes on silica have been intensively studied. Furthermore, surface hydroxy group is very important that may influence the activity of the silica surface [4]. Hydroxylation of SiO_2 surface is an indispensable for a lot of experiments, such as Si wafer direct bonding [5] and polymerization on silica surface [6, 7].

Recently non-equilibrium atmospheric pressure plasma technology has attracted great attention because of its pollution-free process and simple structure [8]. It demonstrates its unique advantages in various applications such as surface modification, thin film deposition and nanoparticle preparation [9]. It has been pointed out that [5, 10] an O_2 or N_2 plasma activation of the silicon surfaces may essentially increase the number of hydroxy groups.

In this chapter, non-equilibrium atmospheric pressure plasma is used to introduce hydrophilicity on oxidized Si wafer surface. For the plasma generation, Ar and Ar/H_2 were use as the working gas. The samples treated with various periods were analyzed based on the X-ray photoelectron spectroscopy (XPS) and contact angle measurements.

2 Experimental details

2.1 Non-equilibrium atmospheric pressure plasma device

A RF capacitive coupled plasma system called “APC”, which is developed by Cresur Corporation, was used as the plasma generating device [11, 12]. The structural illustration of the plasma torch is shown in Fig.2-1. The APC plasma torch consists of two parallel perforated Al electrodes. The inner electrode is connected to a RF power source with frequency of 27.12 MHz through an impedance matching network, while the outer electrode is grounded. The electrode diameter is 9 mm. The diameter of the perforated holes as the plasma nozzles is 1.2 mm and the distance between them is 1.7 mm. The insulator between the electrodes is made of ceramics and the gap spacing between the two electrodes is 1.5 mm.

The schematic diagram of the experimental setup is shown in Fig. 2-2. In the discharge experiment, Ar gas was the working gas at a flow rate of 20 SLPM (standard liter per minute), RF power was maintained at 100 W without reflection, H_2 as an additive gas was added into the Ar working gas at flow rates of 10 SLPM. All flow rates were controlled by a mass flow controller. The distance between the plasma torch head and sample was 3 mm.

2.2 Sample preparation

In this experiment, Si wafers with a dimension of 10 mm×15 mm×0.8 mm were used. The thermal oxide layer prior to plasma treatment is grown on the wafers in Yamato BW201 muffle furnace at 900℃ for 5 min [13]. For this thermally oxidizing process, temperature was raised up to 600℃ in 20 minutes at first, then raised to 900℃ in 40 minutes. After keeping for 5min, it was cooled to room temperature spontaneously.

In the plasma treatments, the wafers were placed on a X-Y stage, which kept a forth and back movement at a rate of 2.0 mm/s in order to achieve the uniformity of the surface treatment.

2.3 Surface characterization.

XPS (X-ray photoelectron spectroscopy) measurements were performed to analyze the surface composition of SiO_2 film with Perkin Elmer ESCA 5600. Mg Kα radiation was employed as an X-ray source (15KV, 400W), and the photoelectron were collected at a takeoff angle 45°. The base pressure of system was below 10^{-7} Torr.

The hydrophilicity of the surface was evaluated in terms of the contact angle of water by aCA-D contact-angle meter, Kyowa Kaimenkagaku Co., LTD., with deionized water. For each sample, measurements were performed at 3 different points. The value of the contact angle was obtained by averaging the results at these 3 points.

3 Results and discussion

3.1 XPS analysis of oxidized Si wafer surfaces

3.1.1 XPS analysis of oxidized Si wafer

Fig.2-3 shows Si 2p spectra of untreated Si wafer and thermally oxidized Si wafer. For the untreated wafer, two peaks indicate the elemental Si peak and the SiO_{2-x} peak which is chemically shifted to higher bind energies. For the heat-treated wafer, a chemical shift of about 4.3 eV is observed. It indicates that after thermally oxidizing, SiO_2 film has covered Si wafer surface [14].

3.1.2 XPS analysis of oxidized Si wafer after plasma treatment

Fig. 2-4 shows XPS survey spectra of thermally oxidized Si wafers without plasma treatment and Ar plasma-treated with different treatment periods. Surface atomic concentration of Si wafer was calculated through the peak area and the sensitivity factor of ESCA system, with results listed in Table 2-1. From Table 2-1, we can see that hydrocarbons or other carbonaceous contaminate can be removed by plasma treatment. Widely known that plasma is very useful to clean material surface.

Fig. 2-5 shows elemental Si 2p peak of the samples thermally oxidized and Ar plasma-treated with different treatment periods. There is no obvious chemical shift observed. The broad O1s of the sample treated by Ar plasma at ambient temperature for 10 minutes in air has been deconvoluted in Fig. 2-6 (b), while the O1s deconvolution of the thermally oxidized sample at 900℃ for 5minutes is shown in Fig. 2-6 (a) as reference. In Fig. 2-6, two component peaks are resolved for O1s peak. The main peak at 532.5±0.5eV is due to SiO_2, while the shoulder peak is attributed to Si–OH (533.8eV) [15]. The concentration of Si-OH is estimated by relative peak areas as percentage of the total area of O1s peak. The analytical results are shown in Fig.2-7 (more details can be found in Table 2-2). Si-OH contents of the samples treated by Ar plasma for 1, 5, and 20 minutes were also estimated in the same way. Compared with the thermally oxidized wafer, the Ar plasma-treated samples have a little higher concentrations of hydroxy group on their surfaces. However, with increasing plasma treatment period, any more increase in concentration of hydroxy group was not ovserved.

The similar results can also be found for the samples treated by Ar/H_2 plasma. Fig. 2-8 shows the O1s peak of thermally oxidized wafer treated by Ar/H_2 plasma at ambient temperature for 10 minutes in air. The O1s spectrum has been deconvoluted as shown in Fig. 2-9, and the

concentration of Si-OH is shown in Fig. 2-10. The XPS analysis indicates the concentration of Si-OH on wafers' surface increases to about 2 times of the values of untreated wafer in 10 minutes treatment and then seems to be saturated.

3.2 Contact angle of water on oxidized Si wafer surfaces

The contact angle can give the information about the macroscopic surface wettability. Fig.2-11 and 2-12 show the change in contact angles of water on the Ar plasma-treated sample and Ar/H_2 plasma-treated sample, respectively. For contact angles evaluation, plasma treatment has more obvious effects than for the results obtained by XPS analysis. It can be seen that contact angles of water on plasma-treated samples decrease dramatically in 10 minutes from 59° to 20°. But with increased plasma treatment period, there is no further obvious decrease in contact angle. The hydroxylation process may be completed within a short period of time during the plasma treatment,.

It is known when water molecule interacts with silica surface water can dissociate and break Si-O forming Si-OH. But many researches show that [5, 16] the reaction enthalpy for a water molecule to be joined to the silica surface is about 4.3 $kcal \cdot mol^{-1}$, which is not sufficient for the disintegration of a water molecule. Hydroxy radical and/or hydrogen radical need to be added for the formation of silanol functional group.

In the previous studies of our lab [12], the emission lines in Ar/H_2 plasma generated by APC plasma torch were observed as listed in Table 2-5 and Fig. 2-13. The emissions were mainly assigned to excited Ar, while the emissions due to H atoms (434.0 nm [19], 486.1 nm, 656.3 nm [20]) were not obvious. The H atoms are considered to be resulted from the dissociation of H_2 by the following reaction [20]:

$$Ar^m + H_2 \rightarrow Ar + H_2^* \rightarrow Ar + H + H \quad (K \sim 10^{-10}\ cm^3 s^{-1})$$

$$Ar^+ + H_2 \rightarrow ArH^+ + H \quad (K \sim 10^{-9}\ cm^3 s^{-1})$$

It is also found that the emission lines located at 308.9 nm and 336 nm are identified as OH and NH emission, respectively [19]. It is assumed that the OH and NH groups were the products of the reaction of H_2, O_2 and N_2 in the impurity of Ar or air [21]. As a result, in Ar plasma process, it seems that the Si-O bond is cleaved by the energy transfer from the metastable argon atom (Ar^m), and the hydroxy group is formed by contact with the atmosphere after plasma irradiation. In Ar/H_2 plasma, H atoms are considered to act in addition to Ar^m. However, the extent of introduction of hydrophilicity into the silicon oxide surface by Ar plasma and Ar/H_2 plasma was not so high. It was considered that the Si-O bond cleaved by the interaction with Ar^m was promptly recombined.

4 Conclusions

In this study, the non-equilibrium atmospheric pressure plasma was used to introduce hydrophilicity on thermally oxidized Si wafer surfaces. The results of XPS analysis and contact angle measurement showed that hydrophilicity can be introduced to the surface of oxidized Si wafer by irradiation with non-equilibrium atmospheric pressure plasma. In the irradiation with Ar plasma, it seems that the Si-O bond is cleaved by the energy transfer from the metastable argon atom (Ar^m), and hydroxy group is formed by contact with the atmosphere after plasma irradiation. In irradiation with Ar/H_2 plasma, H atoms are considered to act in addition to Ar^m. the extent of introduction of hydrophilicity into the silicon oxide surface by Ar plasma and Ar/H_2 plasma was not so high. It was considered that the Si-O bond cleaved by the interaction with Ar^m was promptly recombined.

References

[1] O. Sneh and S. M. George. Thermal stability of hydroxyl groups on a well-defined silica surface. J. Phys. Chem., 99: 4639-4647, 2005.

[2] D. B. Asay and S. H. Kim. Evolution of the Adsorbed Water Layer Structure on Silicon Oxide at Room Temperature. J. Phys. Chem. B, 109: 16760-16763, 2005

[3] O. Sneh, M. A. Cameron, S. M. George. Adsorption and desorption kinetics of H2O on a fully hydroxylated SiO_2 surface. Surface Science, 364: 61-78, 1996.

[4] J. Y. Yang. Study on the behavior of water adsorbed on the SiO_2 surface by using first principles density functional theory (in Chinese). Beijing: Chinese Academy of Sciences' Institute of Physics, 2005.

[5] O. Lichtenberger，J. Woltersdorf. On the atomic mechanisms of water-enhanced silicon wafer direct bonding. Materials Chemistry and Physics, 44: 222-232, 1996.

[6] J. F. Zhang, C. Q. Cui and T. B. Lim. Chemical modification of silicon (100) surface via UV-induced graft polymerization. Chem. Master, 11: 1061-1068, 1999.

[7] G. L. Zhong, M. Mizukami, I. Fukuchi, T. Miyahara and K. Kurihara. Preparation of Nano-films by in situ polymerization of hydrogen-boned macroclusters of N-isopropylacrylamide on silica surface. Chemistry Letters, 24 (2): 228-229, 2005.

[8] G. L. Zhang, K. Hosoi, S. Kuroda. Reduction and Sintering of Copper Nano-Particles by Non-Equilibrium Atmospheric Pressure Plasma Jet. Advanced Science Letters, 19(2): 519-523, 2013.

[9] H. M. Chang, Y. J. Yang, H. C. Li, C. C. Hsu, I. C. Cheng, J. Z. Chen. Preparation of nanoporous TiO_2 films for DSSC application by a rapid atmospheric pressure plasma jet sintering process. Journal of power sources. 234:16-22, 2013

[10] G. L. Sun, J. Zhan, Q.-Y. Tong, S. J. Xie, Y. M. Cai and S. J. Lu. Cool plasma activated surface in silicon wafer direct bonding technology. J. Phys. (Paris), Colloq. C. 49: 79-82, 1988.

[11] X. Fei, S. Kuroda, Y. Kondo, T. Mori, K. Hosoi, J. Mat. Life Soc, 2010.

[12] G. L. Zhang. Reduction and sintering of copper nano-particles by non-equilibrium atmospheric pressure plasma jet. Kiryu: Gunma University, 2012.

[13] P. V. Zant (Writer). Z. S. Han (translator). Microchip fabrication-A practical guide to semiconductor processing, 5th edition. 2010

[14] C. D. Wanger, W. M. Riggs, L. E. Davis, J. F. Moulder and G. E.Muilenberg. Handbook of X-ray photoelectron spectroscopy. Perkin-Elmer Corp., Physical Electronics Division, Eden Prairie, USA, 1979.

[15] J. Viard, E. Beche, D. Perarnau, R. Berjoan and J. Durand. XPS and FTIR study of silicon oxynitride thin films. Journal of the European ceramic society: 17: 2025-2028, 1997.

[16] G.M. Rignanese, J.C. Charlier and X. Gonze. First-principles molecular-dynamics investigation of the hydration mechanisms of the (0001) α-quartz surface. Phys. Chem. Chem. Phys., 6: 1920 – 1925, 2004.

[17] D. Ceresoli. M. Bernasconi, Iarlori, M. Parrinello, and E. Tosatti. Two-Membered Silicon Rings on the Dehydroxylated Surface of Silica. Phys. Rev. Lett., 84 (17): 3887-3890, 2000.

[18] M.H. Du, A. Kolchin, and H.P Cheng. Water-silica surface interactions-A combined quantum-classical molecular. Journal of chemical physics, 119 (13) 6418-6422: 2003.

[19] Q. S. Yu, H, K, Yasuda, An optical emission study on expanding low-temperature cascade arc plasmas. Plasma Chem. Plasma P. 18(4): 461-485, 1998.

[20] B. K. Pawlak, P. Jamroz. An analysis of low frequency discharge in a CH_3SiCl_3-Ar-H_2 mixture

by optical emission spectroscopy and actinometry. Plasma Chem. Plasma P. 30 (5): 641-661. 2010.

[21] M. C. García, M. Varo, P. Martínez. Excitation of Species in an Expanded Argon Microwave Plasma at Atmospheric Pressure. Plasma Chem. Plasma P. 30 (2) -255, 2010: 241.

Tab. 2-1 Surface atomic concentration of thermally oxidized Si wafer after Ar plasma treating for 1 min, 5 min, 10 min and 20 min

Concentration（%）	**Untreated**	**Ar 1min**	**Ar 5min**	**Ar 10min**	**Ar 20min**
O 1s	57.71	62.99	64.11	63.49	62.65
Si 2p	30.55	30.81	31.33	31.64	31.13
C 1s	10.90	6.20	4.56	4.87	6.22

Tab. 2-2 Change in surface chemical components of thermally oxidized Si wafer and thermally oxidized Si wafer treated by Ar plasma for 1 min, 5 min, 10 min and 20 min

	Untreated	**Ar 1min**	Ar **5min**	Ar **10min**	Ar **20min**
Si-O-Si	97.77%	95.16%	95.09%	95.40%	95.24%
Si-OH	2.23%	4.84%	4.91%	4.60%	4.76%
(Si-OH) / (Si-O-Si)	0.02	0.05	0.05	0.05	0.05

Tab. 2-3 Surface atomic concentration of thermally oxidized Si wafer after Ar/H_2 plasma treatment for 1 minute, 5 minutes, 10 minutes and 20 minutes

Concentration (%)	**Untreated**	**Ar/H_2 1min**	**Ar/H_2 5min**	**$Ar//H_2$ 10min**	**Ar/H_2 20min**
O 1s	57.71	62.10	63.65	63.15	63.72
Si 2p	30.55	32.81	32.91	30.55	2.45
C 1s	10.90	5.09	3.43	6.31	3.83

Tab. 2-4 Change in surface chemical components of thermally oxidized Si wafer and thermally oxidized Si wafer treated by Ar/H_2 plasma for 1 min, 5 min, 10 min and 20 min

	Untreated	**Ar/H_2 1min**	**Ar/H_2 5min**	**Ar/H_2 10min**	**Ar/H_2 20min**
Si-O-Si	97.77%	96.80%	94.76%	95.34%	95.29%
Si-OH	2.23%	3.20%	5.24%	4.66%	4.71%
(Si-OH) / (Si-O-Si)	0.02	0.03	0.06	0.05	0.05

Tab. 2-5 Most emission lines observed in Ar/H_2 plasma generated by APC plasma torch at the position of 3 mm down from the plasma torch head and 2 mm side from plasma jet end. The integration time was 100 ns [19-21]

Species	Wavelength (nm)	Transition	Threshold energy (eV)
OH	308.9	$A^2\Sigma^+ \rightarrow X^2\Pi$	-
NH	336	$A^3\Pi \rightarrow X^3\Sigma^-$	**3.7**
Ar	696.5	$2p_2$–$1s_5$	**13.32**
	706.7	$2p_3$–$1s_5$	**13.29**
	714.7	$2p_4$–$1s_5$	**13.28**
	728	$2p_2$–$1s_4$	**13.33**
	738.4	$2p_3$–$1s_4$	**13.3**
	751.4	$2p_5$–$1s_4$	**13.27**
	763.5	4p-4s	**13.17**
	772.4	4p-4s	**13.33**
	794.8	4p-4s	**13.28**
	801.5	4p-4s	**13.15**
	811.5	4p-4s	**13.08**

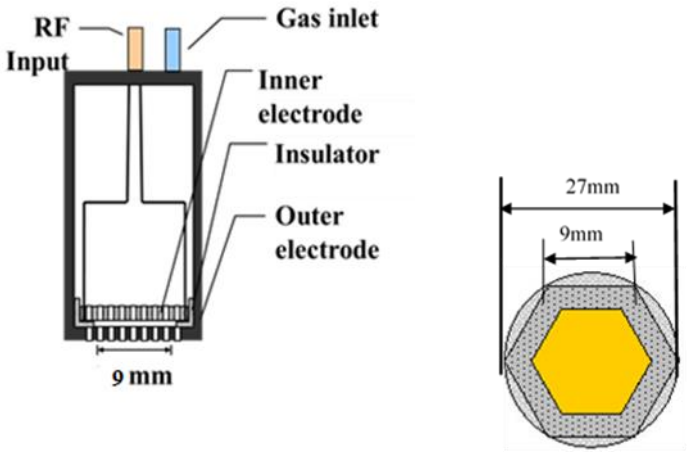

Fig.2-1 Schematic diagram of APC plasma torch.

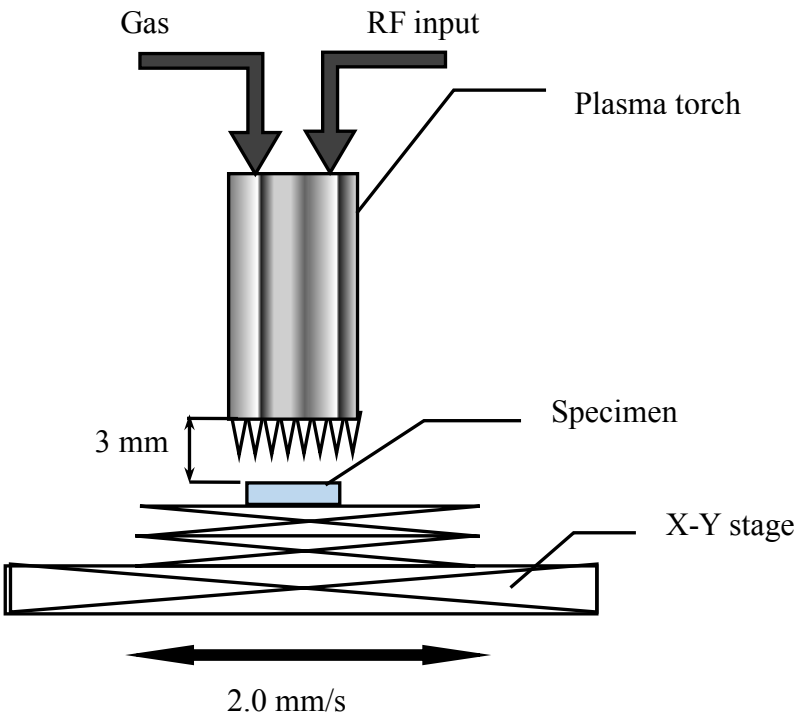

Fig. 2-2 Schematic diagram of the experimental setups for the plasma-treatment of samples

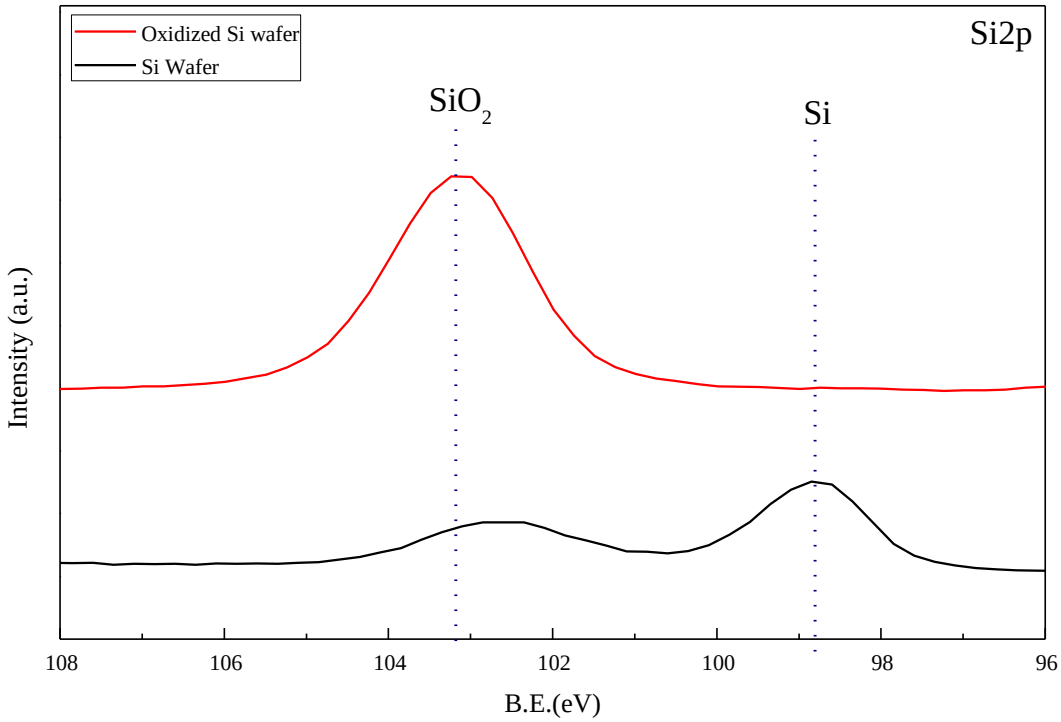

Fig.2-3 Si 2p spectra for Si wafer and thermally oxidized Si wafer at 900℃.

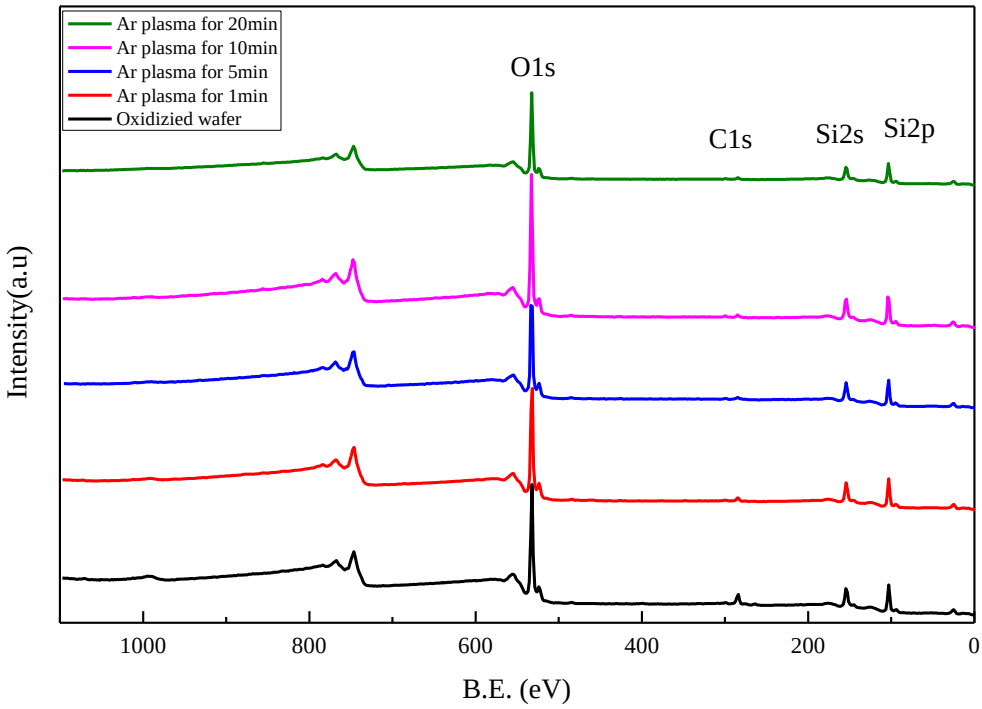

Fig.2-4 Survey spectra for oxidized Si wafers: thermally oxidized at 900℃ for 5 min; Ar plasma treatment for 1 min, 5 min, 10 min, 20 min

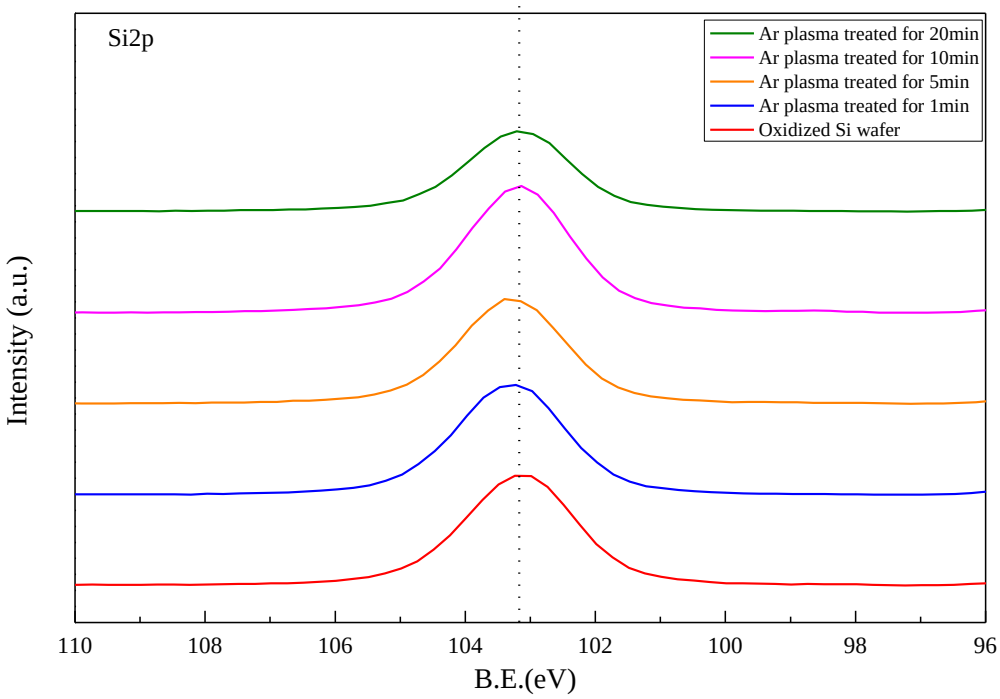

Fig.2-5 Si 2p spectra for oxidized Si wafers: thermally oxidized at 900℃ for 5 min and Ar plasma treatment for 1 min, 5 min, 10 min, 20 min

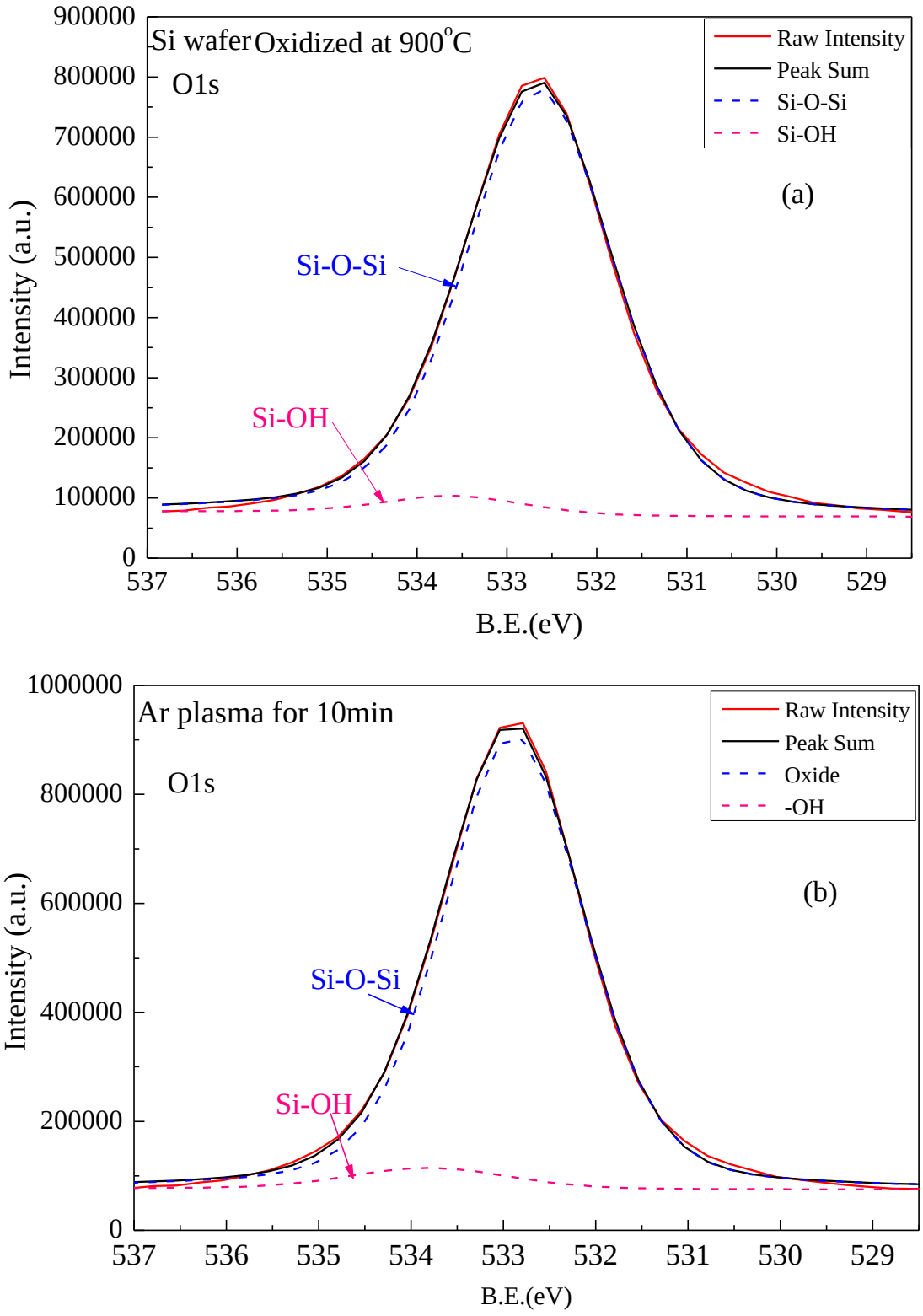

Fig.2-6 (a) XPS spectrum of O1s peak fitting for Si wafers thermally oxidized at 900℃ for 5 min;

(b) XPS spectrum of O1s peak fitting for sample treated by Ar plasma for 10 min;

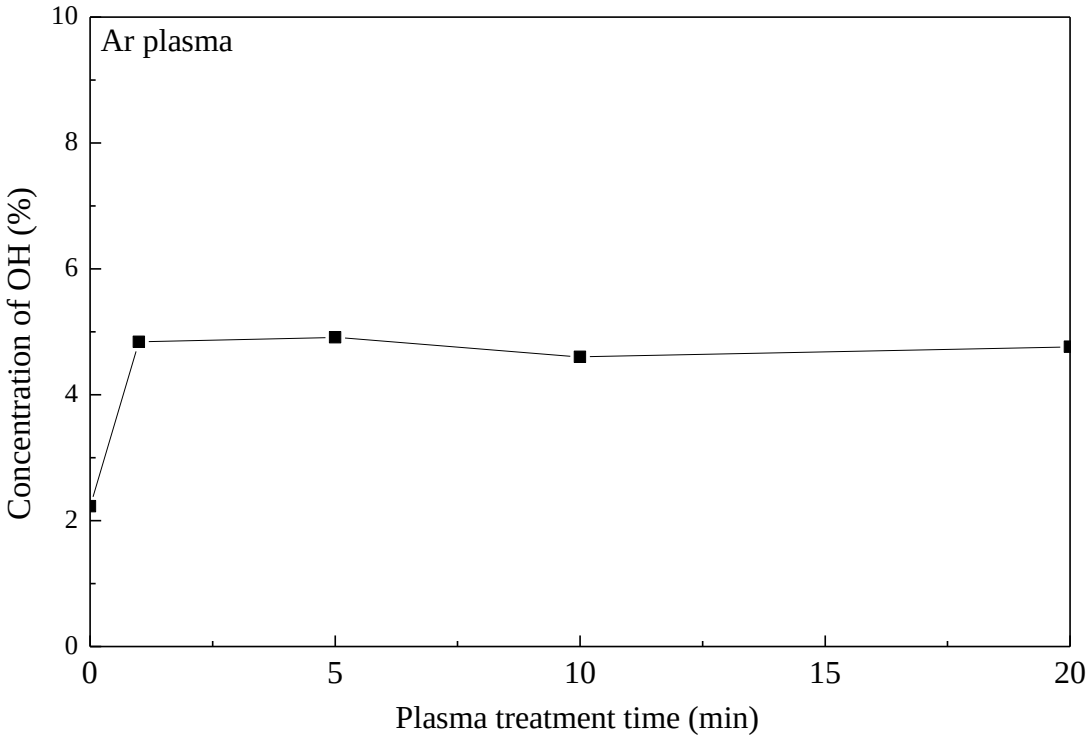

Fig.2-7 Concentration of OH on thermally oxidized Si wafer surface which were treated by Ar plasma under different treating time

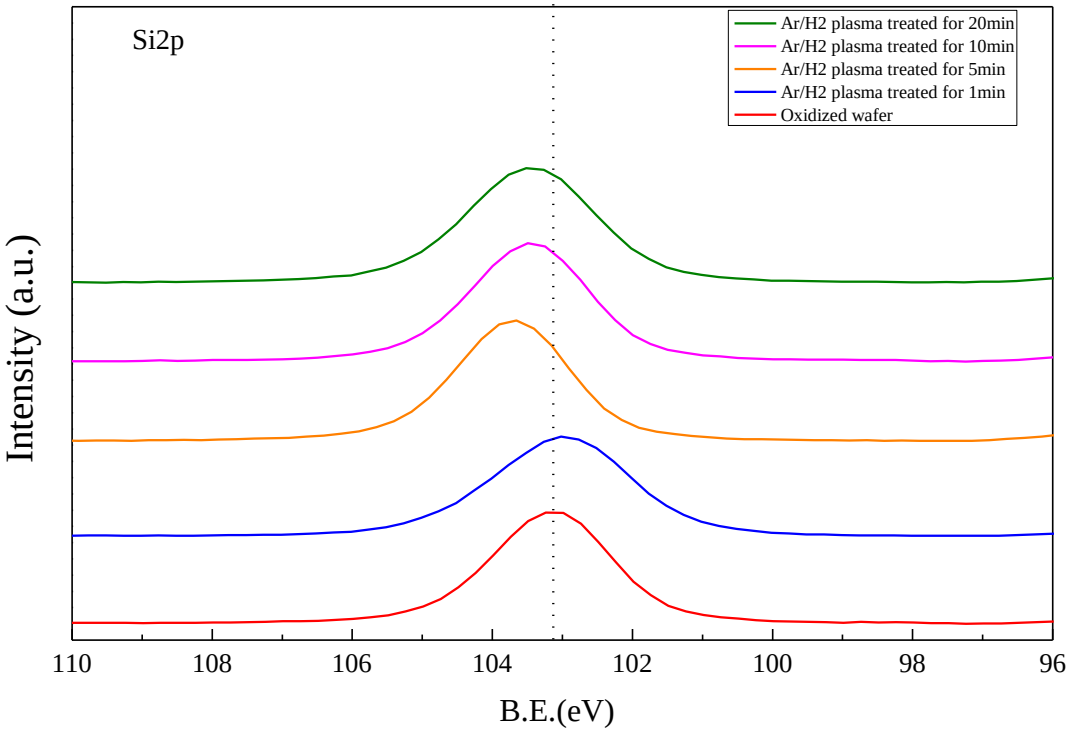

Fig.2-8 Si 2p spectra for samples: thermally oxidized at 900℃ for 5 min and Ar/H_2 plasma treatment for 1 min, 5 min, 10 min, 20 min

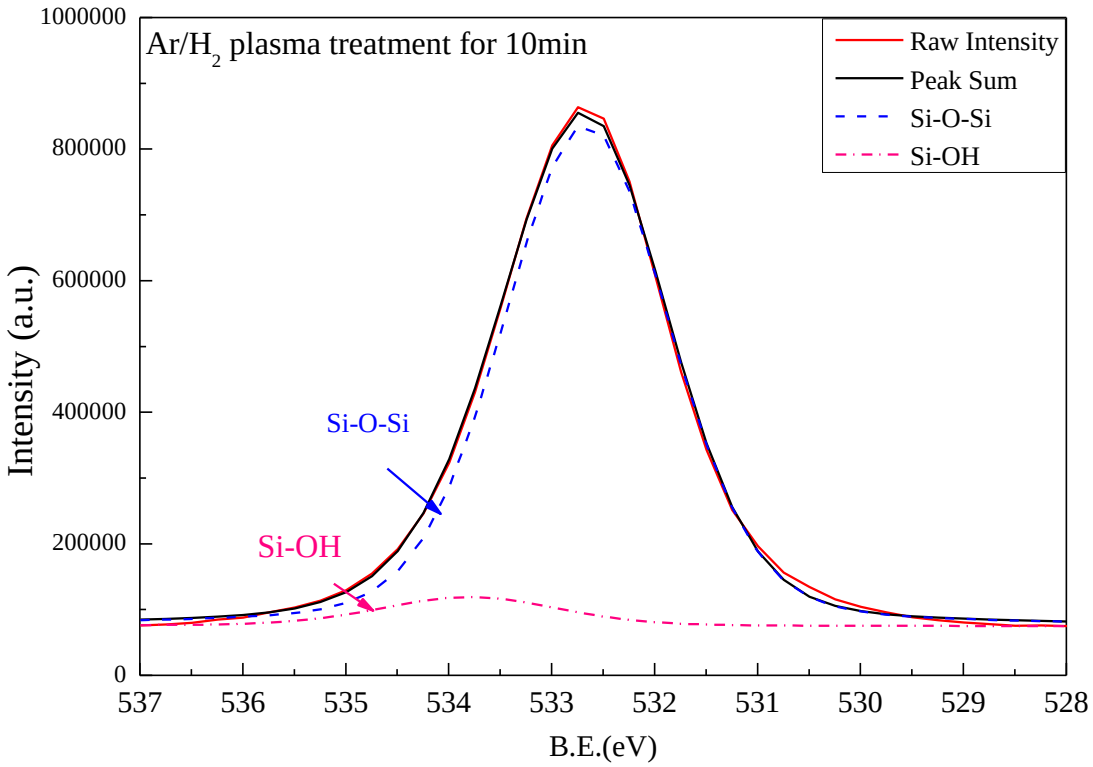

Fig.2-9 XPS spectrum of O1s peak fitting for thermally oxidized Si wafer treated by Ar/H_2 plasma for 10 minutes;

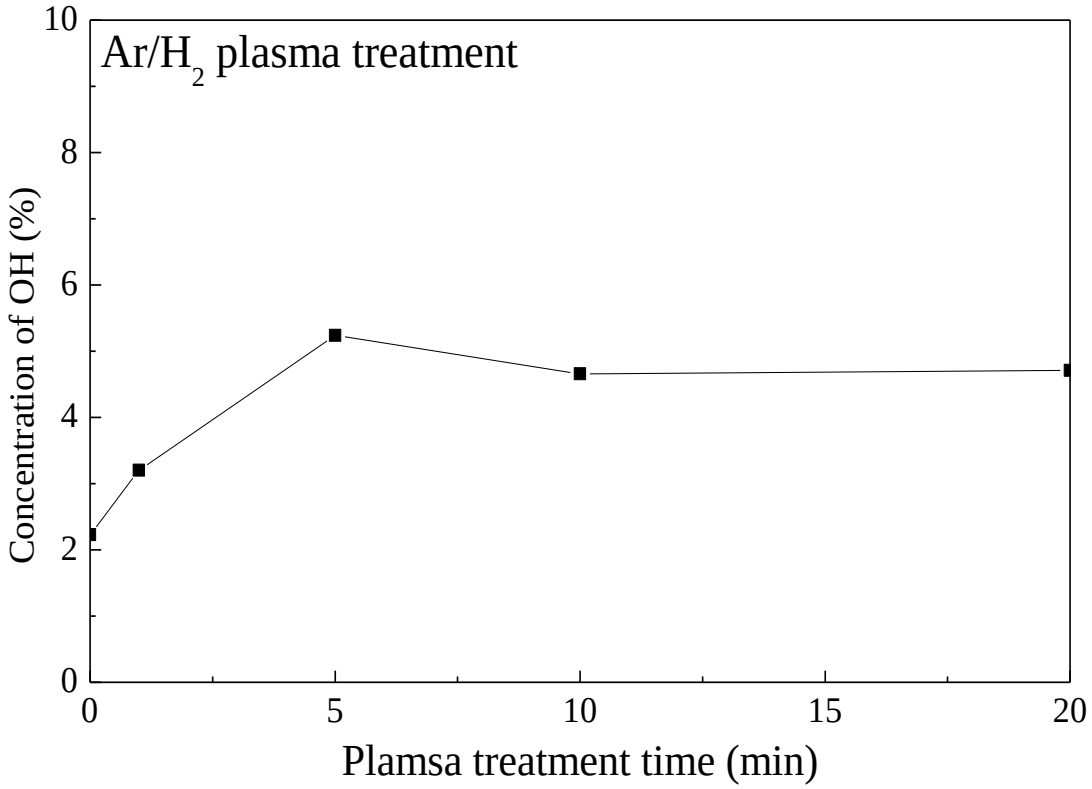

Fig.2-10 Concentration of OH on thermally oxidized Si wafer surface which were treated by Ar/H_2 plasma under different treating time

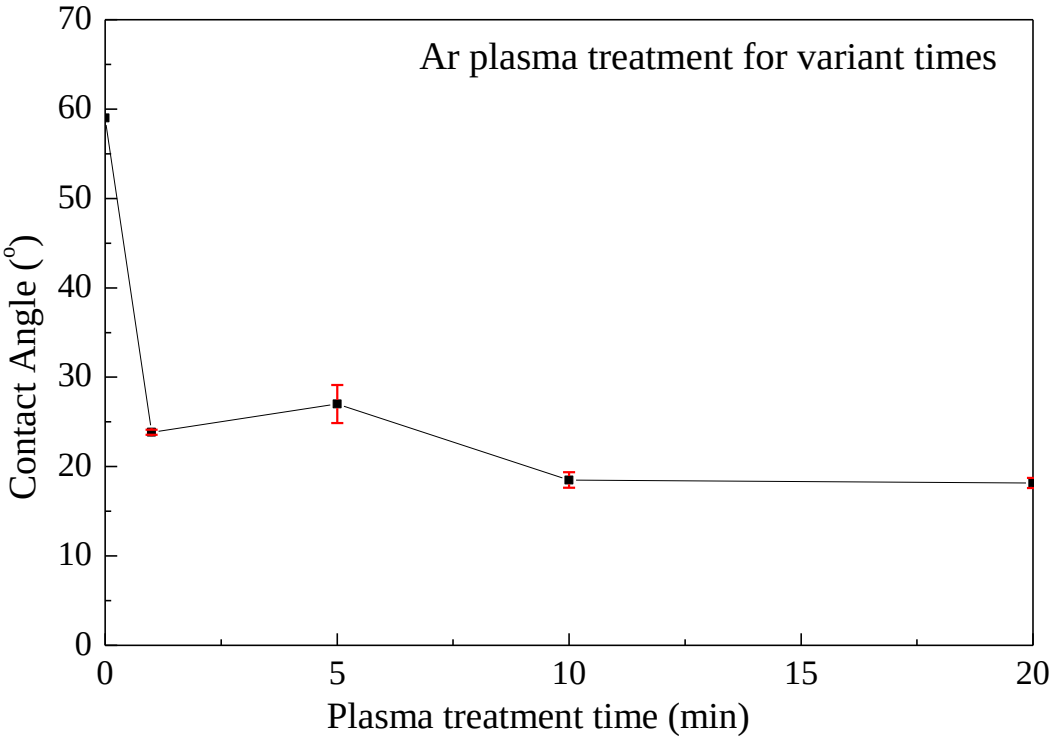

Fig.2-11 Contact angles of thermally oxidized Si wafer treated by Ar plasma for 1 min, 5 min, 10 min and 20 min

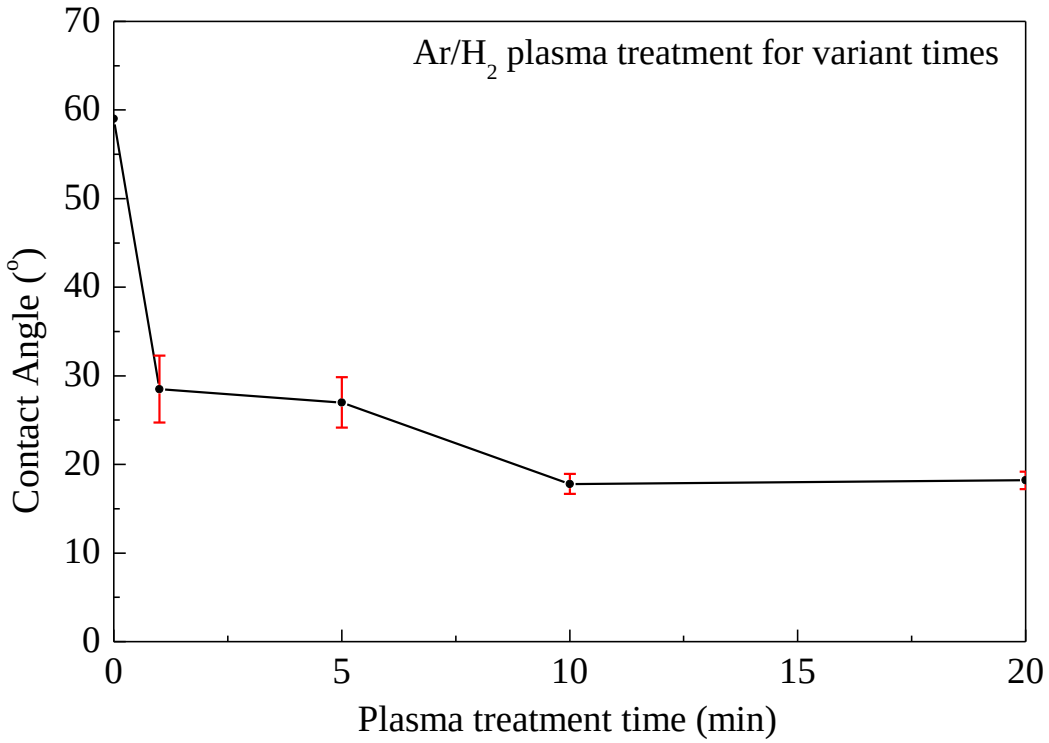

Fig.2-12 Contact angles of thermally oxidized Si wafers treated by Ar/H_2 plasma for 1min, 5min, 10min and 20min

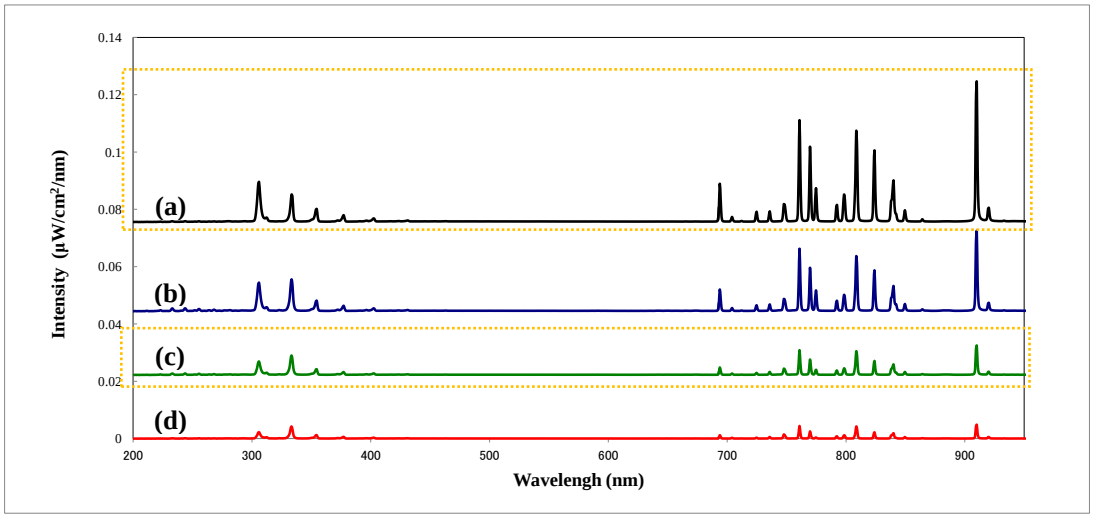

Fig. 2-13 Optical emission spectra from the Ar/H_2 plasma jet with different flow rate of H_2: (a) Ar flow rate =20 L/min without H_2 gas, (b) Ar flow rate =20 L/min and H_2 flow rate =5 mL/min, (c) Ar flow rate =20 L/min and H_2 flow rate=10 mL/min, (d) Ar flow rate =20 L/min and H_2 flow rate=15 mL/min [12]

Chapter 3 Introduction of hydrophilicity onto oxidized Si wafer surfaces by non-equilibrium atmospheric pressure plasma with addition of water vapor

1 Introduction

In chapter 2, we used an APC plasma torch. At ambient condition, Ar and Ar/H_2 plasma jet resulted in the inducing hydrophilicity to surface of oxidized Si wafers. In order to get an obvious result on hydrophilicity introduced by plasma at ambient temperature, more active groups such as OH are desired.

In this chapter, non-equilibrium atmospheric pressure plasma with water vapor is used to introduce hydrophilicity effect on oxidized Si wafer surface. Argon gas is used as working gas and water vapor is also added by bubbling system during plasma discharge.

As we know, surface processes on silica have been intensively studied, with considerable experimental results and conclusions. This is because the high degree of inconsistency between various silica surfaces is attributed to the difference in preparation method [1, 2]. In order to check plasma's applicability, quartz glass irradiated by plasma with water vapor was also studied. The oxidized Si wafers and quartz glass treated under various time were analyzed by X-ray photoelectron spectroscopy (XPS) and contact angle respectively.

Dehydroxylation is also one of the most studied reactions on silica surfaces. Dehydroxylation is important because the reactivity of silica surfaces changes dramatically between the dehydroxylated siloxane phase (Si-O-Si) and the hydrated silanol (Si-OH) surface [2, 3]. The siloxane surface is very inert, but the silanol surface with hydroxy functional groups has high chemical reactivity [4.5].

Therefore, in this chapter, the stability of hydroxy group of wafers and quartz glass treated by Ar plasma with bubbling system is investigated experimentally. In the end, the hydrophilicity effects introduced by difference plasma method shown in chapter 2 and 3 are compared and summarized.

2 Experimental details

2.1 Structure of bubbling system

The schematic diagram of the experimental setups for the plasma-treatment is shown in Fig. 3-1. And the bubbling container is illustrated in Fig.3-2. Deionized water was used for bubbling. The argon gas is introduced from inlet with flow rate of 1 L/min. And the outlet is contact with distributor. This container is put in water bath. Before plasma treatment, we need to decide the optimum temperature of water bath. We put deionized water (about 600mL) in the bottle and record its weight, then heat the bottle by water bath. When the temperature reaches 40℃, 50℃, 60℃, 70℃, 80℃, we check the weight of deionized water again and calculate the loss of water. Considering the lab safety, we cannot set the temperature of water bath too high. The result was shown in Fig.3-3. It can be seen that at 80□, loss of water increased dramatically to reach its maximum. Therefore 80□ was chosen as the experiment temperature.

2.2 Sample preparation

In this experiment, Si wafers with a dimension of 10 mm×15 mm×0.8 mm are used. The thermal oxide layer prior to plasma treatment is grown on samples in Yamato BW201 muffle furnace at 900℃ for 5 minutes. Silica glass (by TGK CO., LTD) cut into 15 mm×15 mm×0.5 mm is used for comparison.

In the discharge experiment, Ar gas was the working gas, at a flow rate of 20 L/min, and RF powers were maintained at 100 W without reflection. Water vapor was added by Ar gas which was introduced through tubes below plasma torch at a flow rate of 1 L/min. And the flow rates were controlled by a mass flow controller. The distance between the plasma torch head and sample was 3 mm.

2.3 Surface characterization

XPS (X-ray photoelectron spectroscopy) measurements are conducted to analyze the surface composition of SiO_2 film with Perkin Elmer ESCA 5600. Mg Kα radiation is employed as an X-ray source (15 KV, 400 W), and the photoelectron are collected at a takeoff angle 45°. The base pressure of system is below 10^{-7} Torr.

The hydrophilicity of the surface is evaluated with contact angle measurement, by CA-D contact-angle meter with deionized water. For each sample, measurements were performed at 3 different points. The final value of the contact angle was obtained by averaging the results at these 3 points.

2.4 Analysis of surface hydroxy group by derivatization XPS

A lot of oxide surfaces are with hydroxy group which can play an important role [6]. As we discussed above, the concentration of hydroxy group has a great effect on thermally oxidized Si wafer surface, thereby affecting all the devices made of SiO_2. Therefore, the measurement for hydroxy group of oxide surfaces has a practical significance. Some methods have been examined in estimating the surface hydroxy groups [7]. It has been reported [8] that $LiAlH_4$- GC was used to analyze the hydroxy group content of organosilane. Later this method was certified to measure the

surface hydroxy group of silica which is used as filler in rubber [9]. Morimoto et al. [10-12] have studied the metal oxide surface by measuring the water content by means of the successive-ignition-loss method. On the other hand, Fripiat et al. [13] adopted Zerewitinoff's method to determine active hydrogen in the analysis of the water content on silica gel.

In last chapter, hydrophilicity was characterized by XPS and contact angle. From the results of hydrophilicity of thermally oxidized Si wafer, we can see that contact angle shows an obvious improvement on wettability. But this is only a qualitative analysis. XPS can be used as a quantitative analysis to give us a quantization information on hydroxy group content of oxide surface. But XPS generally shows little or no significant binding energy shift between oxide and hydroxide species. Therefore, the hydroxide present on the oxide matrix is not easily identified by XPS [14, 15]. Moreover, we know water can adsorb onto a hydrophilic silicon oxide surface at room temperature [16], and the bond energy of O1s for adsorbed H_2O is close to Si-O-Si at about 532.5 eV in XPS analysis. Water maybe disturb us to check the evidence of Si-OH existence. The XPS analysis of hydroxide species can be significantly enhanced when used in conjunction with chemical labeling. So derivatization of Si-OH is carried out.

For labeling method, a reagent containing a tag element (not part of the surface studied) is used to selectively react with the -OH group and the tag element is subsequently analyzed using XPS. But this method must meet two criteria. First, the extraction procedure employed has to remove all the unreacted and adsorbed reagent. A sample containing no hydroxide must be subjected to the same derivatization and extraction procedure to meet the first requirement. Second, the derivatization must be completed in the XPS sampling depth region. In the case of functional groups other than OH, evidence for this is generally achieved by comparing the concentration of the tag

element in the derivatized sample and the concentration of the functional group determined by XPS. If an appropriate stoichiometric ratio is obtained, the derivatization is completed in the XPS sampling region [17].

In this part, labeling method for silanol analysis by derivatization XPS was used. This method is to use tridecafluoro-1, 1, 2, 2-tetrahydrooctyl dimethyl-chlorosilane, FOCS for short, as the derivatization reagent. We will apply this method to quantify the Si-OH on the surface of thermally oxidized Si wafer.

2.4.1 Derivatization reaction

In this experiment, Si wafers treated by thermally oxidized in muffle furnace at 900℃ for 5 minutes were used. FOCS (made by Gelest, the structure was shown in Fig. 3-4) was used as the derivatization agent, and chloroform (made by Wako) as the dilution solvent.

For derivatization treatment, FOCS: chlorlform =1:100 (volume ratio) solution was prepared. Thermally oxidized Si wafers before and after plasma treatment were soaked into derivatization solution for 1 hour at room temperature. Then we rinse the samples by chloroform in ultraphonic cleaning machine for 1 hour. After cleaning, the samples were dried under low pressure (10^{-5} Torr) for 12 hours [18, 19].

2.4.2 XPS measurements

XPS measurements are conducted to analyze the derivated SiO_2 layer of thermally oxidized Si wafer surface by using Perkin Elmer ESCA 5600. Mg Kα radiation is employed as an X-ray source (15 KV, 400 W), and the base pressure was below 10^{-9} Torr. Integrated peak areas and atomic sensitivities provided by Physical Electronics were used for determination of atomic composition.

In order to better study derivatization on SiO_2 surface, the photoelectrons are collected at a takeoff angle of 15°, 45° and 75°.

3 Results and discussion

3.1 Results of oxidized Si wafer surfaces

3.1.1 XPS analysis of oxidized Si wafer

The broad O1s of the samples treated by Ar plasma with bubbling system at ambient temperature for 10 minutes in air have been deconvoluted, as can be seen in Fig. 3-5 (O1s deconvolution of the thermally oxidized sample as reference was shown in chapter 2, Fig. 2-5 (a)). In Fig. 3-5, two component peaks are resolved for O1s peak. The main peak at 532.5±0.5 eV indicates that SiO_2 with shoulder peak attribute to Si–OH (533.8 eV) [20]. The concentration of Si-OH is estimated by relative peak areas as percentage of the total area of the O1s peak. The analytical results are shown in Fig.3-6 (More details can be obtained from Tab. 3-1). Si-OH contents of samples treated by Ar plasma with bubbling system for 1, 5, and 20 minutes were also estimated in the same way. Compared with thermally oxidized wafer, the increase of Si-OH on Ar/H_2O plasma-treated samples' surface is about 3%. As plasma treating time increases, there is a small increasing trend in the concentration of hydroxy group.

3.1.2 Contact angle of water on oxidized Si wafer surfaces

Contact angle can give information about the macroscopic surface wettability. Fig.3-7 illustrates the contact angles of thermally oxidized Si wafers treated by Ar/H_2O plasma. For contact angles evaluation, plasma treatment has a more significant effect than those characterized by XPS analysis.

It can be seen that the contact angles of plasma-treated samples decrease dramatically: it can drop down to below 10°. But with increased plasma treating time, there is not an obvious decrease in contact angles. This means that under plasma treatment, this hydroxylated process may be completed within a short period of time, about 1 min.

3.1.3 Analysis of surface hydroxy group by derivatization XPS

In this experiment, the OH group can be labeled through Si-OH group with FOCS and the dehydrochlorination reaction would occur between them. The content of Si can be analyzed by analyzing the content of F. Since one Si atom is equivalent to one Si-OH, we can use the following -formula to represent Si_{OH}/Si_{all}:

$$\frac{Si_{OH}}{Si_{all}} = \frac{\left[\frac{RSF_{Si2p}}{RSF_{F1s}}\right]\frac{1}{13}\left[F_{1s}\right]}{\left[Si_{2p}\right]-\frac{\left[RSF_{Si2p}\right]}{\left[RSF_{F1s}\right]}\frac{1}{13}\left[F_{1s}\right]} = \frac{\left[RSF_{Si2p}\right]\left[F_{1s}\right]}{13\left[RSF_{F1s}\right]\left[Si_{2p}\right]-\left[RSF_{Si2p}\right]\left[F_{1s}\right]} \quad (5.1)$$

$[F_{1s}]$ Count number of fluorine atom (Atomic Concentration of F)

$[Si_{2p}]$ Count number of silicon atom (Atomic Concentration of Si)

$[RSF_{F1s}]$ Relative sensitivity factors of fluorine atom

$[RSF_{Si2p}]$ Relative sensitivity factors of silicon atom

XPS survey spectra of derivatized SiO_2 treated by Ar/H_2O plasma for 20 minutes are shown in Fig. 3-8. XPS survey spectra were measured under an escape angle of 15°, 45° and 75°, respectively. As we know, the depth of XPS measurement can be decided by the escape angle, for measuring with 15°, we can get information of outermost surface of SiO_2. From survey spectra, F element can be detected, indicating that derivatization had occurred. Comparing these three spectra in Fig.3-8, we can clearly see that the F band of sample measured under 15° escape angle was more intense. From

Tab. 3-2, we can also observe the phenomenon of more -OH on outermost surface. Under escape angle of 15°, XPS survey spectra of derivatized SiO_2 without plasma treatment and treated by Ar/H_2 plasma and Ar plasma with bubbling for 20 minutes are illustrated in Fig. 3-9. It can be seen that samples without plasma treatment, F band was less intense.

SiOH/Siall of SiO_2 with different treating condition and takeoff angles are shown in Fig. 3-10. This is like what we discussed in former chapter that –OH characterized by XPS deconvolution of O1s. Referring to Tab. 3-3, the concentration of hydroxy group was still small, with the maximum being only 3.3%. But we can find that the thermally oxidized wafer treated by Ar/H_2O plasma treatment has more hydroxy group on its surface than untreated one, as shown in Fig.3-11.

Although there were many successful cases of chemical labeling used in facilitating the XPS analysis of functional groups on polymer, only limited work has been done in inorganic. I think this labeling method can't reflect all the quantity of –OH on wafer's surface. But it can be used to compare the results introduced by different plasma treatment.

3.2 Results of quartz glasses

3.2.1 XPS analysis of quartz glass

As we know, plasma can improve surface wettability of thermally oxidized Si wafer by treating surface oxidation layer of wafers. In order to check plasma's applicability to silica that with different structures according to different Si interatomic distances, quartz glass irradiated by Ar/H_2O plasma was also discussed. Fig. 3-12 (a). Fig. 3-12 (b) show the deconvolution of the main peak O1s of samples that were untreated and Ar/H_2O plasma at ambient temperature for 10 minute as Si-O-Si peak and Si-OH peak. The position of Si-O-Si peak at 532.5±0.5 eV with Si-OH peak at 533.8 eV

[20]. The concentration of Si-OH is estimated by relative peak areas as percentage of the total area of the O1s peak. The analytical results are shown in Fig.3-13 (More details can be found in Tab. 3-4.) Si-OH content of samples treated by Ar/H_2O plasma for 1, 5 and 20 minutes were also estimated in the same way. Compared with untreated quartz glass, we observed the same phenomenon as thermally oxidized Si wafer: The concentration of Si-OH on Ar/H_2O plasma-treated quartz glass' surface increases about 4%. As plasma treating time increases, there is a less obvious increasing trend in the concentration of hydroxy group.

3.2.2 Contact angle of water on quartz glasses

Fig. 3-14 shows the contact angles of quartz glasses treated by Ar/H_2O plasma under different treating time. We also can see plasma treatment has a more significant effect than those characterized by XPS analysis. It can be seen that the contact angles of plasma-treated quartz glasses decrease dramatically: drop down below 10°. But with increased plasma treating time, there is also not an obvious decrease in contact angles.

3.3 Stability of hydroxy group

The thermally oxidized Si wafers after Ar/H_2O plasma treatment for 10 minutes are stored in vacuum (in vacuum chamber with pressure of about 10^{-5} Torr) and in atmosphere (in a Petri dish) respectively, and the changes in water contact angles of samples under different storage time are illustrated in Fig.3-15. The quartz glass used for comparison is also treated by Ar/H_2O plasma treatment for 10 minutes and stored under the same conditions.

From Fig.3-15, as time goes on, contact angles will restore gradually. We can see that in the initial one day, both thermally oxidized wafer and glass's contact angles have an obvious increase with

storage time. After one day, the increase of contact angles become slow. This is because dehydroxylation reaction (2SiOH—Si-O-Si +H_2O) happens on silica surfaces [21-25]. Dehydroxylation is very important because the reactivity of silica surfaces changes dramatically between the dehydroxylated siloxane phase (Si-O-Si) and the hydrated silanol (Si-OH). The sketch of dehydroxylation is shown in Fig. 3-16, where neighboring surface hydroxy groups that are hydrogen-bonded together (vicinal) have been indicated to be desorbed easily as H_2O [2, 4, 22]. So the active surface restore inert siloxane surface. Consequently, contact angles increase.

We also can see that contact angles of samples stored in ambient are smaller than those stored in vacuum. Under atmospheric conditions, due to existence of water molecules, water would adsorb onto hydrophilic silicon oxide surface, and adsorbed water can induce some wettability, so contact angles of samples stored in ambient are smaller than them stored in vacuum.

In Fig. 3-17, changes in water contact angles of thermally oxidized Si wafer and quartz glass under different storage time are compared. For thermally oxidized Si wafer, the distance between Si atoms may be shorter than that in quartz glass, so that it would be easier to occur dehydroxylation reaction in thermally oxidized Si wafer. Thermally oxidized wafer would increase contact angle of water during storage faster than quartz glass.

4 Comparison of hydrophilicity introduced by difference plasma methods

In chapter 2 and 3, thermally oxidized Si wafer was treated by plasma by different methods: Using Ar and Ar/H_2 as working gas respectively, and inducing water vapor during Ar plasma discharge. The concentration of OH on oxidized Si wafer surface treated by plasma for 10 minutes is shown in

Fig. 3-18. Comparing these three methods, we can conclude that plasma irradiating can improve the concentrations of hydroxy group on their surfaces, but this increase was not very obvious, at about 3.5%.

Fig. 3-19 demonstrates the contact angles of water on oxidized Si wafer surface treated by plasma for 10 minutes. The contact angles of plasma-treated samples decrease dramatically, especially those samples treated by plasma with bubbling system, as the angle decreases from 59° to less than 10°.

5 Conclusions

In this study, the non-equilibrium atmospheric pressure plasma with bubbling system which can introduce water vapor during plasma irradiating was used to improve the hydrophilicity of thermally oxidized Si wafer surfaces. The XPS results show that the concentration of silanol on surface of wafers treated by plasma with bubbling system could increase. With increased treating time, there is no remarkable change in the concentration of hydroxy group. But the contact angles can show an obvious effective: After plasma treatment, the contact angle dropped dramatically from 59° down to 10°. It strongly suggests that Ar/H_2O plasma could enhance the hydrophilicity of oxidized Si wafer. With plasma treatment for 1 minute, the contact angle could decrease to about 10°. As time goes on, the contact angle stabilized at 10°.

In order to investigate the influence of the structure of silicon oxide on the introduction of hydrophilicity by non-equilibrium atmospheric pressure plasma, quartz glass was treated with Ar/H_2O plasma. Furthermore, the stability of the hydrophilicity introduced on the silicon oxide surface was investigated. The amount of surface silanol and the water contact angle of the quartz glass treated with Ar/H_2O plasma changed like the surface silicon oxide wafer. The amount of

surface silanol increased from 1.8% to 5.7%, and the contact angle decreased from 63 º to 10 º or less. In order to confirm the stability of the hydrophilicity of the silicon oxide surface introduced by Ar/H_2O plasma, change with time of the contact angle was observed. Surface silicon oxide wafers and quartz glass were stored in air and in vacuo after Ar/H_2O plasma treatment. It was revealed that the contact angle gradually increased with storage time. It is believed that adjacent silanols dehydrated and condensed to form siloxane bonds. The rate of increase in the contact angle of quartz glass was slower than that of the surface silicon oxide wafer, but this was considered to be due to the difference in distance of Si atoms.

In this chapter, a characterization method for various name labeling approaches was discussed. The surface hydroxy group on plasma treated thermal oxidized Si wafer can be successfully determined by reaction of the OH group with tridecafluoro-1, 1, 2, 2-tetrahydrooctyl dimethyl-chlorosilane (FOCS) and subsequent electron spectroscopy for chemical analysis for fluorine which has high sensitivity. In order to better study hydroxy group on different depths of SiO_2 surface, photoelectrons are collected at a takeoff angle of 15°, 45°and 75°. For the labeling method, the concentration of silanol on surface of wafers treated by plasma with bubbling system is higher than the untreated wafer and Ar/H_2 plasma treated wafer. Another conclusion we get is that as depth of surface increases, the OH content will decrease. Plasma treatment can have an obvious effect on the outermost surface of samples. But the concentration of hydroxy group by labeling method was still small. Maybe this method has limited applicability to inorganic

References

[1] Borello, E.; Zecchina, A.; Morterra, C. Infrared study of methanol adsorption on Aerosil. I.

Chemisorption at room temperature. J. Phys. Chem. 71(9): 2938-2945, 1967.

[2] R. K. Ile. The Chemistry of Silica, 2nd ed.; Wiley: New York, Chapter 6, 1979.

[3] C. P. Tripp, M. L. Hair. Measurement of polymer adsorption on colloidal silica by in situ transmission Fourier transform infrared spectroscopy. Langmuir, 9 (12): 3523-3529, 1993.

[4] R. L. White, et al., Diffuse reflectance infrared spectroscopic characterization of silica dehydroxylation. A. Appl. Spectrosc, 44 (1), 1990: 69-75.

[5] S. H. Garofalini, Molecular dynamics computer simulations of silica surface structure and adsorption of water molecules. J. Non-Cryst. Solids, 120 (1-3): 1-12 , 1990.

[6] D. P. Xu, Y. X. Xia, Y. F. Li. Determination of hydroxyl groups on the surface of particulate oxides (in Chinese). Chemistry. 5, 1981：25-26, 33.

[7] T. Morimoto, H. Naono. Water content on metal oxides. I. Water content on silica gel, magnesium oxide, zinc oxide, and titanium dioxide. Bulletin of the Chemical Society of Japan, 46 (7): 2000-2003, 1973.

[8] Institute of chemistry, Chinese Academy of Science, Room 5, Team 4. Determination of Si hydroxy group in siloxane by gas chromatography with lithium aluminum hydride (in Chinese). Chinese Journal of Analytical Chemistry, 3(5): 372-378, 1975.

[9] Y. F. Li. Y. X. Xia. D. P. Xu. G. L. Li. Analysis of hydroxyl groups on the surface of silicon dioxide used in rubber filler (in Chinese). Chinese Journal of Analytical Chemistry, 8(4): 389-389, 1980.

[10] T. Morimoto, K. Shiomi, and H. Tanaka. The heat of immersion of aluminum oxide in water. Bulletin of the Chemical Society of Japan. 37 (3): 392-395, 1964.

[11] T. Morimoto, M. Nagao, and F. Tokuda. Desorbability of chemisorbed water on metal oxide

surfaces. I. Desorption temperature of chemisorbed water on hematite, rutile and zinc oxide. Bulletin of the chemical society of Japan, 41 (7), 1968: 1533-1537.

[12] T. Morimoto, M. Nagao, and J. The Adsorption of Water on SiO_2, Al_2O_3, and $SiO_2 \cdot Al_2O_3$. The Relation between the Amounts of Physisorbed and Chemisorbed Water. Bulletin of the Chemical Society of Japan, 44 (5): 1282-1288, 1971.

[13] J. J. Fripiat and J. Uytterhoeven, Hydroxyl content in silica gel “aerosol”. J. Phys. Chem., 66 (5): 800-805, 1962.

[14] M. Miller and R.. L..Ana1. X-ray photoelectron spectroscopy of thermally treated silica (SiO_2) surfaces. Chem. 57: 2341-2349. 1985.

[15] D. Harvey and R. Linton. Chemical characterization of hydrous ferric oxides by X-ray photoelectron spectroscopy. Anal. Chem. 53: 1684-1688, 1981..

[16] D. B. Asay and S. H. Kim. Evolution of the Adsorbed Water Layer Structure on Silicon Oxide at Room Temperature. J. Phys. Chem. B, 109: 16760-16755, 2005.

[17] T. A. D. R. Gnanasekaran and D. D. Deppe. Quantification of surface hydroxides using chemical labeling and XPS. Surface and interface analysis. 18: 141-146, 1992.

[18] N. Takahashi, H. Mori, Y. Kimoto, T. Ohmori and A. Murase. Analysis of Silanol on DLC-Si Surfaces by Derivatization XPS (in Japanese). Surf. Sci., 26 (8): 492-494, 2005.

[19] T. A. Dang. Enhancement of electron spectroscopy for chemical analysis of surface silanol in silicon nitride through chemical derivatization. Journal of Vacuum Science & Technology A 9 (3): 1406-1410, 1991.

[20] J. Viard, E. Beche, D. Perarnau, R. Berjoan and J. Durand. XPS and FTIR study of silicon oxynitride thin films. Journal of the European ceramic society, 17: 2025-2028, 1997.

[21] O. Sneh, S. M. George. Thermal stability of hydroxyl groups on a well-defined silica surface. J. Phys. Chem., 99: 4639-4647, 1995.

[22] D. W. Sindorf, G. E. Maciel. Silicon-29 NMR study of dehydrated/rehydrated silica gel using cross polarization and magic-angle spinning. J. Am. Chem. SOC., 105: 1487-1493, 1983.

[23] J. Y. Yang. Study on the behavior of water adsorbed on the SiO_2 surface by using first principles density functional theory (in Chinese). Beijing: Chinese Academy of Sciences' Institute of Physics, 2005.

[24] B.C. Bunker et al., Surf. Sci. 210, 406 (1989); 222, 95 (1989); A.Grabbe et al., U.S. Patent No. 5736245 (1998)

[25] L. H. Dubois, B. R. Zegarski. Bonding of alkoxysilanes to dehydroxylated silica surfaces: a new adhesion mechanism. J. Phys. Chem. 97 (8): 1665-1670, 1993.

[26] M.H. Du, A. Kolchin, and H.P. Cheng. Water-silica surface interactions-A combined quantum-classical molecular. Journal of chemical physics, 119 (13): 6418-6422, 2003.

Tab. 3-1 Change in surface chemical components of thermally oxidized Si wafer and thermally oxidized Si wafer treated by Ar/H_2O plasma for 1 min, 5 min, 10 min and 20 min

	Untreated	Ar/H_2O 1min	Ar/H_2O 5min	Ar/H_2O 10min	Ar/H_2O 20min
Si-O-Si	97.77%	95.35%	95.63%	94.72%	94.06%
Si-OH	2.23%	4.65%	4.37%	5.28%	5.94%
(Si-OH) / (Si-O-Si)	0.02	0.05	0.05	0.06	0.06

Tab.3-2 XPS data of atomic concentration for sample treated under different conditions

		RSF		Atomic Concentration %	
	Takeoff Angle	**Si 2p**	**F 1s**	**Si 2p**	**F 1s**
Ar/H_2 plasma treating for 20min	15°	0.317	1	28.77	11.92
	45°			30.97	7.61
	75°			31.36	6.24
Ar/H_2O plasma treating for 20min	15°	0.317	1	27.70	10.47
	45°			31.12	5.53
	75°			31.88	4.32
Untreated	15°	0.317	1	27.54	6.04
	45°			31.01	4.57
	75°			31.65	3.29

Tab.3-3 Relation with different treating conditions and Si_{OH}/Si_{all}

	Takeoff Angle	Si_{OH}/Si_{all}
Ar/H_2 plasma treating for 20min	15°	2.99%
	45°	1.39%
	75°	1.05%
Ar/H_2O plasma treating for 20min	15°	3.29%
	45°	1.93%
	75°	1.55%
Untreated	15°	1.71%
	45°	1.15%
	75°	0.81%

Tab. 3-4 Change in surface chemical components of quartz glass treated by Ar/H_2O plasma for 1 min, 5 min, 10 min and 20 min

	Untreated	Ar/H_2O 1min	Ar/H_2O 5min	Ar/H_2O 10min	Ar/H_2O 20min
Si-O-Si	98.19%	96.49%	96.28%	95.21%	94.25%
Si-OH	1.81%	3.51%	3.72%	4.79%	5.75%
(Si-OH) / (Si-O-Si)	0.02	0.04	0.04	0.05	0.06

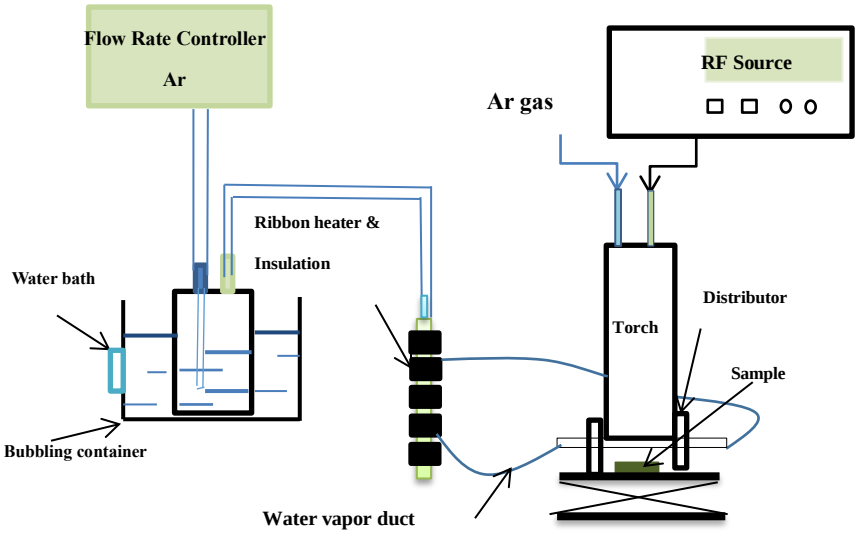

Fig. 3-1 Schematic diagram of the experimental setups for the plasma-treatment of samples

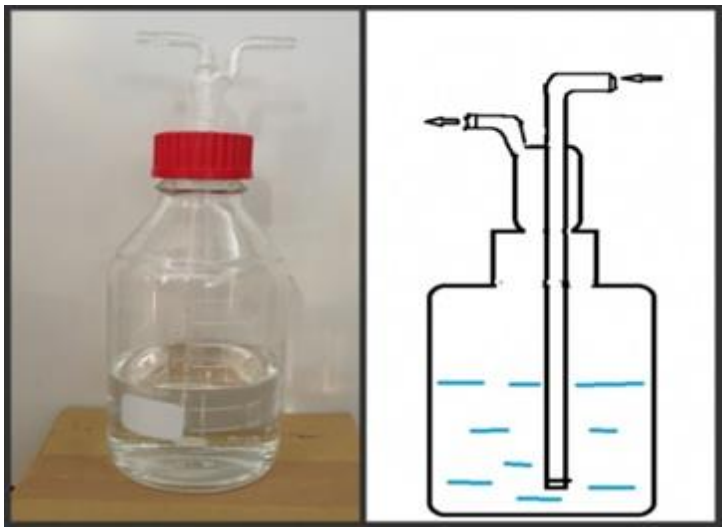

Fig.3-2 Schematic diagram of bubbling container

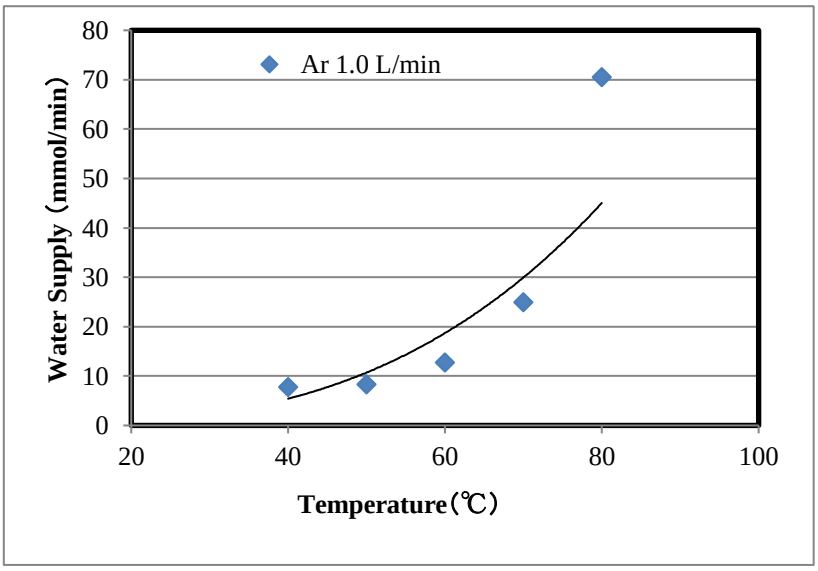

Fig.3-3 Water supply-Temperature

Fig.3-4 The structure of tridecafluoro-1, 1, 2, 2-tetrahydrooctyl dimethyl-chlorosilane (FOCS)

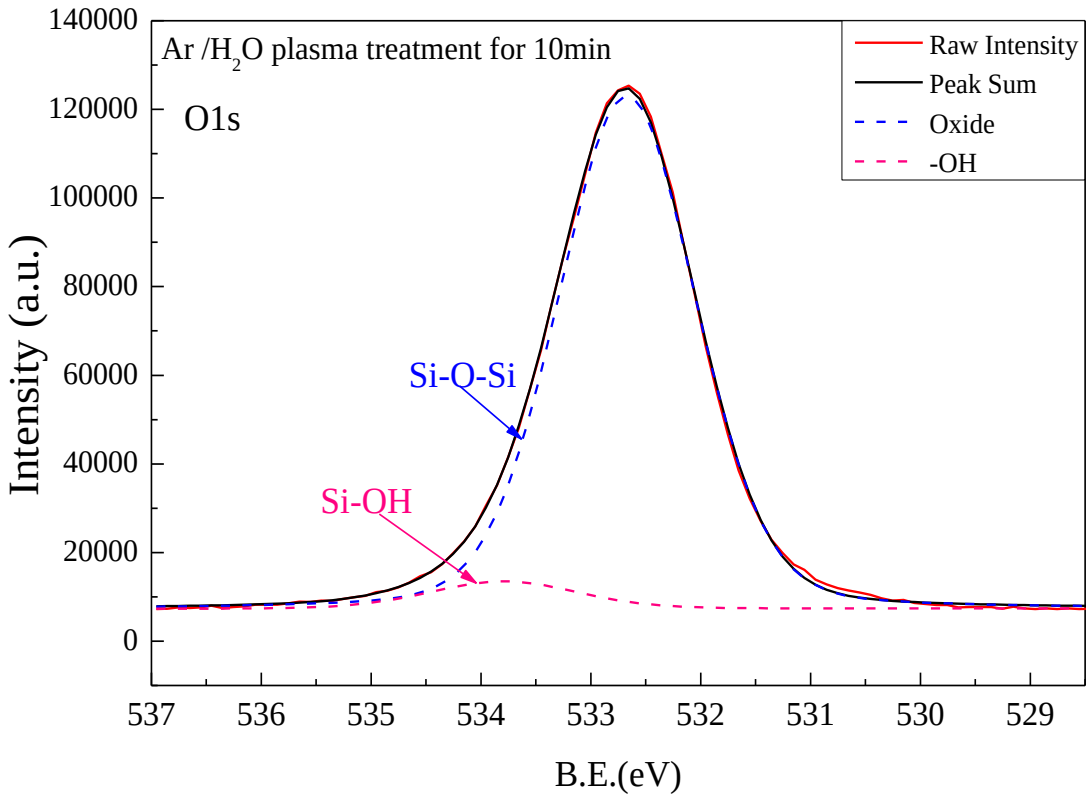

Fig.3-5 XPS spectrum of O1s peak fitting for thermally oxidized Si wafer treated by Ar/H_2O plasma for 10 min;

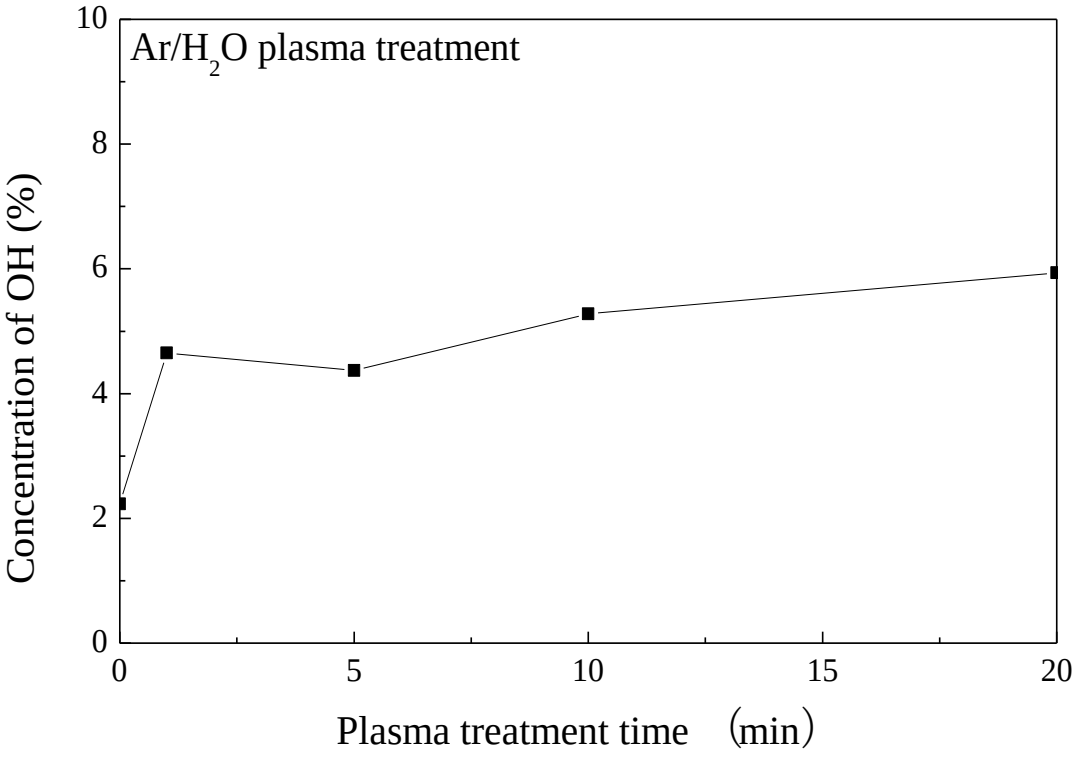

Fig. 3-6 Concentration of OH on thermally oxidized Si wafer surface which were treated by Ar/H_2O plasma for different treating time

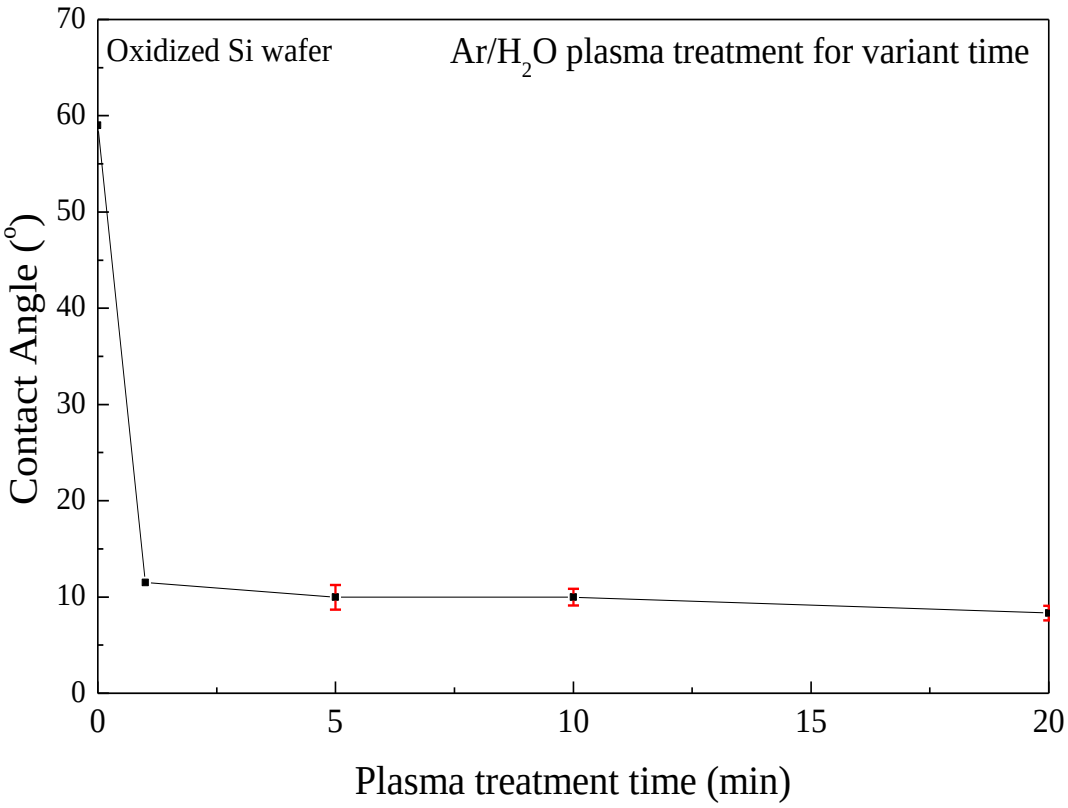

Fig.3-7 Contact angles of thermally oxidized Si wafer treated by Ar/H_2O plasma for 1 min, 5 min, 10 min and 20 min

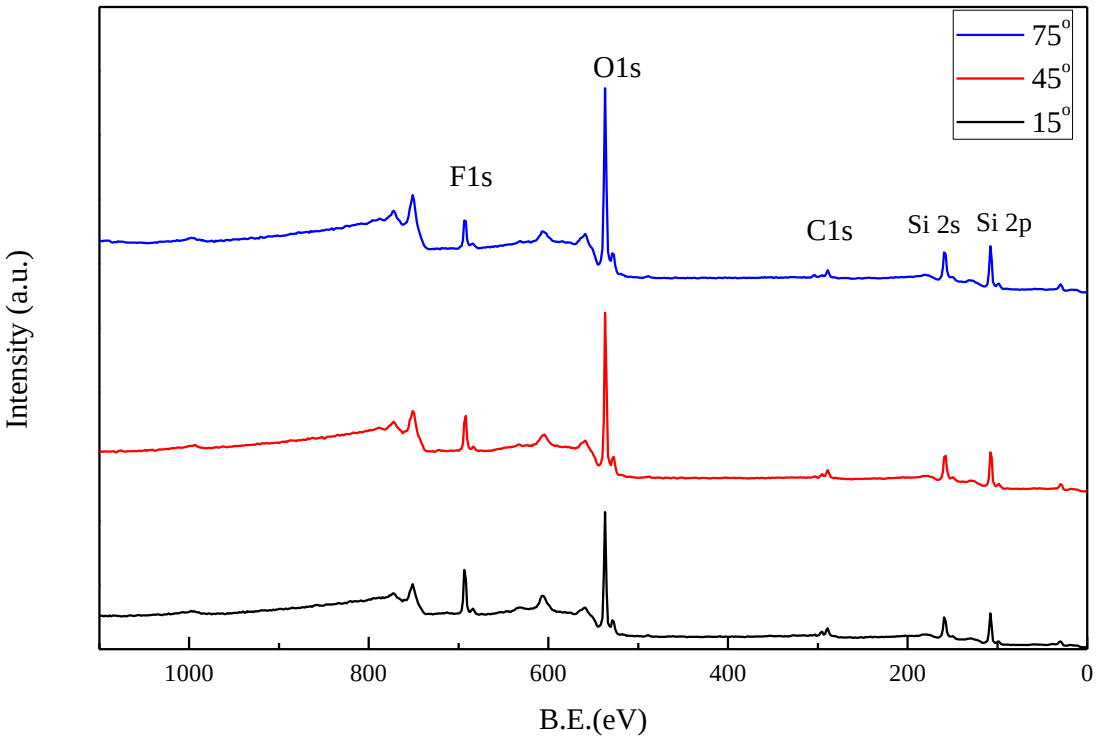

Fig. 3-8 XPS of FOCS derivatized SiO_2 treated by Ar/H_2O plasma for 20 min with different takeoff angles.

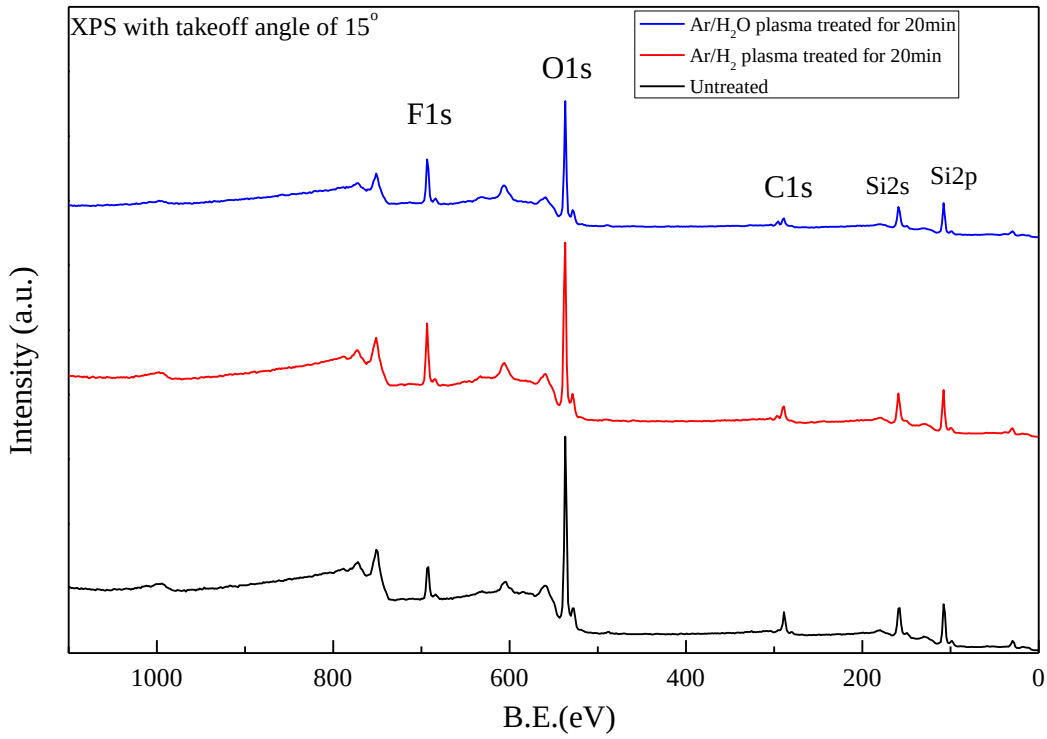

Fig. 3-9 XPS of FOCS derivatized SiO_2 without plasma treating and treated by Ar/H_2 plasma and Ar/H_2O plasma for 20 min with takeoff angle of 15°

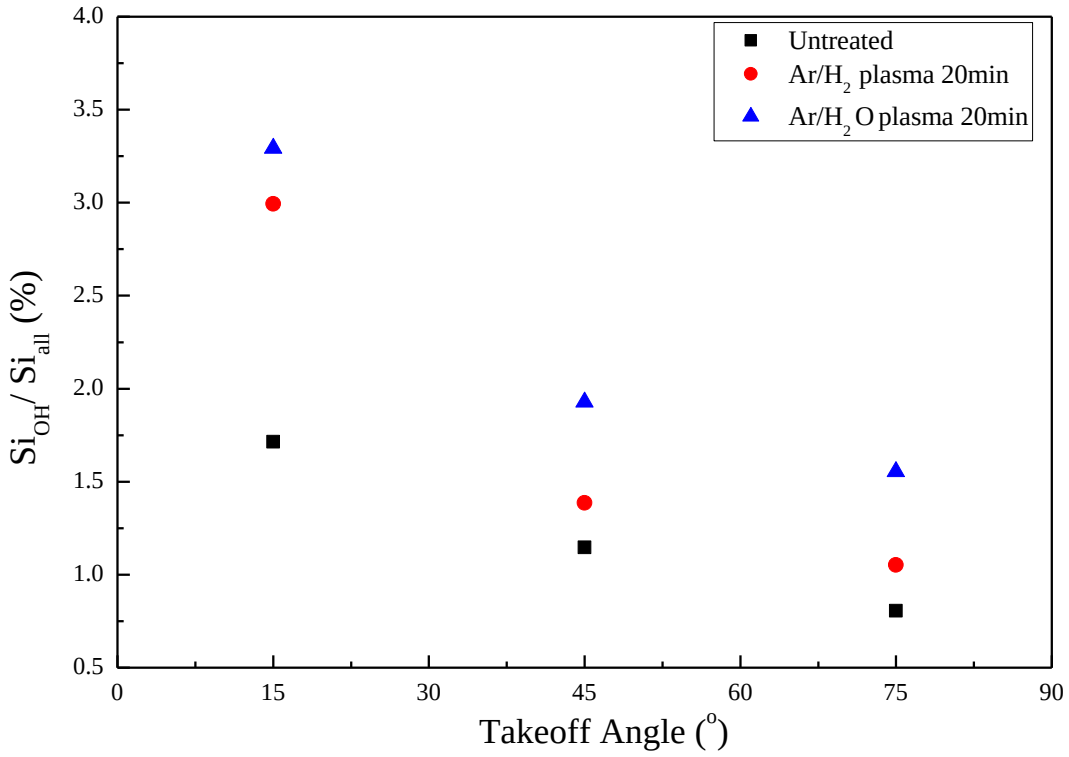

Fig.3-10 Relation with different treating condition and Si_{OH}/Si_{all}

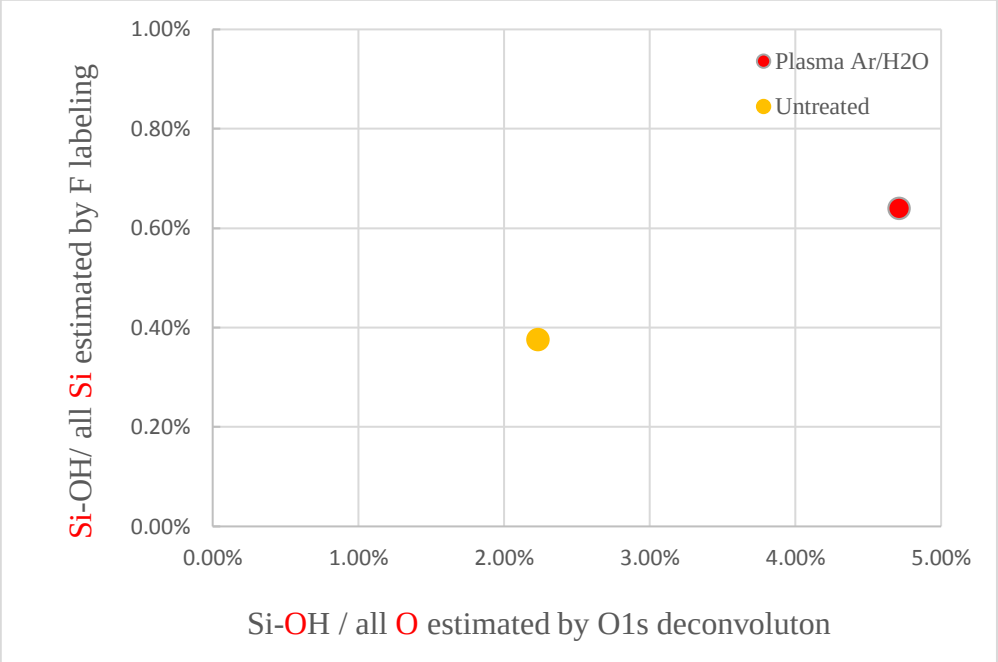

Fig.3-11 Relationship between Si-OH contents estimated by O1s deconvolution and F-labeling

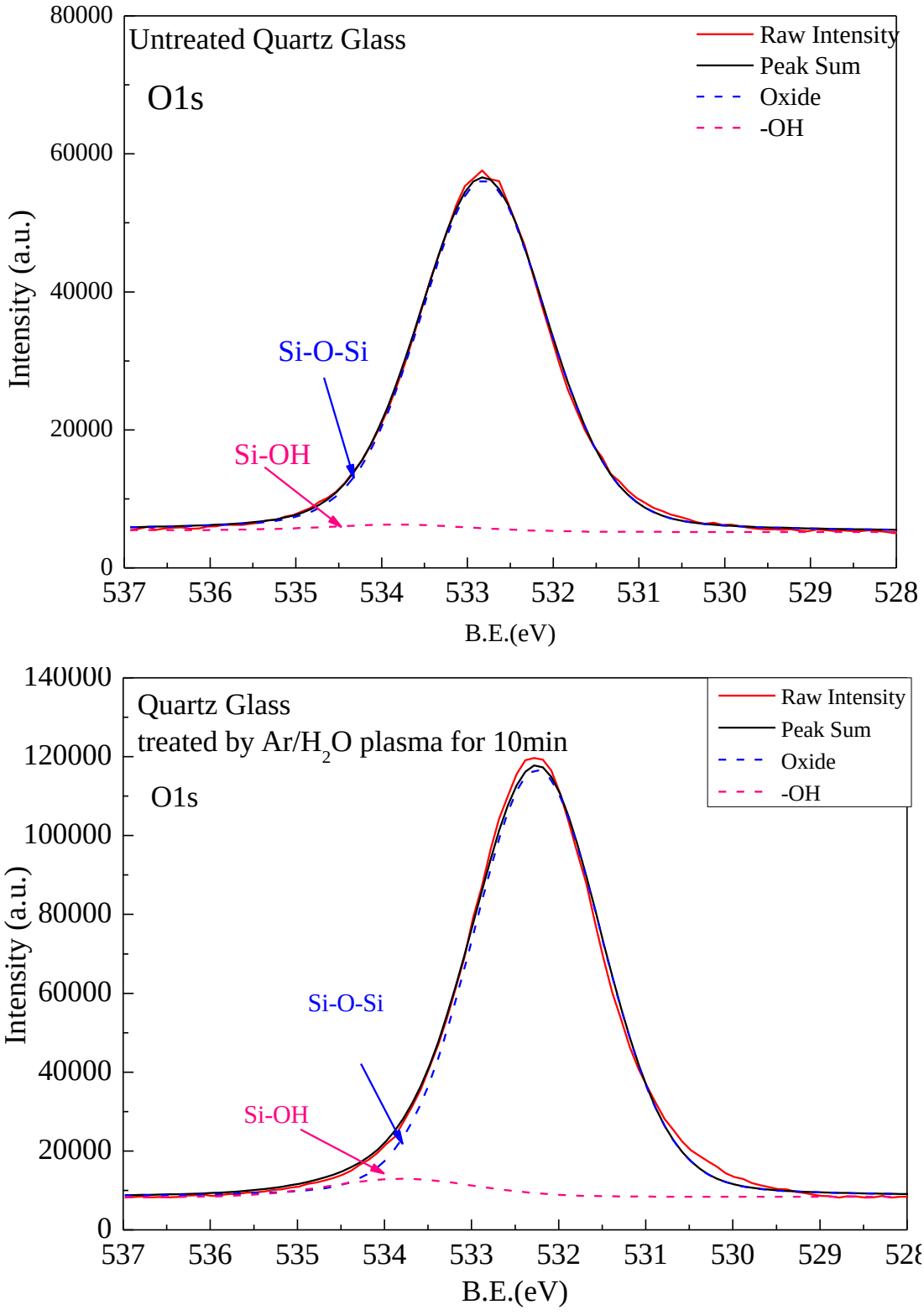

Fig.3-12 XPS spectrum of O1s peak fitting for (a) untreated quartz glass and (b) glass treated by Ar/H_2O plasma for 10 min;

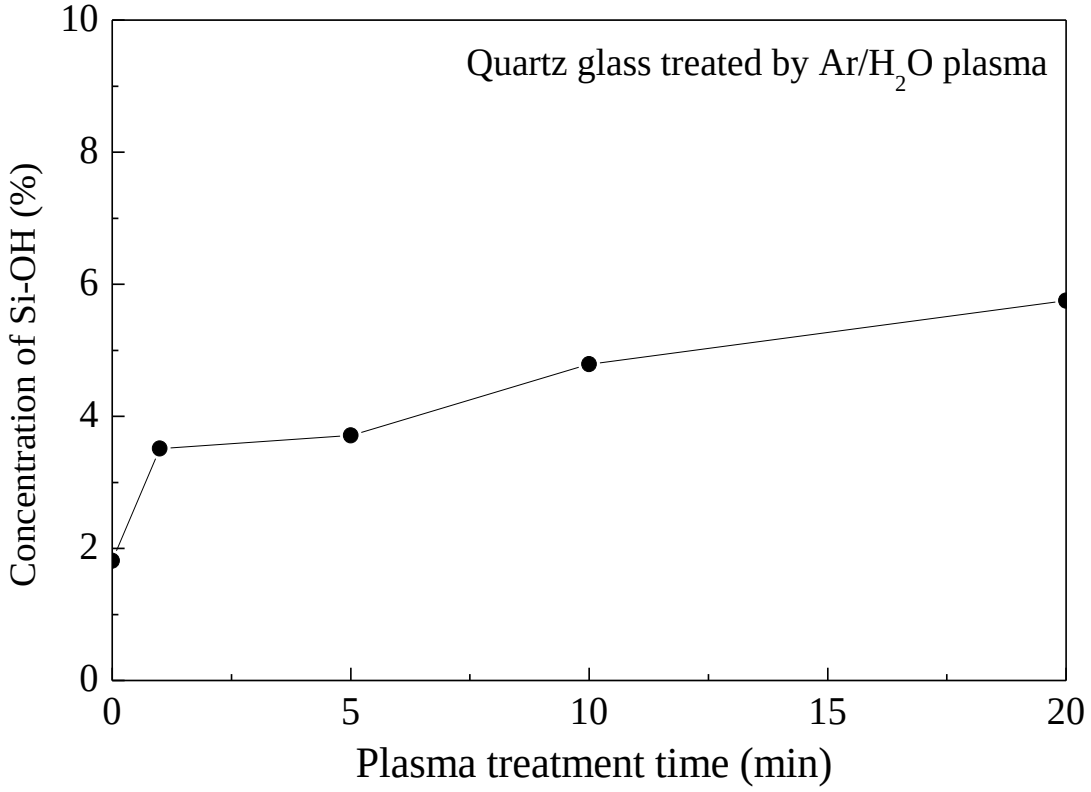

Fig. 3-13 Concentration of OH on quartz glass surface which were treated by Ar/H_2O plasma for different treating time

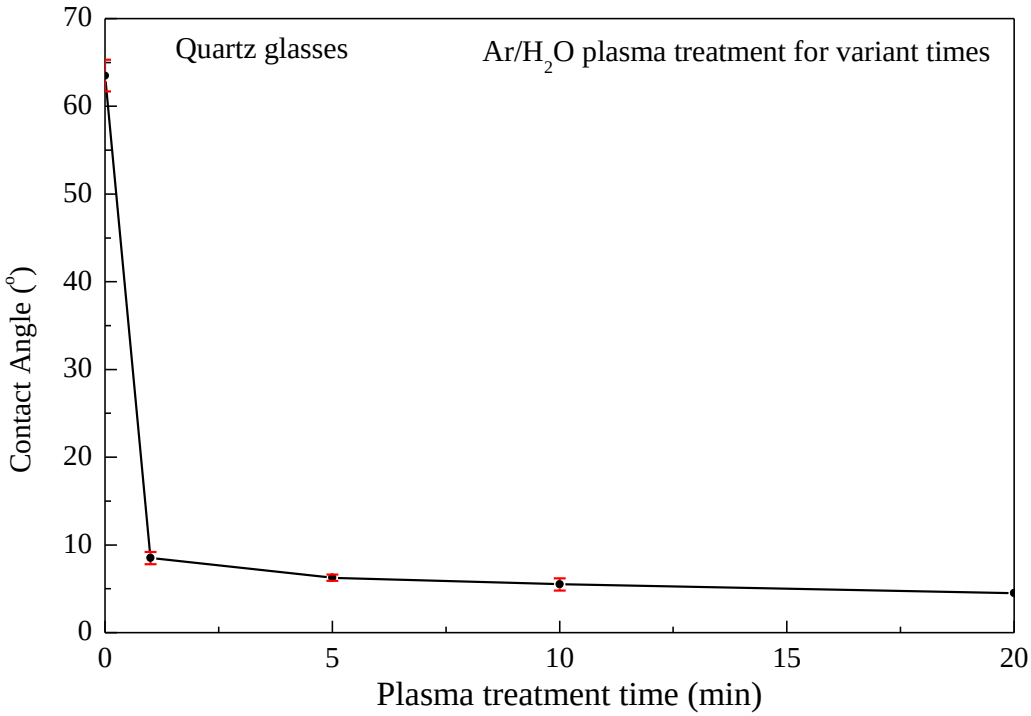

Fig. 3-14 Contact angles of quartz glass treated by Ar/H_2O plasma for 1 min, 5 min, 10 min and 20 min

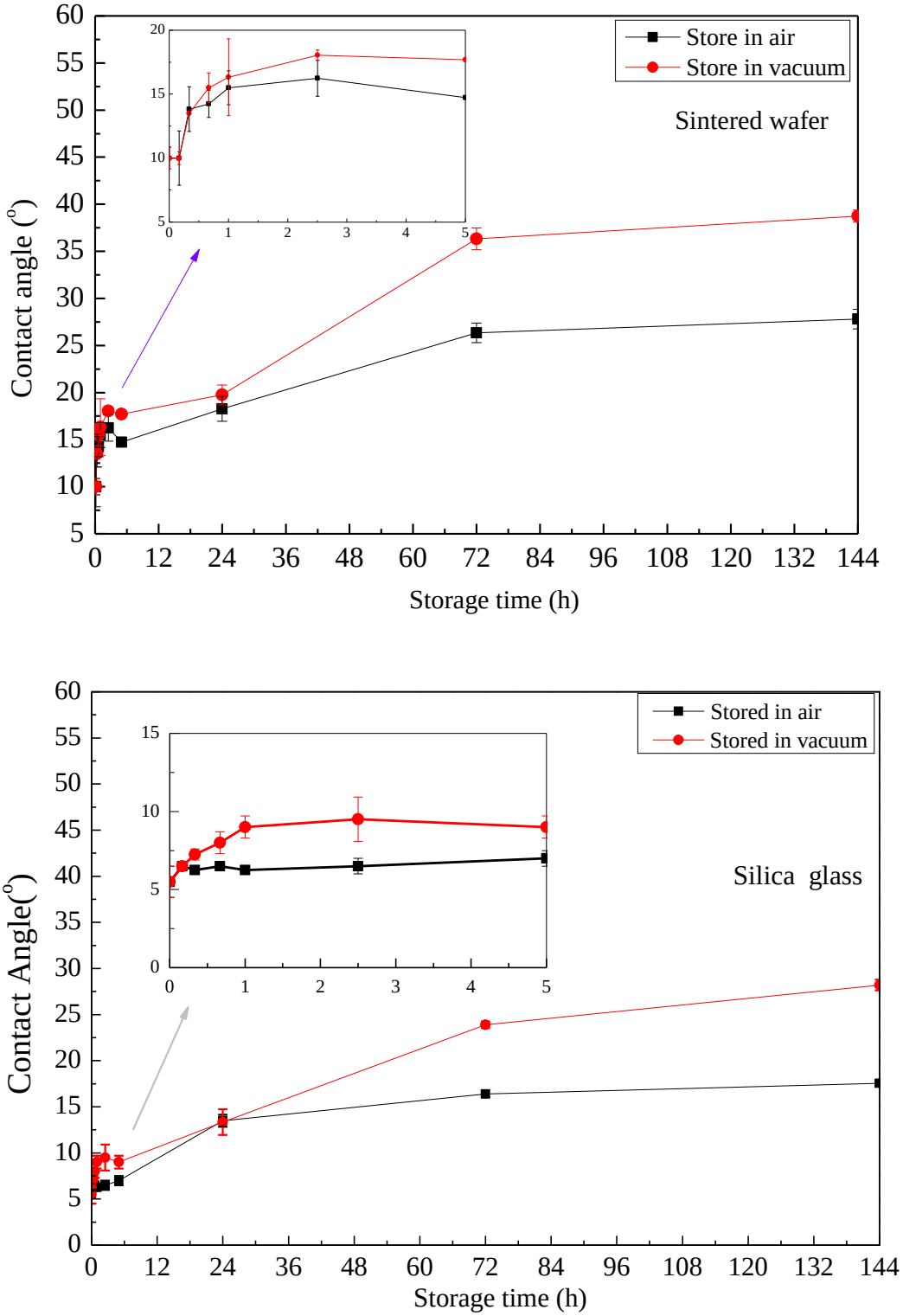

Fig.3-15 Changes of contact angles of Ar/H_2O plasma treated (top) thermally oxidized Si wafer and (below) quartz glass under different storage times

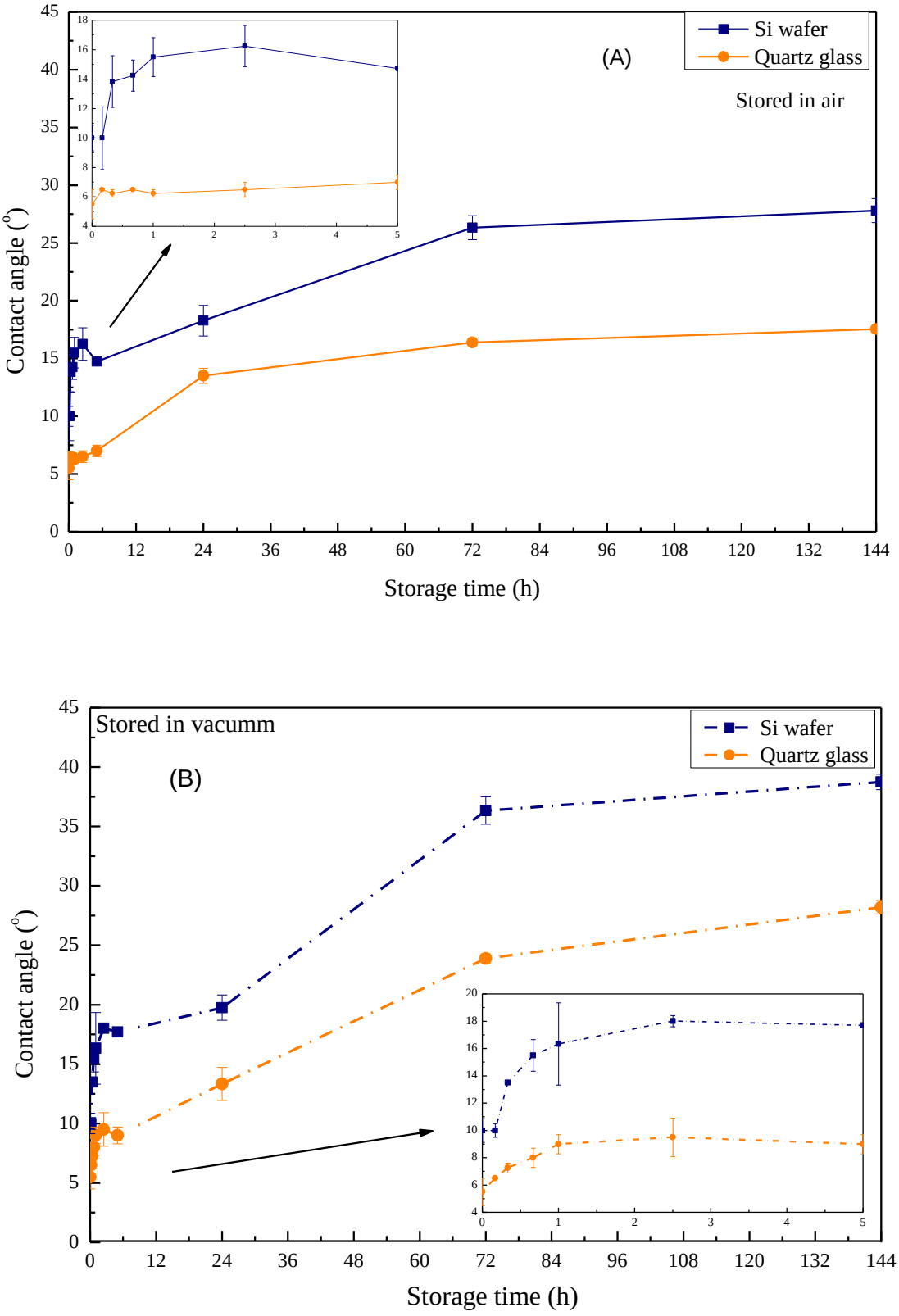

Fig.3-16 Compared the changes of contact angles of Ar/H_2O plasma treated thermally oxidized Si wafer and quartz glass under different storage times stored in (A) air and (B) vacuum

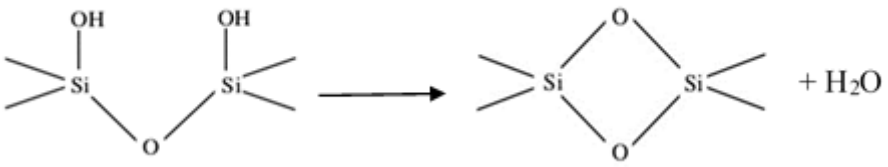

Fig.3-17 Sketch of the dehydroxylation reaction

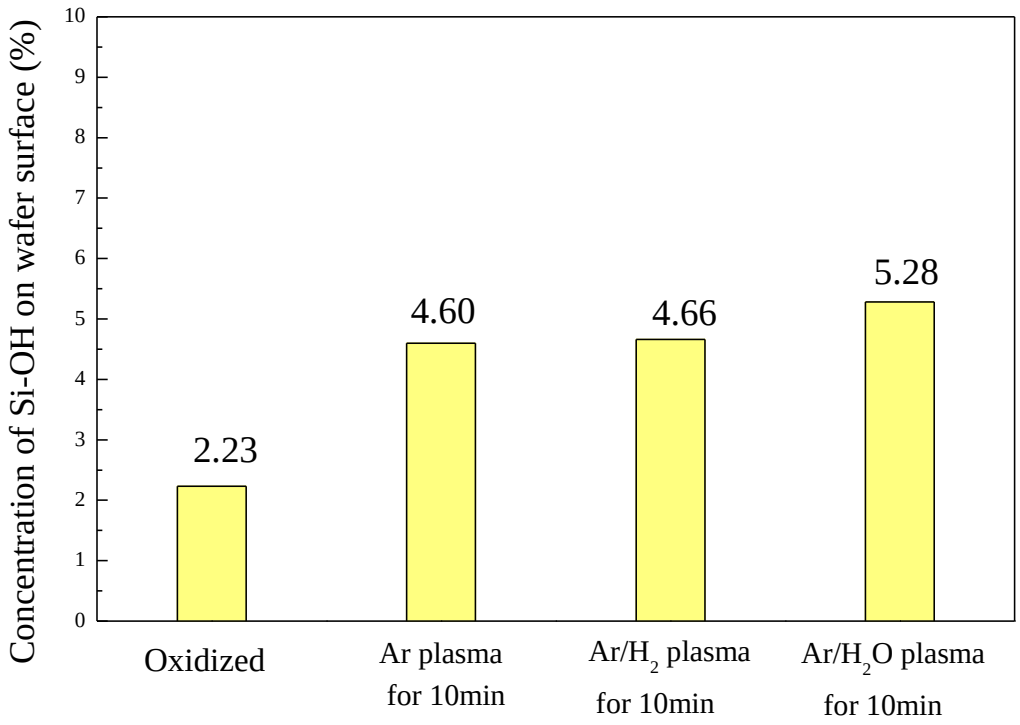

Fig. 3-18 Concentration of OH on thermally oxidized Si wafer surfaces which were treated by different methods

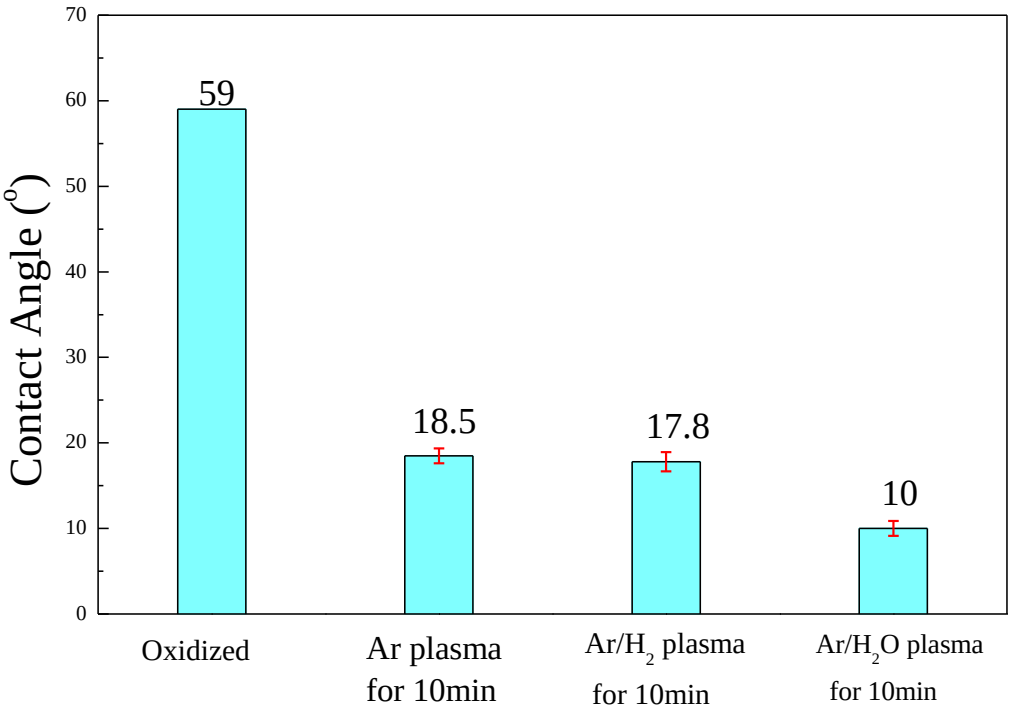

Fig. 3-19 Contact angles of thermally oxidized Si wafer surfaces which were untreated and treated by different methods

Chapter 4 Comparison of hydrophilicity on TiO_2 film surfaces introduced by non-equilibrium atmospheric pressure plasma with or without addition of water vapor

1 Introduction

Not only because of the properties of titanium dioxide (TiO_2) material itself but also the modifications of the TiO_2 material host (e.g., with inorganic and organic dyes) and on the interactions of TiO_2 materials with the environment [1], since its commercial production in the early 20th century, TiO_2 has been widely used in daily chemical products [2-6], environmental fields [7-9] and energy field [10-13].

In recent years, photovoltaics based on TiO_2 nanocrystalline material have been widely studied [10, 14-18]. Nanocrystalline TiO_2 film can be used as a photocatalyst electrode in dye-sensitized solar cells (DSSCs), because it is physically and chemically stable at standard temperature and normal pressure. Hydrophilic property of the TiO_2 surface plays an important role in increasing the dye adsorption and thus enhancing the efficiency of DSSCs power generation [19].

It is well known that plasma treatment is a very effective technology to modify sample surface by a strong interaction with the plasma containing electrons, ions, radicals, and neutral molecules. The plasma treatment is suggested to increase oxide vacancy and hydrophilic property of nano-structured TiO_2.

In this chapter, non-equilibrium atmospheric pressure plasmais used to increase hydrophilicity

effect on TiO_2 surface. Effects of plasma treatment on TiO_2 surface hydrophilicity and the stability of hydroxy group of TiO_2 films treated by Ar plasma with bubbling system are investigated experimentally. At the end of the chapter, the quantification of MK-2 dye which used in dye sensitized solar cells (DSSC) is studied.

2 Experimental details

2.1 Sample preparation

The processes of the nano-particles sintering are represented in Fig. 4-1 [20, 21]. In fact, as shown in Fig. 4-1 (a), in order to stabilize TiO_2 nano-particles, usually polymeric dispersant is added into the TiO_2 nano-paste as the additive, which would greatly reduce the conductivity of the TiO_2 nano-paste and prevent the nano-particles sintering. To remove the polymer additives in the paste, heat-treatment is generally carried out, as shown in Fig. 4-1 (b). If we heat the sample at an appropriate temperature, the polymer dispersant would be decomposed as shown in Fig 4-1 (c), which is considered as one of the most important process for TiO_2 nano-particles sintering. Fig. 4-1 (d) shows the sintered state of the TiO_2 nano-particles, which requires much energy.

The "TiO_2 nano-paste" supplied by Taiyo yuden Co., Ltd. is composed of TiO_2 particles with an average grain diameter of 25 nm (P25) and the polymer additives are used as the binder. The TiO_2 nano-paste is printed onto glass by using squeeze printing method with c.a. 0.02 mm thick and c.a. 1.9 cm^2 active area. After printing, samples were dried in an oven at 100℃ for 10 minutes, then put in a muffle furnance at 450℃ for 30 minutes to remove the binder [22, 23]

During plasma discharge, Ar gas was used as the working gas at a flow rate of 20 L/min, and RF powers were maintained at 100 W without reflection. Water vapor was added by Ar gas which was

introduced through tubes below plasma torch at a flow rate of 1 L/min. All flow rates were controlled by a mass flow controller. The distance between the plasma torch head and sample was 3 mm.

2.2 Surface characterization

XPS (X-ray photoelectron spectroscopy) measurements are conducted to analyze the surface composition of SiO_2 film by using Perkin Elmer ESCA 5600. Mg Kα radiation is employed as an X-ray source (15 KV, 400 W), and the photoelectron are collected at a takeoff angle 45°. The base pressure of system is below 10^{-7} Torr.

The hydrophilicity of the surface is evaluated in terms of contact angle, which is measured by CA-D contact-angle meter with deionized water at least 3 times, and the results are averaged.

The UV-vis absorption spectra of the dye-loaded transparent film and the dye solutions were recorded on a JASCO UV-560 spectrophotometer [24].

3 Results and discussion

3.1 XPS analysis of TiO_2 surfaces

XPS analysis was carried out to determine alterations in surface charge states of TiO_2 thin film and functionalities at the surface after Ar plasma and Ar/H_2O plasma treatment. Fig. 4-2 and Fig. 4-3 illustrate the deconvolution of resolution Ti2p XPS spectra of untreated, Ar plasma-treated and Ar plasma with bubbling system treated TiO_2 thin films at 100W for 10 minutes. The Ti2p XPS spectrum of untreated and plasma-treated TiO_2 films are fitted with four peaks, which correspond to titanium oxide (Ti^{4+}) and titanium sub-oxide (Ti^{3+}) in $Ti2p_{1/2}$ and Ti^{4+} and Ti^{3+} in $Ti2p_{3/2}$ respectively [23], as shown in Fig. 4-2 (a) ~ (c). The surface stoichiometry is estimated by relative

peak areas as percentage of the total area of the Ti2p peak, and the analytical results are shown in Tab. 4-1 and 4-2. Changes in oxidation state of Ti for TiO_2 films treated by Ar plasma and Ar plasma with bubbling system for 1, 5 and 20 minutes are also estimated in the same way. After Ar plasma treatment for 40 min, the Ti^{4+} surface state in the Ti2p region decreased from about 94.29% to 90.85%, and Ti^{3+} increased from 5.71% to 9.15%. Similarly, with TiO_2 treated Ar plasma with bubbling system for 40 minutes, the Ti^{4+} surface state in the Ti2p region decreased to 90.10%, while Ti^{3+} increased to 9.90%. It is observed, as shown in Fig. 4-2, that Ti^{4+} is changed to Ti^{3+} by the reaction of Ti^{4+} with the electrons and this change enhances the hydrophilic state of TiO_2 surface as indicated by the increase in OH^-, which can be deduced from XPS O1s spectra, as shown in Fig. 4-3. As plasma treatment time increases, there is a less obvious increasing trend in Ti^{3+}.

The broads O1s of TiO_2 films treated by Ar plasma and Ar ph bubbling system for 40 minutes are fitted and deconvoluted into three peaks in the XPS spectra, as shown in Fig 4-3. The main peak at 529.5eV indicates oxygen in O^{2-} (TiO_x), with two shoulder peaks attributing to Ti-OH (531.2 eV) group and H_2O (532 eV) respectively. The intensity of the O1s' peak of Ti-OH increased after the TiO_2 thin film was treated by plasma. The concentration of Ti-OH is estimated by relative peak areas as percentage of the total area of the O1s peak. The analytical results are displayed in Fig.4-4 (More details can be found in Tab. 4-3 and 4-4). Ti-OH content of samples treated by Ar plasma and Ar plasma with bubbling system for 1, 5 and 20 minutes are also estimated in the same way. Comparing Ar plasma and Ar/H_2O plasma treatment, we can find that Ar/H_2O plasma treatment has a more obvious effect on samples' surface, as the increase of Ti-OH is higher. With increased plasma treating time, the concentration of Ti-OH will increase as well.

3.2 Contact angle of water on TiO_2 film surfaces

Contact angle can give information about the macroscopic surface wettability. Fig.4-5 shows contact angles of TiO_2 thin films treated by Ar plasma and Ar/H_2O plasma respectively. For contact angles evaluation, plasma treatment has a more significant effect than those characterized by XPS analysis. It can be seen that contact angles of plasma-treated samples drop below 10°. But with increased plasma treating time, there is no further obvious decrease in contact angles. Additionally, from Fig. 4-5 we can find that the contact angles of samples treated by Ar/H_2O plasma were smaller than those treated by Ar plasma.

For TiO_2, plasma irradiation may create surface oxygen vacancies at bridging sites, resulting in the conversion of relevant Ti^{4+} sites to Ti^{3+} sites [26, 27] which are favorable for dissociative water adsorption, which is shown as follows:

$$TiO_2 + \text{Energy} \rightarrow e_{CB}^- + h_{VB}^+$$

$$e_{CB}^- + Ti^{4+} \rightarrow Ti^{3+}$$

These oxygen vacancies presumably influence the affinity to chemisorbed water of their surrounding sites, forming hydrophilic areas.

We know TiO_2 has photocatalysis under UV irradiation, and in plasma discharge there may generated UV. In order to verify effect of plasma on hydrophilicity, TiO_2 films covered with quartz glass was treated by Ar plasma for 10 min. And then compared its contact angle results with film directly irradiated Ar plasma for 10 min. Quartz glass will obstruct active particle in plasma and let UV penetrate. The contact angle results are shown in Fig. 4-6. From figure, we know contact angle of TiO_2 film directly irradiated Ar plasma for 10 min reduced by half, from 14.1° to 6.6°, while TiO_2 film with quartz glass only decrease 1°. So we draw a conclusion that plasma can improve

hydrophilicity on TiO_2 nanocrystalline films surfaces.

3.3 Stability of hydroxy group

The samples after plasma treatment with bubbling system for 10 minutes are stored in vacuum (in vacuum chamber with pressure of about 10^{-5} Torr) and atmosphere (in a Petri dish) respectively, and the changes in water contact angles of samples under different storage duration are shown in Fig.4-7.

From Fig.4-7, we can see that during the first day, contact angles had an increasing trend with storage time. After one day; the increase of contact angles was not obvious. With long term storage, oxygen vacancies may trap electron or active group or react with other gas from the air, thereby losing activity (-OH) gradually, and the chemisorbed hydroxy groups are replaced by oxygen [25, 28-33]. Under macroscopic, contact angles will increase gradually. That is why hydrophilicity on surface of plasma irradiated TiO_2 films has a certain longevity. We also can see that the contact angles of samples stored in ambient are smaller than those stored in vacuum. The same as silicon dioxide, under atmospheric conditions, water would adsorb onto TiO_2 surface. On TiO_2 film's surface photo-electronic transferring may occur by surface state (Ti^{3+} and O_2^-) and adsorbed water. This can decrease probability of electron-cavity compounding [34], oxygen vacancies would be long-lived when films store in air. So contact angles of films stored in ambient are smaller than them stored in vacuum.

4 Application of non-equilibrium atmospheric pressure plasma treatment to dye-sensitized solar cell

As mentioned above, it is known that titanium can exist in sub-oxide forms such as Ti_2O_3 in a

nanocrystalline TiO_2 film. The oxygen vacancies due to such sub-oxides are surface defects from the perspective of DSSCs. These surface defects are expected to significantly influence the performance of the cell. Modifying the surface structure of the TiO_2 film is one of the strategies adopted for improving the solar-to-electricity conversion efficiency [35–38]. We have discussed that Ar plasma treatment can increase Ti^{3+} surface state of TiO_2 film. In this part, we will investigate the effect of plasma treatment on quantification of MK-2, which is used as dye in DSSC. The information and structure of MK-2 Dye are illustrated in Tab. 4-5 and Fig. 4-8 [39] respectively.

4.1 Measurement of dye adsorption

Adsorption of dye per unit area can be calculated by adsorbance of desorption solution and standard adsorption curve of dye. By using standard dye solution, the adsorbance can be determined directly and the working curve can also be drawn. The process of quantification is listed as below [40, 41]: ① Prepare desorption agent; ② Prepare standard solution, and draw the standard curve of the concentration and adsorbance; ③ Put the dye-loaded samples in desorption agent for a certain period, and measure the adsorbance of desorption agent which dissolved dye; ④ Get the value of concentration, and calculate the amount of MK-2 adsorbed.

The mixture solvent of THF/toluene (volume ratio of 2/8) was used as the desorption agent. In this report the solution with concentration of 0.0011, 0.0017, 0.0034, 0.0051, 0.0068 mmol/L was prepared as standard solution, and THF/toluene mixture solvent was used as reference. At first the 0.0017 mmol/L dye solution was chosen to measure adsorption spectra from 300 nm to 700 nm.

Fig. 4-9 displays the UV-vis absorption spectra of the MK-2 dye solution with concentration of 0.0017 mmol/L. From Fig.4-8, we can see that at 477 nm, the absorbance is highest. We therefore

measure the absorbance of every standard solution at 477 nm. Fig.4-10 is standard curve of the relation between concentration and absorbance of Dye MK-2 solution at 477 nm. Standard curve equation (4-1) is obtained after analysis and regression:

$$y=78.634x \qquad (4\text{-}1)$$

In equation 4-1, y is absorbance; x is concentration of Dye MK-2, mmol/L. The correlation coefficient of $r^2=0.999>0.99$, this means these data are reliable.

After plasma treating, we put the dye-loaded TiO_2 films in desorption agent for a period, then the film was withdrawn from the desorption agent. After that the surplus desorption agent was absorbed by tissue, then we measure the UV-Vis absorbance of desorption agent from 300 nm to 700 nm, find the value of absorption at 477 nm. We then calculate the concentration according to Equation 4-1, and calculate the adsorption capacity (Q) in term of following equation 4-2.

$$Q=(C\times V)/S \qquad (4\text{-}2)$$

In equation 4-2, Q is adsorption capacity of Dye MK-2, mol/cm^2; C is concentration of Dye MK-2, mol/L; V is volume of desorption agent, L; S is area of TiO_2 film, cm^2.

I my experiment, after plasma treating, TiO_2 films were immersed in 0.3 mM dye solution in darkness. After an hour, take dye-loaded films out of dye solution (the surplus dye solution is absorbed by tissue) and soak them into desorption agent (THF/toluene mixture solvent [39],) for one day to withdraw dye from the films. Then dilute the desorption agent with THF/toluene mixture solvent to 4mL. In the end measure UV-Vis absorbance of diluted desorption agent from 300 nm to 700 nm, find the value of absorption at 477 nm. And calculate the concentration according to equation 4-1, and the adsorption capacity (Q) in term of equation 4-2. The performance of desorption is displayed in Fig.4-11.

4.2 Quantity of dye adsorption

In this experiment, the quantity of dye adsorption for TiO_2 nano-film treated by Ar plasma and Ar /H_2O for 20 minutes are evaluated. The untreated film is also measured as reference.

From Fig 4-11, we can see that TiO_2 film treated by Ar /H_2O plasma has more quantity of dye adsorption, so it is clear that the adsorption of the MK-2 dye on the TiO_2 film will increase with increased concentration of hydroxy group. The reason for the increased dye uptake by the TiO_2 film after plasma treatment can be explained on the basis of the interaction between hydroxy group of titanium on the TiO_2 surface and the –COOH groups of the MK-2 dye molecules [42]. The interaction between plasma-treated TiO_2 and –COOH groups of the dye can be represented by the equation as follows:

$$Ti–OH + HOOC–R \leftrightarrow Ti–OOC–R + H_2O$$

Where Ti–OH stands for the hydroxylated TiO_2 surfaces, and HOOC–R represents the MK-2 dye with Ti-OH anchoring carboxylic acid groups [43]. Oxygen vacancies can be created during plasma treatment. This will improve affinity to chemisorbed · OH, forming hydrophilicity domains. As mentioned above, plasma treatment with bubbling has a more obvious effect than Ar plasma treatment on hydrophilicity, so it also has more quantity of dye adsorption.

5 Conclusions

In this study, the non-equilibrium atmospheric pressure plasma with water vapor during plasma irradiating, was used to improve hydrophilicity on TiO_2 nanocrystalline films surfaces. The XPS results show the reduction of plasma, and oxygen vacancy will be created during plasma process. After a 40 minute-long Ar plasma treatment, the Ti^{4+} surface state decreased from about 94.29% to

90.85%, and Ti^{3+} increased from 5.71% to 9.15%. Similarly, with treatment by Ar plasma with bubbling system for 40 minutes, the Ti^{4+} surface state decreased to 90.10%, and Ti^{3+} increased to 9.90%. The concentration of Ti-OH on surface of TiO_2 films, after being treated by plasma with bubbling system, could increase. With increased plasma treatment time, the concentration of Ti-OH will increase. The contact angles can demonstrate an obvious result: After plasma treatment, the contact angle dropped dramatically, as it can drop below 10°. It strongly suggests that Ar/H_2O plasma could enhance the hydrophilicity of TiO_2 nanocrystalline films. With plasma treatment for 5 minutes, the contact angle could decrease to 10°. To conclude, as time goes on, contact angle has a small change.

The hydrophilicity on TiO_2 nanocrystalline films surfaces after treatment by plasma with bubbling has a certain longevity. Because oxide vacancy loses its activity, contact angles will restore gradually as storage time increases, no matter if the samples are stored in vacuum or in atmosphere. But contact angles of samples stored in atmosphere can keep smaller contact angles than those stored in vacuum.

Compared with untreated ones, Ar plasma treated and Ar /H_2O plasma treated TiO_2 films, plasma treated films had more quantity of dye adsorption than untreated film. As Ar /H_2O plasma treatment has the most obvious effect on hydrophilicity, it also has the most dye adsorption.

References

[1].BO. X, Chen, S. S. Mao. Titanium dioxide nanomaterials: synthesis, properties, modifications, and applications. Chem. Rev. 107: 2891−2959-2007.

[2] Pfaff, G.; Reynders, P. Angle-Dependent Optical Effects Deriving from Submicron Structures of Films and Pigments. Chem. Rev. 99 (7): 1963-1982 1999.

[3] Salvador, A.; Pascual-Marti, M. C.; Adell, J. R.; Requeni, A.; March, J. G. Analytical methodologies for atomic spectrometric determination of metallic oxides in UV sunscreen creams. J. Pharm. Biomed. Anal., 22: 301-306, 2000.

[4] Zallen, R., Moret, M. P. The optical absorption edge of brookite TiO_2. Solid State Commun.137, 154-157, 2006.

[5] J. H. Braun, A. Baidins, R. E. Marganski. TiO_2 pigment technology: a review. Prog. Org. Coat., 20: 105-138, 1992.

[6] S. A. Yuan, W. H.Chen; S. S.Hu. Fabrication of TiO_2 nanoparticles/surfactant polymer complex film on glassy carbon electrode and its application to sensing trace dopamine. Mater. Sci. Eng. C, 25: 479-485, 2005.

[7] A. Fujishima, K. Honda. Electrochemical Photolysis of Water at a Semiconductor Electrode. Nature, 238: 37-38, 1972.

[8] A. Fujishima, Rao, T. N.; D. A Tryk. Titanium dioxide photocatalysis. J. Photochem. Photobiol. C, 1, 1-21, 2000.

[9] D. A. Tryk, A. Fujishima, K. Honda. Recent topics in photoelectrochemistry: achievements and future prospects. Electrochimca Acta, 45: 2363-2376, 2000.

[10] M. Grätzel. Photoelectrochemical cells. Nature, 414: 338-344, 2001.

[11] A. Hagfeldt, M. Grätzel. Light-Induced Redox Reactions in Nanocrystalline Systems. Chem. Rev., 95: 49-68, 1995.

[12] A. L. Linsebigler, G. Lu, J. T. Yates. Photocatalysis on TiO_2 Surfaces: Principles, Mechanisms, and Selected Results. Chem. Rev., 95: 735-738, 1995.

[13] Millis, A.; L; H., S. An overview of semiconductor photocatalysis. J. Photochem. Photobiol. A, 108: 1-35, 1997

[14] M. J. Grätzel, Perspectives for dye-sensitized nanocrystalline solar cells. Prog. Photovolt., 8: 171-185, 2000.

[15] M. J. Grätzel, Sol-Gel Processed TiO_2 Films for Photovoltaic Applications. Sol-Gel Sci. Technol, 22: 7-13, 2001.

[16] M. J. Grätzel, Dye-sensitized solar cells. Photochem. Photobiol. C, 4: 145-153, 2003.

[17] M. J. Grätzel, Conversion of sunlight to electric power by nanocrystalline dye-sensitized solar cells. Photochem. Photobiol. A: 164, 3-14, 2004.

[18] M. J. Grätzel, Dye-sensitized solid-state heterojunction solar cells. MRS Bull. 30: 23-27, 2005.

[19] Y. Kim, B. J. Yoo, et al., Low-temperature oxygen plasma treatment of TiO_2 film for enhanced performance of dye-sensitized solar cells. Journal of Power Sources, 175: 914–919. 2008.

[20] N. Terada. Fine pattern formation by ink-Jet printing using conductive nano-paste and its application (Tutorial series-the basic technology course of conductive adhesives for electronics devices Part 2(5)) (in Japanese). JIEP, 11: 300-306, 2008.

[21] G. L. Zhang. Reduction and sintering of copper nano-particles by non-equilibrium atmospheric pressure plasma jet. Kiryu: Gunma University, 2012.

[22] M. Samiee, J. Luo. Enhancing the visible-light photocatalytic activity of TiO_2 by heat treatments in reducing environments. Materials Letters, 98: 205–208, 2013.

[23] H. J. Kim, J. Kim, B. Hong. Effect of plasma treatment with various gases on nanocrystalline TiO_2 for dye-sensitized solar cell. Applied Surface Science. 274: 171–175, 2013.

[24] Z. S Wang, N. Koumura, et al., Hexylthiophene-Functionalized Carbazole Dyes for Efficient Molecular Photovoltaics: Tuning of Solar-Cell Performance by Structural Modification. Chem. Mater., 20: 3993–4000, 2008.

[25] R. Wang, K. Hashimoto, A. Fujishima. Light-induced amphiphilic surfaces. Nature., 388: 431-432, 1997

[26] A. N. Shultz, et al., Comparative second harmonic generation and X-ray photoelectron spectroscopy studies of the UV creation and O_2 healing of Ti^{3+} defects on (110) rutile TiO_2 surfaces. Surface Sci., 339: 114–124, 1995.

[27] T. Berger, O. Diwald, et al., Hydrogen activation at TiO_2 anatase nanocrystals. Chemical Physics, 339: 138–145, 2007.

[28] J. Shen, H. Dong, et al., A study of hydrophilicity of titanium dioxide thin films prepared by Sol- Gel method (in Chinese). Vacuum science and technology (China), 6 (20), 385-388, 2000.

[29] W. Göpel, G. Rocker, R. Feierabend. Intrinsic defects of TiO_2 (110): Interaction with chemisorbed O_2, H_2, CO, and CO_2 Phys. Rev. B, 28: 3427–3438, 1983.

[30] J. M. Pan, B. L. Maschhoff, U. Diebold, T. E. Madey, Interaction of water, oxygen, and hydrogen with TiO_2 (110) surfaces having different defect densities. Sci. Technol. A 10 (): 2470–2476, 1992.

[31] U. Diebold, J. Lehman, T. Mahmoud, M. Kuhn, G. Leonardelli, W. Heben-streit, M. Schmid, P. Varga. Intrinsic defects on a TiO_2 (110) surface and their reaction with oxygen: a scanning tunneling microscopy study. Surf. Sci., 411: 137–153, 1998.

[32] J. Weidmann, Th. Dittrich, E. Konstantinova, I. Lauermann, I. Uhlendorf, F. Koch. Influence of oxygen and water related surface defects on the dye sensitized TiO_2 solar cell. Solar energy material and solar cells. 56: 153–165, 1999.

[33] Hugenschmidt, M. B., Gamble, L. and Campbell, C. T. The interaction of H_2O with a TiO_2 (110) surface. Surface Sci, .302: 329-340, 1994.

[34] X. J. Li, G. J. Qiao, J. R. Chen. Mechanism of oxygen vacancy of titanium oxide modified by the radio frequency plasma in photocatalytic degradation. Journey of Chinse ceramic society.. 34 (12): 1466-1469, 2006

[35] L. Kavan, M. Gra¨tzel, J. Rathousky´, A. Zukal, Nanocrystalline TiO_2 (anatase) electrodes: surface morphology, adsorption, and electrochemical properties. J. Electrochem. Soc. 143: 394–400, 1996.

[36] K. H. Jung, J. S. Hong, R. Vittal, K.-J. Kim, Enhanced Photocurrent of Dye-Sensitized Solar Cells by Modification of TiO_2 with Carbon Nanotubes. Chem. Lett. 31: 864–865, 2002.

[37] N. Papageorgiou, C. Barbé, M. Grätzel, Morphology and Adsorbate Dependence of Ionic Transport in Dye Sensitized Mesoporous TiO_2 Films. J. Phys. Chem. B, 102: 4156–4164, 1998.

[38] C.J. Barbé, F. Arendse, P. Comte, M. Jirousek, F. Lenzmann, V. Shklover, M. Grätzel, J. Nanocrystalline Titanium Oxide Electrodes for Photovoltaic Applications. American Ceram. Soc. 80: 3157–3171, 1997.

[39] ZS. Wang, N. Koumura, Y. Cui, M. Takahashi, et al., Hexylthiophene-functionalized carbazole dyes for efficient molecular photovoltaics: Tuning of solar-cell performance by structural modification. Chem. Mater., 20: 3993–400, 2008.

[40] M. Yu. Preparation of dye sensitized solar cell and influencing factors (in Chinese). South China University of Technology: 2012.

[41] J. J. Fan. Preparation of TiO_2 nanosheets-based dye-sensitized solar cell (in Chinese). Wuhan University of Technology: 2012.

[42] Y. Kim, B. Jin Y. et al., Low-temperature oxygen plasma treatment of TiO_2 film for enhanced performance of dye-sensitized solar cells. Journal of Power Sources. 175: 914–919, 2008.

[43] M. Aizawa, Y. Morikawa, Y. Namai, H. Morikawa, Y. Iwasawa, J. Phys. Chem. B 109: 18831–18838, 2005.

Tab. 4-1 Change in oxidation state of Ti for TiO_2films treated by Ar plasma for 5 min, 10 min, 20 min and 40 min

	Untreated	**Ar 5min**	**Ar 10min**	**Ar 20min**	**Ar 40min**
Ti^{4+}2p	94.29%	94.86%	94.75%	91.93%	90.85%
Ti^{3+}2p	5.71%	5.14%	5.25%	8.07%	9.15%
Ti^{4+}/ Ti^{3+}	16.53	18.47	18.05	11.39	9.93

Tab. 4-2 Change in oxidation state of Ti for TiO_2 films treated by Ar/H_2O plasma for 5 min, 10 min, 20 min and 40 min

	Untreated	**Ar/H_2O 5min**	**Ar/H_2O 10min**	**Ar/H_2O 20min**	**Ar/H_2O 40min**
Ti^{4+}2p	94.29%	94.90%	92.75%	90.99%	90.10%
Ti^{3+}2p	5.71%	5.10%	7.25%	9.01%	9.90%
Ti^{4+}/ Ti^{3+}	16.53	18.61	12.79	10.10	9.11

Tab. 4-3 Change in surface chemical components of TiO_2 film treated by Ar plasma for 5 min, 10 min, 20 min and 40 min

	Untreated	Ar 5min	Ar 10min	Ar 20min	Ar 40min
O_{oxide}	93.68%	94.56%	95.13%	95.00%	95.08%
-OH	3.99%	4.03%	4.24%	4.93%	4.85%
H_2O	2.34%	1.42%	0.63%	0.06%	0.07%
OH/Oxide	0.043	0.042	0.045	0.052	0.051

Tab. 4-4 Change in surface chemical components of TiO_2 film treated by Ar/H_2O plasma for 5 min, 10 min, 20 min and 40 min

	Untreated	Ar/H_2O 5min	Ar/H_2O 10min	Ar/H_2O 20min	Ar/H_2O 40min
O_{oxide}	93.68%	93.37%	93.88%	93.36%	89.18%
-OH	3.99%	5.27%	5.59%	6.47%	8.66%
H_2O	2.34%	1.36%	0.53%	0.17%	2.1%
OH/Oxide	0.043	0.056	0.059	0.069	0.097

Tab. 4-5 Information on MK-2 Dye

Synonyms	2-Cyano-3-[5‴-(9-ethyl-9H-carbazol-3-yl)-3′, 3″, 3‴, 4-tetra n-hexyl-[2, 2′, 5′, 2″, 5″, 2‴]-quarter thiophen-5-yl] acrylic acid
Formula	$C_{58}H_{70}N_2O_2S_4$
Molecular Weight	955.45 g/mol
CAS-No.	1037440-21-3
Appearance	Solid
Melting point/range	181 - 185 °C

Tab. 4-6 The determination of adsorbed MK-2 of TiO_2 thin films treated by different method

	Untreated	**Ar plasma 20min**	**Ar/H_2O 20min**
Adsorption (1×10^{-8}mol/cm^2)	3.02	4.05	5.52

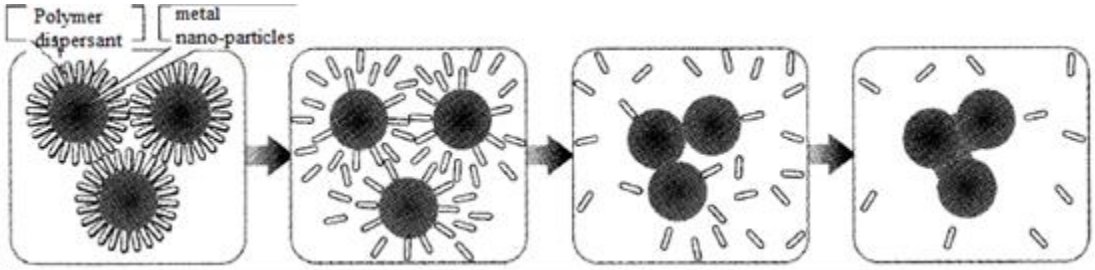

Fig. 4-1 The process of heat-treatment and sintering for metal nano-paste. At ambient temperature without treatment (a), heat-treatment (b), decomposition of the polymer additive (c), sintering of metal nano-particles (d) [20, 21].

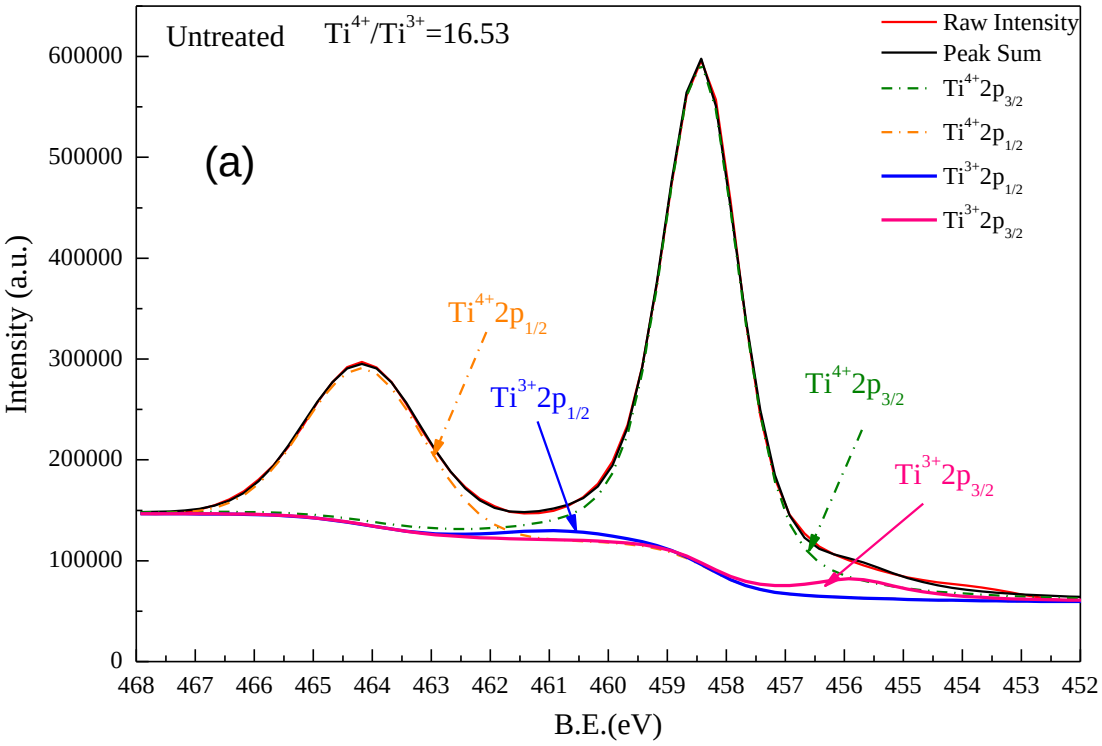
Untreated
Ti4+/Ti3+=16.53
(a)
Raw Intensity
Peak Sum
Ti4+2p3/2
Ti4+2p1/2
Ti3+2p1/2
Ti3+2p3/2
Intensity (a.u.)
B.E.(eV)

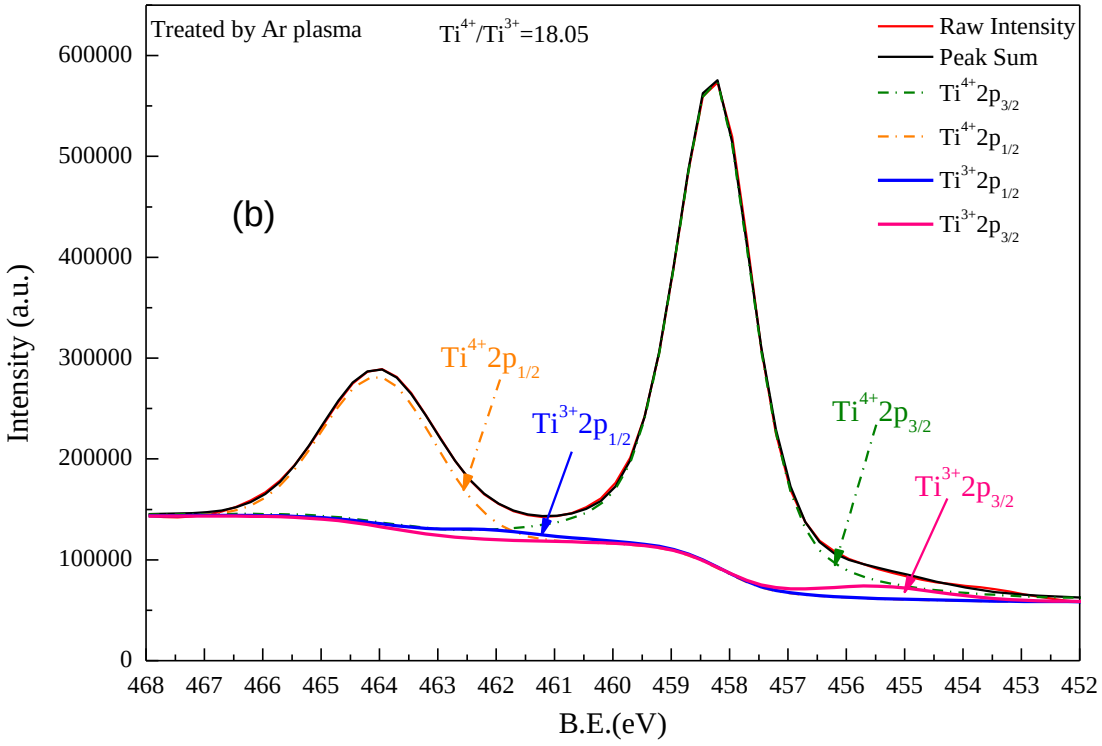
Treated by Ar plasma
Ti4+/Ti3+=18.05
(b)
Raw Intensity
Peak Sum
Ti4+2p3/2
Ti4+2p1/2
Ti3+2p1/2
Ti3+2p3/2
Intensity (a.u.)
B.E.(eV)

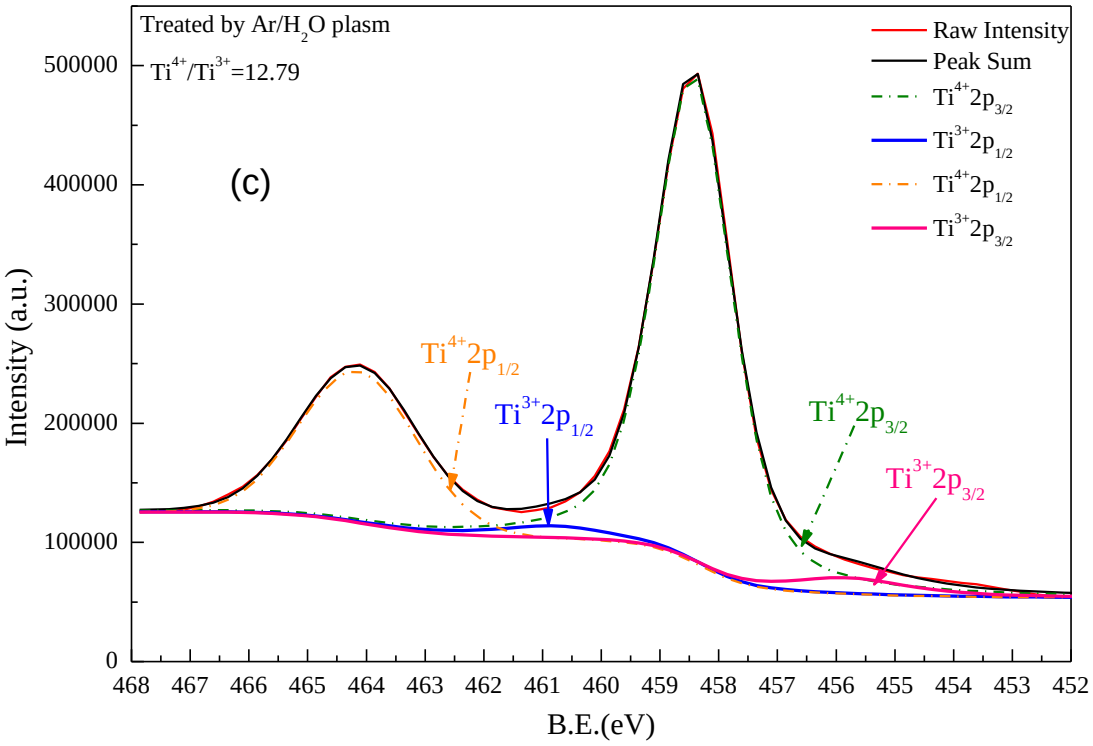

Fig.4-2 (a) XPS spectrum of Ti2p peak fitting for TiO_2 films: (a) untreated; (b) TiO_2 film treated by Ar plasma for 10 min; (c) TiO_2 film treated by Ar/H_2O plasma for 10 min

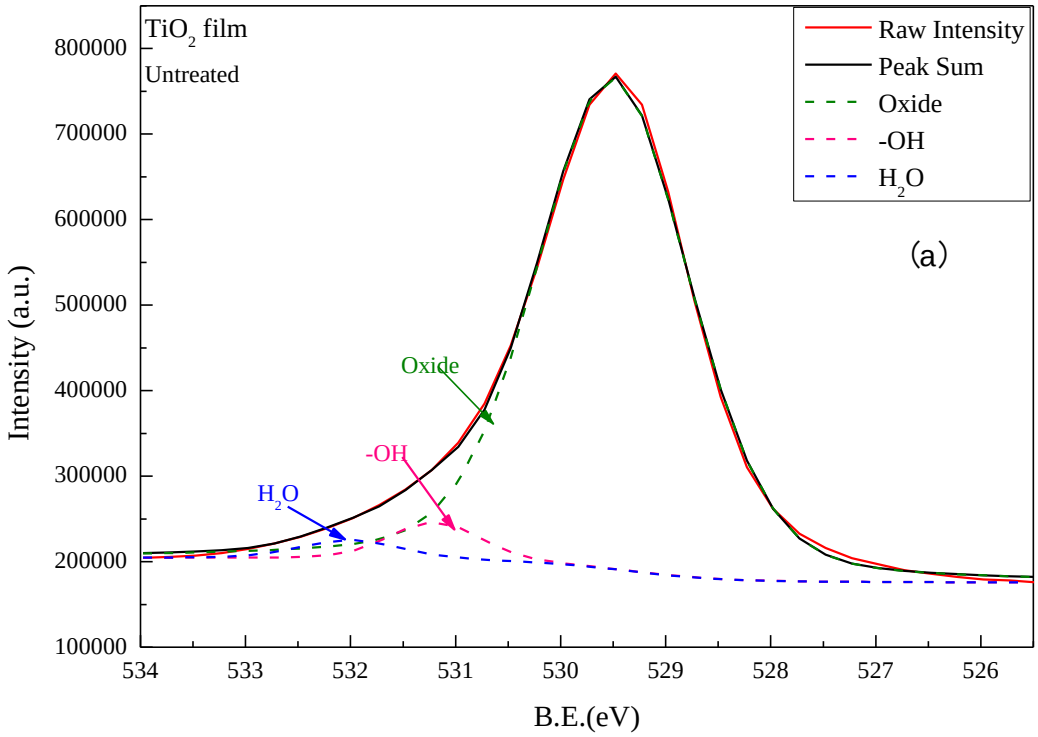
TiO2 film
Untreated
Raw Intensity
Peak Sum
Oxide
-OH
H2O
(a)
Oxide
-OH
H2O
Intensity (a.u.)
B.E.(eV)
800000
700000
600000
500000
400000
300000
200000
100000
534
533
532
531
530
529
528
527
526

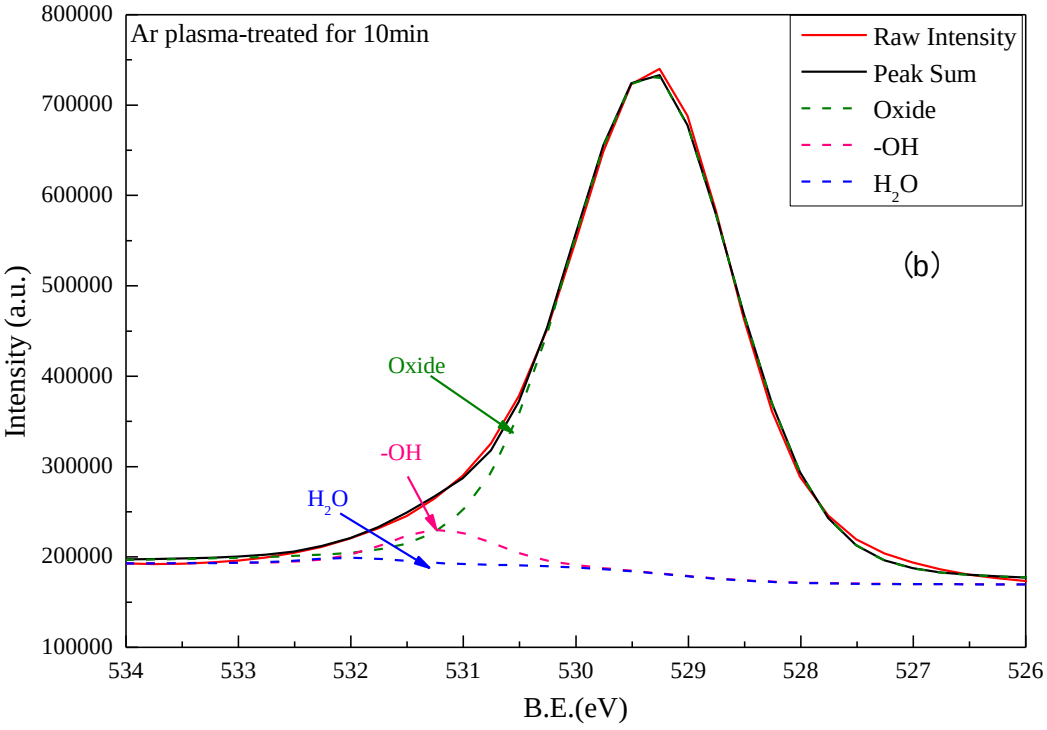
Ar plasma-treated for 10min
Raw Intensity
Peak Sum
Oxide
-OH
H2O
(b)
Oxide
-OH
H2O
Intensity (a.u.)
B.E.(eV)
800000
700000
600000
500000
400000
300000
200000
100000
534
533
532
531
530
529
528
527
526

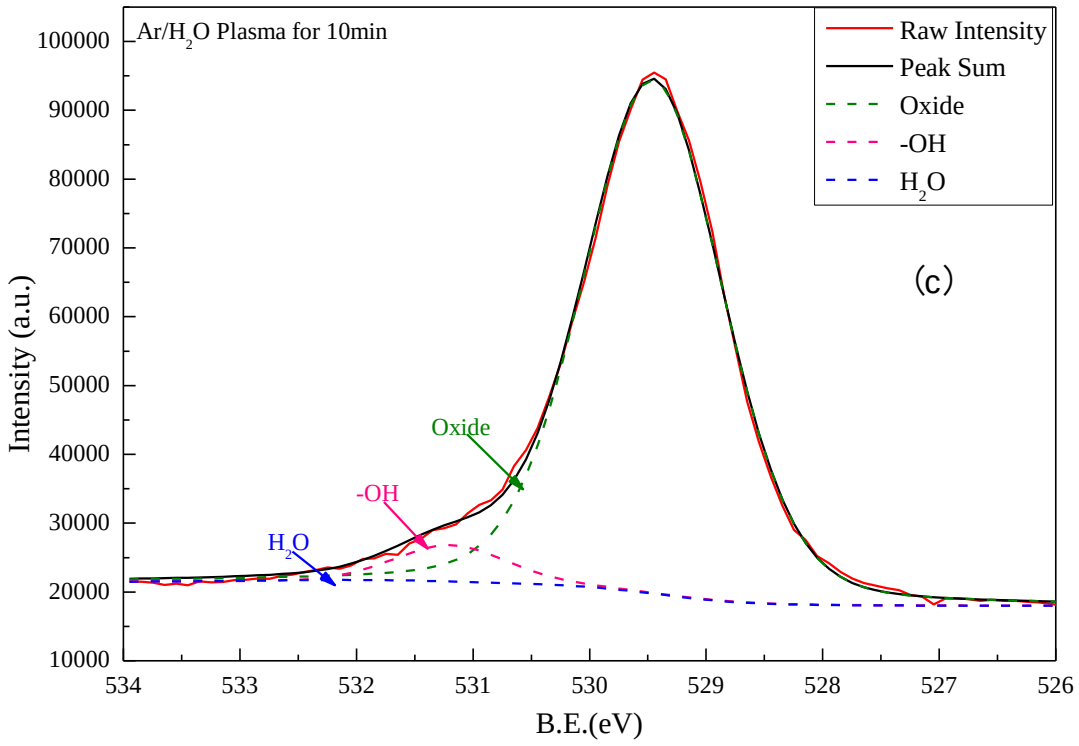

Fig.4-3 XPS spectrum of O1s peak fitting for TiO_2 films: (a) untreated; (b) TiO_2 film treated by Ar plasma for 10 min; (c) TiO_2 film treated by Ar/H_2O plasma for 10 min

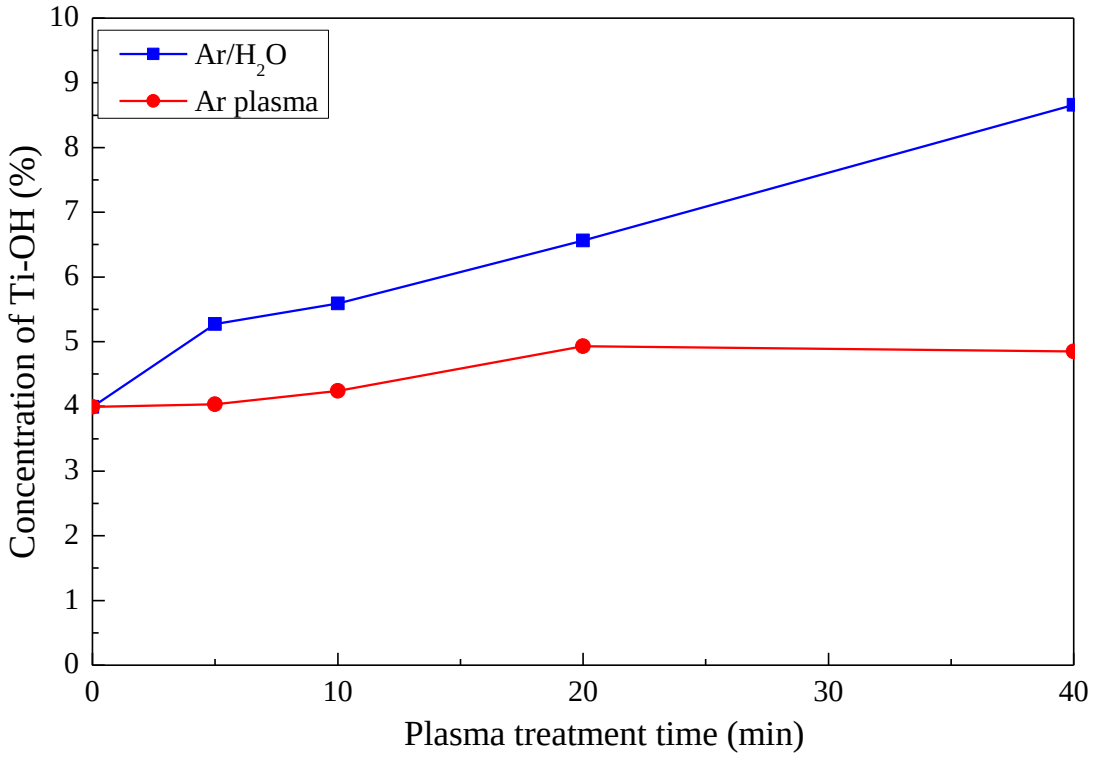

Fig.4-4 Concentration of OH on TiO_2 film surfaces which were treated by Ar plasma and Ar/H_2O plasma for different treating time

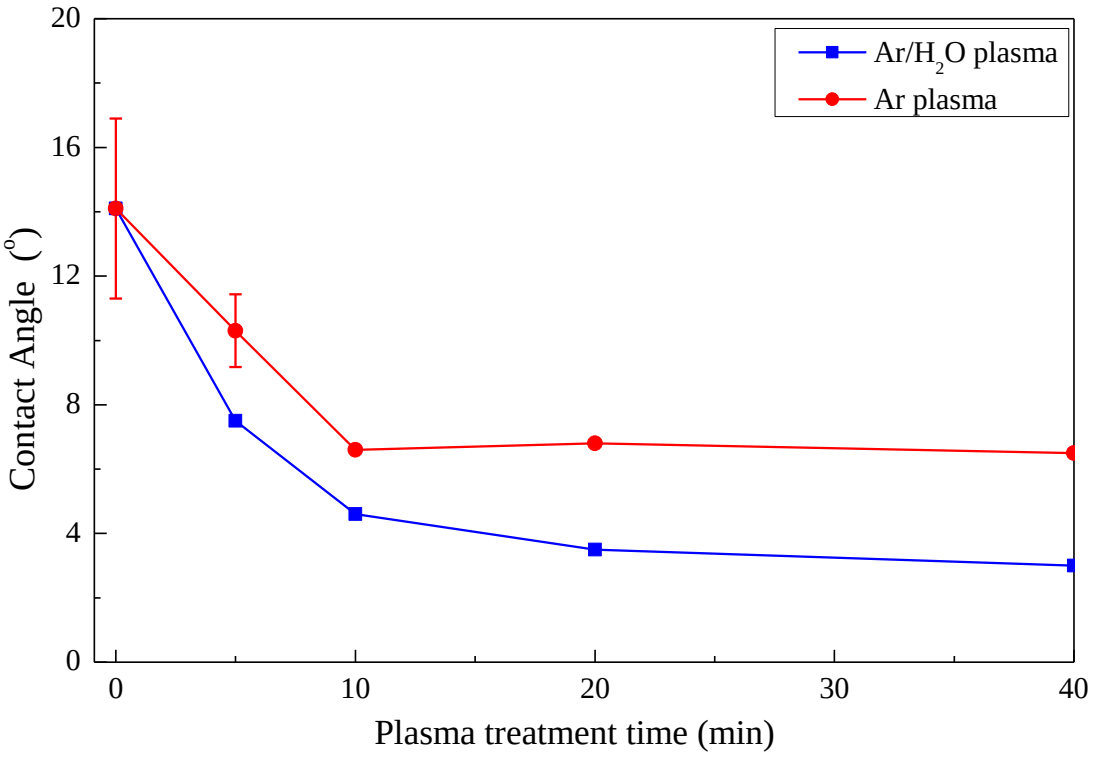

Fig.4-5 Contact angles on TiO_2 film surfaces which were treated by Ar plasma and Ar/H_2O plasma for different treating time

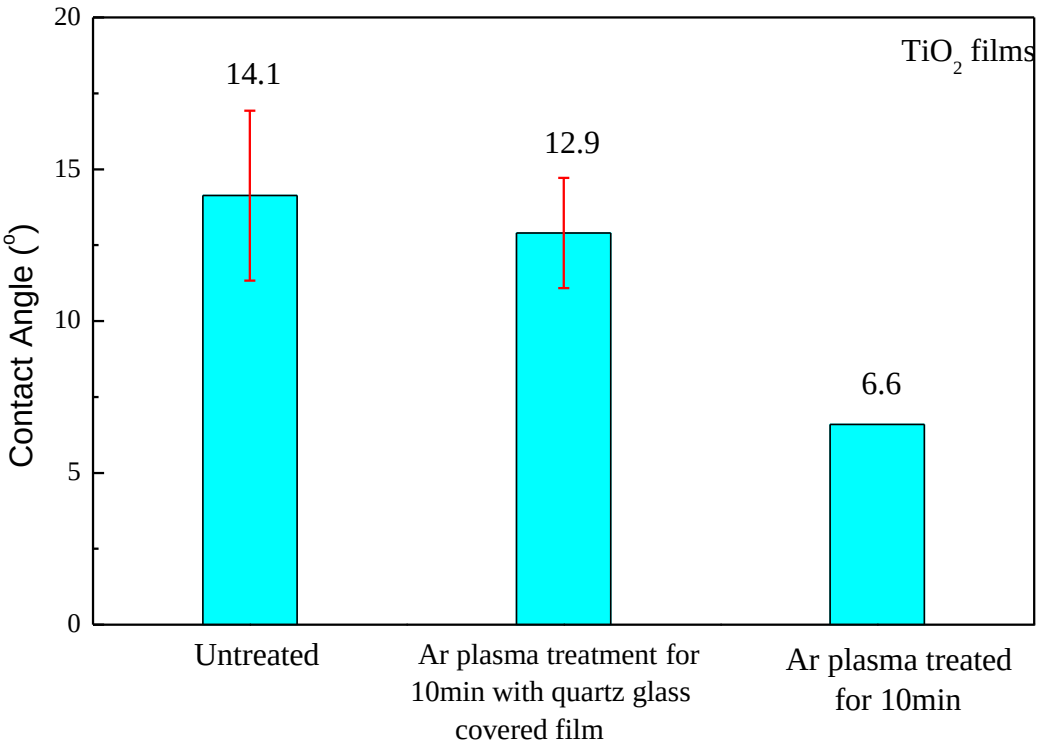

Fig.4-6 Discussion of effect of UV in plasma irradiation

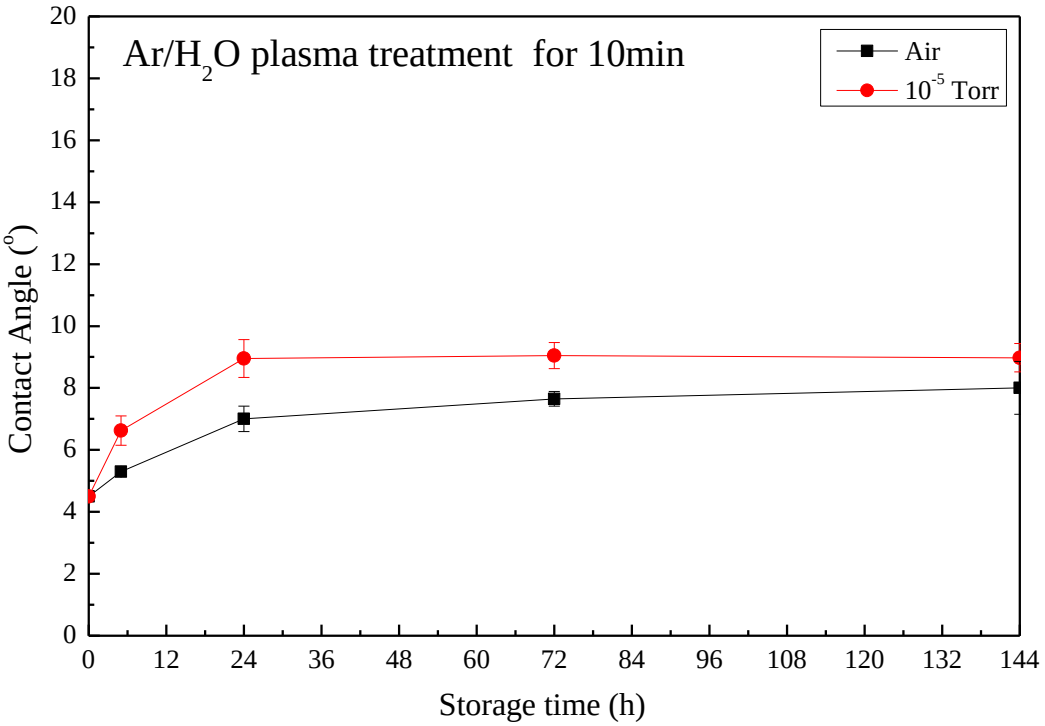

Fig.4-7 Changes of contact angles of plasma treated after different storage times

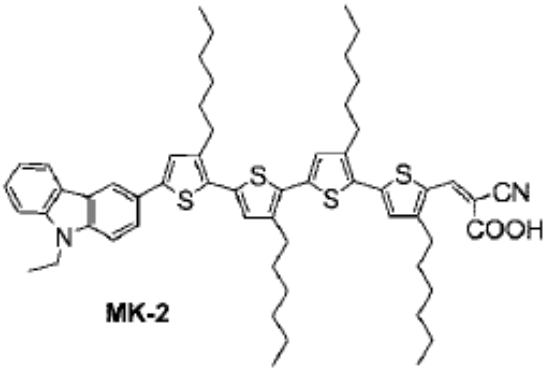

Fig.4-8 The structure of MK-2

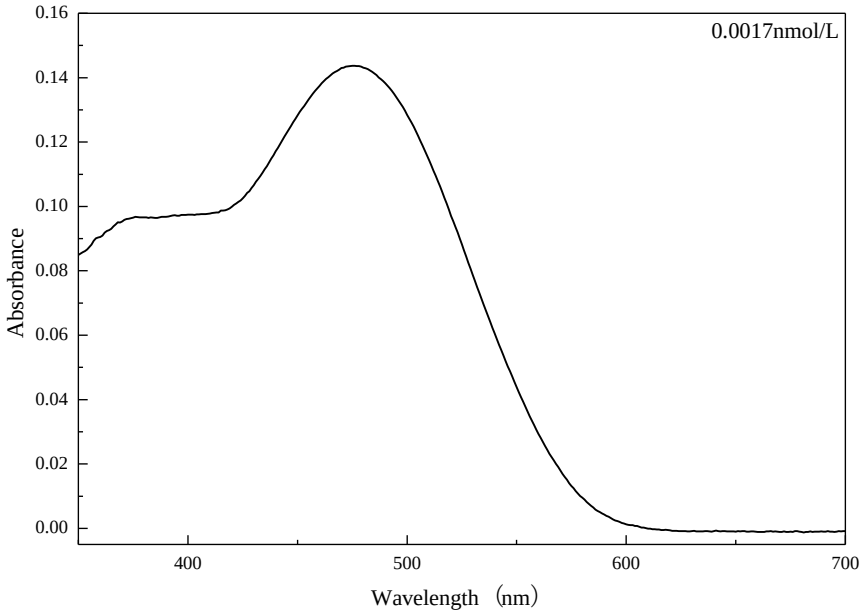

Fig.4-9 The absorbance curve of Dye MK-2 solution with concentration of 0.0017 mmol/L

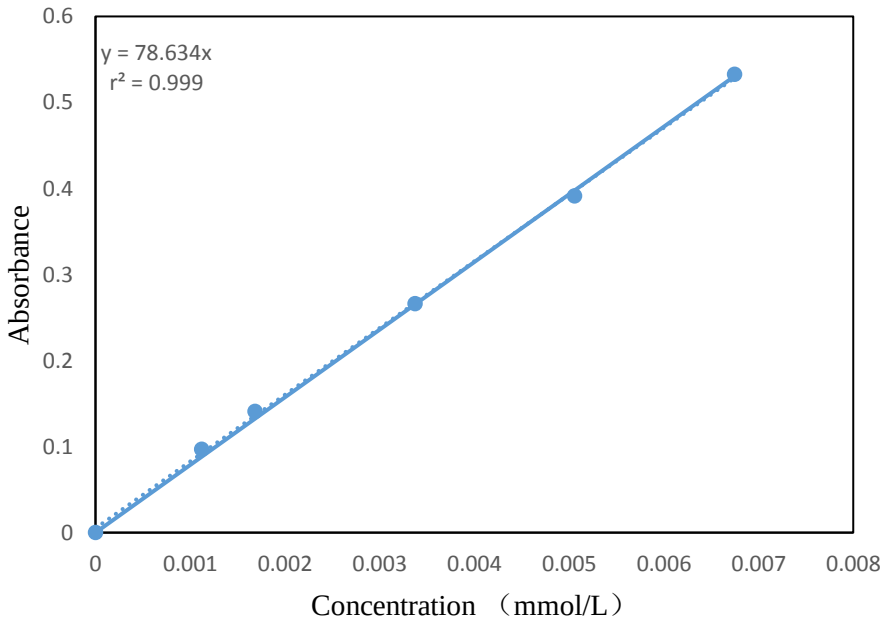

Fig.4-10 Standard curve of the relation between concentration and absorbance of the Dye MK-2 solution

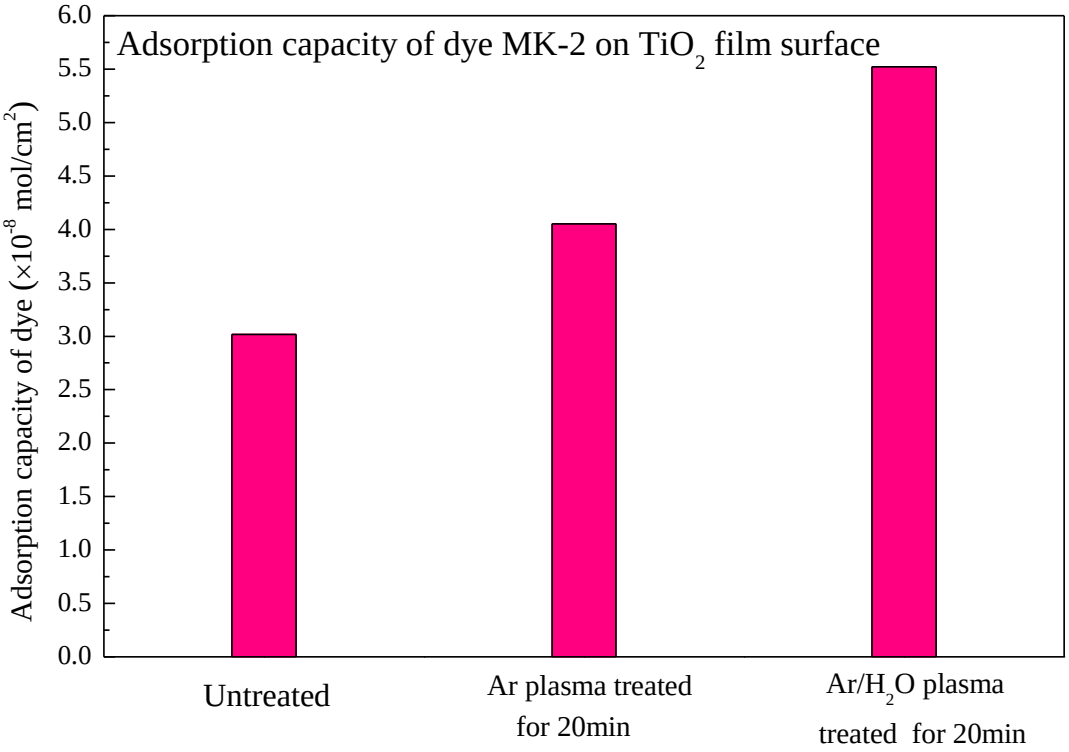

Fig.4-11 Evaluation of adsorbed dye MK-2 on TiO_2 films' surface

Chapter 5 Conclusions and prospect

1 Conclusions

The aim of this study is to apply non-equilibrium atmospheric pressure plasma jets in electronics industry, e.g. the semiconductor industry and solar cell area, to simplify the production process, reduce the production cost and improve the performance of materials. We discussed the application of non-equilibrium atmospheric pressure plasma to oxide such as silica and titanium dioxide which are widely used in electronics industry. In order to improve the shortcoming of less hydrophilicity surface of oxidized Si wafer and TiO_2 monocrystalline film, we introduce hydroxy group or reduce (create oxide vacancy) on their surfaces by using non-equilibrium atmospheric pressure plasma jet generated with three kinds of gases, which is Ar, Ar/H_2 and Ar/H_2O (water vapor was introduced by bubbling system). The longevity of hydrophilicity introduced by plasma was also investigated. We confirmed that hydrophilization process onto the oxidized Si wafers and TiO_2 films by plasma at ambient temperature could be finished within 1 minute in atmosphere.

In chapter 2, the non-equilibrium atmospheric pressure plasma generated with 2 kinds of working gases (Ar and Ar/H_2) was used to introduce hydrophilicity effect on thermally oxidized Si wafer surfaces. The results of XPS analysis and contact angle measurement showed that hydrophilicity can be introduced to the surface silicon oxide wafer surface by irradiation with non-equilibrium atmospheric pressure plasma. In the irradiation with Ar plasma, it seems that the Si-O bond is cleaved by energy transfer from the metastable argon atom (Ar^m) which is the active species, and hydroxy group is formed by contact with the atmosphere after plasma irradiation. In irradiation with Ar/H_2 plasma, H atoms are considered to act in addition to Ar^m. However, slight introduction of

hydrophilicity into the silicon oxide surface by Ar plasma and Ar/H_2 plasma was observed. It was considered that the Si-O bond cleaved by the interaction with Arm was promptly recombined.

In order to efficiently generate hydroxy groups, it was considered effective to coexist with H_2O. In chapter 3, the non-equilibrium atmospheric pressure plasma with bubbling system which can introduce water vapor during plasma irradiating was used to improve hydrophilicity on thermal oxidized Si wafer surfaces. The XPS results show that, the amount of surface silanol increased from 2.5% to 5.9%. Also, the water contact angle showed a drastic drop, decreasing from 59 º to less than 10º. With increasing treating time, there is not an obvious change in concentration of hydroxy group. It strongly suggests that Ar/H_2O plasma could enhance hydrophilicity of oxidized Si wafer. With plasma treatment for 1 minute, the contact angle could decrease to 11°. In conclusion, as time goes on, contact angle stabilized at about 10°.

In order to investigate the influence of the structure of silicon oxide on the introduction of hydrophilicity by non-equilibrium atmospheric pressure plasma, quartz glass was treated with Ar/H_2O plasma. Furthermore, the stability of the hydrophilicity introduced on the silicon oxide surface was investigated. The amount of surface silanol and the water contact angle of the quartz glass treated with Ar/H_2O plasma changed like the surface silicon oxide wafer. The amount of surface silanol increased from 1.8% to 5.7%, and the contact angle decreased from 63 º to 10 º or less. In order to confirm the stability of the hydrophilicity of the silicon oxide surface introduced by Ar/H_2O plasma, change with time of the contact angle was observed. Surface silicon oxide wafers and quartz glass were stored in air and in vacuo after Ar/H_2O plasma treatment. It was revealed that the contact angle gradually increased with storage time. It is believed that adjacent silanols dehydrated and condensed to form siloxane bonds. The rate of increase in the contact angle of quartz

glass was slower than that of the surface silicon oxide wafer, but this was considered to be due to the difference in distance of Si atoms.

In this chapter, a characterization method for various name labeling approaches was discussed. The surface hydroxy group on thermally oxidized Si wafer after plasma treatment can be successfully determined by reaction of the OH group with tridecafluoro-1, 1, 2, 2-tetrahydrooctyl dimethyl-chlorosilane (FOCS) and subsequent electron spectroscopy for chemical analysis for fluorine which has high sensitivity. In order to better study hydroxy group on different depths of SiO_2 surface, photoelectrons are collected at a takeoff angle of 15°, 45°and 75°. For the labeling method, the concentration of silanol on surface of wafers treated by plasma with bubbling system is higher than the untreated wafer and Ar/H_2 plasma treated wafer. Another conclusion we get is that as depth of surface increases, the OH content will decrease. Plasma treatment can have an obvious effect on the outermost surface of samples.

Based on the above results, in chapter 4, the influence of non-equilibrium atmospheric pressure plasma on titanium oxide is studied. As a sample, a titanium oxide film prepared by coating titanium oxide nanoparticles on a glass plate was used. Ar/H_2O plasma was generated with using APC. In order to confirm the surface hydrophilicity, the Ti^{4+} / Ti^{3+} ratio and the hydroxy group concentration were estimated based on the XPS measurement and the water contact angle was evaluated. The results of XPS analysis and water contact angle measurements showed that hydroxy groups were introduced into titanium oxide surface by atmospheric pressure non-quilibrium plasma. The energy transfer from Arm seems to have resulted in cleavage of the Ti-O bonds to generate oxygen defects and additionally to hydroxy groups. By plasma irradiation, the ratio of Ti^{4+} / Ti^{3+} decreased from 16.5% to 9.1% and the amount of hydroxy groups increased from 4.0% to 8.7%. Also, the contact

angle decreased to 10 º or less. We also confirmed the stability of the hydrophilicity introduced on the titanium oxide film surface by Ar/H_2O plasma. After the Ar/H_2O plasma treatment, the titanium oxide film was stored in air and in vacuo, and the water contact angle gradually increased with the storage time. In addition, it was revealed that the titanium oxide film treated with Ar/H_2O plasma increased the adsorption amount of the dye. It can be expected that introduction of hydrophilicity into oxide by non-equilibrium atmospheric pressure plasma contributes to performance improvement of dye sensitized solar cell.

2 Prospect

We reach the objectives of the study, based on those approaches and the conclusions introduced in previous chapters. As for further study in future, it is necessary to find optimum characterization methods on quantitative analysis of hydroxy group on oxidized Si wafer surface. In addition, I also hope to further investigate the detailed properties of DSSC cells, to verify practicability of TiO_2 nano-particles by non-equilibrium atmospheric pressure plasma in solar cells field.

List of publications

1. Introduction of hydrophilicity onto silicon oxide by non−equilibrium atmospheric pressure plasma with several working gases

   Chen Long, Katsuhiko Hosoi, Shin-ichi Kuroda

   Journal of Materials Life Society, vol. 31 (2019), in press

   Related to Chapter 2 and 3

2. Introduction of hydroxy group onto titanium oxide by non−equilibrium atmospheric pressure plasma for the enhancement of dye adsorption

   Chen Long, Katsuhiko Hosoi, Shin-ichi Kuroda

   Journal of Materials Life Society, vol. 31 (2019), in press

   Related to Chapter 4

Acknowledgement

First and foremost, I would like to show my deepest appreciation to my supervisor, Dr. Shin-ichi Kuroda, a respectable, responsible scholar, who has provided me with valuable guidance and assistance in every stage of the writing of this thesis, especially after I left university and started working overseas. Without his instruction, kindness and patience, I could not have completed my thesis. His keen and vigorous academic observation enlightens me not only in this thesis but also in my work now and future.

I shall extend my gratitude to Dr Kawai for his kind encourage and help during my study in Gunma University.

I wish to give special thanks to Professor Kyomen, Professor Tobishima, Professor Itabashi, and Professor Morimoto for their invaluable suggestions and comments to this thesis.

A deep gratitude is also given to all the members of Kuroda Laboratory, especially to Dr. Hosoi and the members of plasma group, for their warm guidance and assistance. We have formed profound friendship during the experiments.

I also hope to express my appreciation to Cresur Corporation for providing plasma devices and Taiyo yuden Co., Ltd for the sample support.

Moreover, I wish to give thanks to Japan Students Services Organization for providing me the scholarship and other various supports during my study in Japan.

Lastly, my thanks would go to my family for their great confidence in me all through these years.

I also owe my sincere gratitude to Yin Yichun, Huang Lingqi and Ma Haiyang, Zhao Meichao who gave me significant help and suggestions on my research; as well as my friends who share their time listening to me and helping me work out my problems during the difficult course of the thesis; my colleague Nii Daisuke, Liu xubing, Huang Mudan, with whose understanding and support, I can give more attention on this paper.